2012-01-01

A Novel Method For The Curing Of Metal Particle Loaded Conductive Inks And Pastes

David Adrian Roberson
University of Texas at El Paso, droberson@miners.utep.edu

A NOVEL METHOD FOR THE CURING OF METAL PARTICLE LOADED CONDUCTIVE INKS AND PASTES

DAVID ADRIAN ROBERSON

Materials Science and Engineering

APPROVED:

Eric W. MacDonald, Ph.D., Chair

Ryan B. Wicker, Ph.D.

Lawrence E. Murr, Ph.D.

Geoffrey B. Saupe, Ph.D.

Cristian E. Botez, Ph.D.

Benjamin C. Flores, Ph.D.
Interim Dean of the Graduate School

DEDICATION

For Adriana and Austin.

A NOVEL METHOD FOR THE CURING OF METAL PARTICLE LOADED CONDUCTIVE INKS AND PASTES

by

DAVID ADRIAN ROBERSON, B.S., M.S.

DISSERTATION

Presented to the Faculty of the Graduate School of

The University of Texas at El Paso

in Partial Fulfillment

of the Requirements

for the Degree of

DOCTOR OF PHILOSOPHY

Materials Science and Engineering

THE UNIVERSITY OF TEXAS AT EL PASO

May 2012

ACKNOWLEDGEMENTS

The five day trip between Richmond, Virginia and El Paso, Texas that my family and I embarked on starting August 19, 2009 marked the beginning of a new era in our lives. The actual road trip itself was extremely hard because we had to stop every 200 miles or so as my 15 month old son, Austin, hated to ride in the car. I thank the state of Tennessee for having very nice rest stops. Five days earlier, I had been encouraged to start the pursuit of my doctorate, by Lawrence E. Murr via an unexpected e-mail, and the Fall semester was to start on the twenty fourth. Applying to the Ph.D. program was one of many shots in the dark I had taken during the six months that lay between the bankruptcy of my former employer and that moment when I had to make a decision; remain on unemployment and bob around like a bottle in the ocean and wait for whatever job came around or make a conscientious effort to change the circumstance of my life and the lives of my family. I thank Dr. Murr for giving me the opportunity to make a choice.

Funding for the research my dissertation is composed of came from the NSF LSAMP Bridge to the Doctorate Program under grant number HRD-0929727. I was the recipient of a Mr. and Mrs. MacIntosh Murchison Engineering Scholarship, specifically the Patricia and Jonathan Rogers Scholarship. I also received a Dodson Dissertation Fellowship.

My thanks to the students and staff in the W.M. Keck Center for 3D Innovation as well as the staff in the LSAMP office for the help and support I received during the pursuit of my Doctorate. Also, I thank my classmates, the faculty and staff in the Department of Metallurgical and Materials Engineering for their friendship and support. Thank you to Brandon Aguirre in the UTEP NanoMIL for his help and expertise in profilometry. Thanks to Donny Chen and Cliff Boyd at nScrypt, Inc. for printing test samples for me. Thanks to Dr. Mike Irwin and Richard Olivas for help with the UVO cleaner and the Dimatix materials printer. My thanks to Rodolfo Salas and Danny Muse for their help with SolidWorks and for their willingness to engage me in brain-stimulating conversation. Thanks to Cassie Soto for her development of the LabView program. I thank my committee members— Dr. MacDonald, Dr. Wicker, Dr. Murr, Dr. Saupe and Dr. Botez— for their guidance in my endeavor to

earn a Ph.D., particularly the input following the presentation of my dissertation proposal as it helped shape the overall focus of this dissertation.

I am extremely thankful for the love and support given to me by my wife, Adriana and my son, Austin. The opportunity to earn my Ph.D. came in tumultuous times and with a large amount of sacrifice. Their faith in me allowed me to complete this chapter in our lives.

Heb. 11:1

ABSTRACT

The emerging technology of printed microelectronics involving the use of conductive inks in conjunction with standard printing techniques offers a fast and low waste method for creating microelectronics compared with standard manufacturing processes. A clear path to the creation of flexible electronics is present due to the ease of printing on flexible substrates. Moreover, creation of novel 3D structural electronics is possible via the integration of printing technologies and additive manufacturing (AM) techniques.

A key obstacle to the manufacturing of flexible and structural electronics comes from the temperature restrictions imposed by the substrates, which are typically polymeric. This hindrance has the effect of limiting the thermal cure cycles necessary to create the maximum electrical performance of conductive traces printed with conductive ink, which must be thermally cured. Whether the ink has micro-scale conductive particles, nano-scale conductive particles, or is organometallic in nature, all conductive inks need some sort of thermal curing to perform properly.

The research presented in this dissertation entails the development of a curing technique which creates the optimal electrical performance in conductive traces created from conductive ink on both flexible and 3D polymeric substrates. The utilization of ohmic heating in conjunction with and in lieu of thermal curing is shown to decrease the resistivity of conductive traces printed form conductive inks and pastes. Microstructural characterization was performed on successful and unsuccessful (electrically failed) specimens. A process characterization of the creation of a via/interconnect system in a 3D freeform was made and involved electrical characterization and printable conductor selection. Initial research involving electrical and microstructural characterization of the thermal curing process is presented along with novel findings showing the impact of inkjet printing procedure on the resulting electrical resistivity. Also, a failure analysis of a component from a direct write equipment set was made.

TABLE OF CONTENTS

LIST OF TABLES

LIST OF FIGURES

LIST OF EQUATIONS

CHAPTER 1: INTRODUCTION

The goal of this work was to develop a curing method for conductive ink which can be used alternatively to thermal curing methodologies or in conjunction with thermal and other curing techniques. The main curing method explored will be the employment of ohmic curing in order to improve the electrical characteristics of printed conductive traces. Electrical characterization—namely resistance—and mechanical properties such as adhesion to the substrate and cyclic testing of ink cured on flexible substrates will be compared to those of thermally cured processes. Integration with additive manufacturing (AM) in order to create 3D structural electronic devices will be investigated. The effects of utilizing ohmic curing in conjunction with other curing methods, namely thermal curing, will also be characterized.

1.1 Research Motivation

Printed microelectronics involving conductive ink is an emergent industry with distinct advantages over conventional electronic manufacturing methods which entail the use of lithography and deposition necessitating several steps to create a functional product. The ability to directly print a functional conducting, semiconducting, or insulating substance directly onto a substrate opens the door to numerous applications such as the creation of flexible and structural (or 3D microelectronics) manufacturing. Alone, the Flexible Electronics Industry is expected to generate $300 billion by 2028 [1].

The utilization of conductive ink in the printing of electrodes and conductive pathways as a replacement for traditional metallization methods has been demonstrated in numerous applications such as the manufacturing of solar cells, radio frequency identification devices (RFIDs), and glucose sensors [2–4]. Several examples involving the combination of printing techniques to create functional electronic devices are a testament to the potential of this manufacturing methodology. One example is the combination of gravure and ink jet printing in the creation of functional junction transistor in a 5-step process [5].

The main advantage printing methodologies have over standard metallization techniques are the ability to create conductive paths in one to two steps. An example of a typical metallization process is seen in Figure 1.1 where a minimum of six steps are required to perform the total metallization process. It is also worth considering that multiple steps also require different equipment sets such as lithography and etching machines and that the typical metallization process is relatively wasteful compared to direct printing techniques as excess mask and conductive material must be removed to create the conductive path.

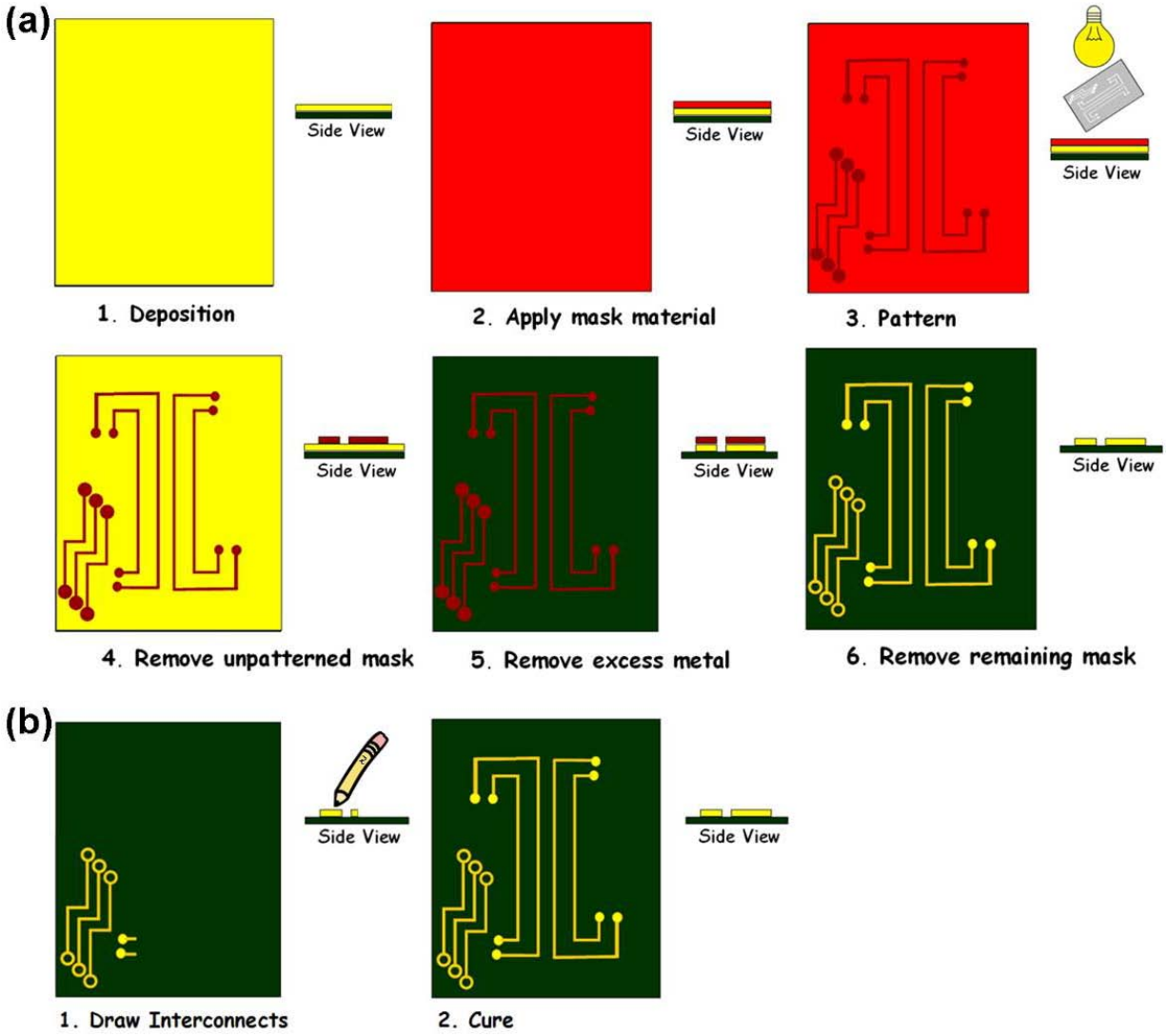

Figure 1.1: (a) The typical 6-step metallization process for creating conductive paths. A direct print technique **(b)** is capable of creating the same end product in as little as two steps.

The use of conductive ink in microelectronics manufacturing presents numerous opportunities for the development of new materials processing. A critical step is the process of curing the ink in order to gain optimal electrical performance. Currently, the norm is thermal processing to the point where most commercially available conductive inks have specified thermal curing parameters [6–8]. There are several examples of the scientific characterization of thermally processing particle-based—both nanoparticle and microparticle based—conductive inks as well as the resulting microstructure and electrical performance [9–12].

The main limitation to thermally curing conductive ink comes from the need for both the substrate and the conductive trace to be subjected to the process. For example, if polycarbonate is utilized as a substrate material, adherence to the temperature limitation of 150°C—the glass transition temperature of polycarbonate—would have to be obeyed. This temperature is below the manufacturing recommended curing temperature for DuPont CB028, (DuPont, Wilmington, DE, USA) [8] a commercially available conductive ink.

Problem Statement

In order to expand the use of conductive ink in microelectronics manufacturing, curing methods must be developed which can optimize the electrical performance of the printed conductive path without being governed by limitations imposed by inherent material properties of the substrate of choice.

1.2 Microstructure and Conductivity

In the following sections the fundamental concepts of the factors controlling the electrical performance of particulate conductive inks are presented. The concepts presented here are necessary to understand the driving force of the overall research. The information conveyed is based on a literary review as well the results of preliminary research. Section 1.2.1 provides an overview of the microstructural features pertinent to the performance of conductive ink. Section 1.2.2 covers percolation theory of conduction as it pertains to particulate conductive ink. Section 1.2.3 explains the concepts behind the sintering process and the relationship with conductivity.

The relationship between the characteristics of grains and conductivity will be covered in 1.2.4 and experimental examples of microstructural effects will be demonstrated in section 1.2.5.

1.2.1 Pertinent Microstructures

The microstructural characteristics of particle-based conductive ink are the key aspect of overall electrical performance of the printed line. The effect of temperature applies to both microparticle and nanoparticle-based inks in that the higher the curing temperature, the lower the resultant resistance will be for a given cure time. The effects of temperature on microstructure and resistance of a printed line have been well characterized [9, 11–14]. Based on these references, there are three resultant microstructures due to curing at various temperatures: 1.) a microstructure in which the particles are essentially lying next to each other in which the conductivity is governed by percolation theory; 2.) a sintered microstructure in which the curing process has led to necking of the conductive particles; and 3.) a microstructure in which a solid film composed of grains and some voids. It is important to note that the three resultant microstructures mentioned above occur at temperatures below the melting temperatures of the conducting particles. From the point of view of the conducting particles, all processing occurs in the solid state.

Percolation Theory

Percolation theory was described by Saraf *et al.* [14] for a silver flake conductor with a polymeric binder. The concepts of Percolation Theory is best explained by depicting the thermal cure process as is seen in Figure 1.2 where a correlation between the decrease in binder, or which ever media the ink particles are suspended in, is made with an increase in the conductivity of a printed trace. From this point of view the suspension media is separating the conductive particles, therefore, less separation due to less suspension media equates to an increase in conductivity. The key concept here is that if there is a greater contact area between the conductive particles, there will be less resistance in a printed line. The vertically linear area of the graph in Figure 1.2 designated by the number 2 is known as the percolation threshold of the

particle/binder system. It is during this region of the curing process in which conductivity is achieved as the amount of binder has decreased to a level sufficient enough to allow conduction by way of the particles physically touching one another. In the process described above , the conclusion can be drawn that the method used to process a printable conductor should be efficient at decreasing the amount of binder present in the conductor/binder system in order to be effective.

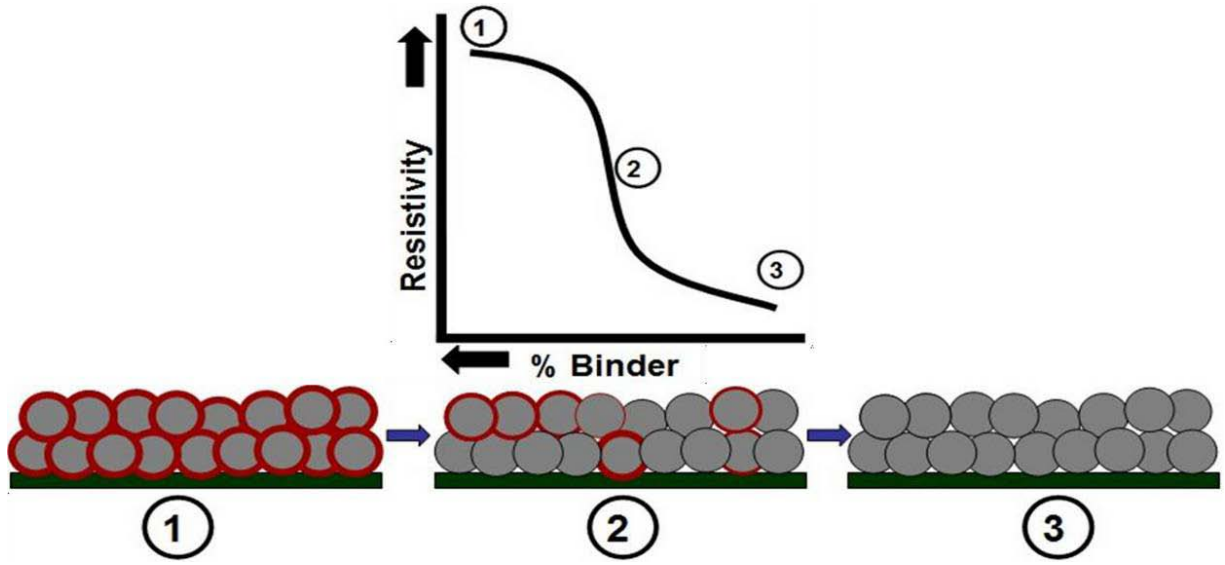

Figure 1.2: Depiction of percolation theory. As the ink or paste is cured, the substance separating the conductive particles, represented by red circles, decreases. As the contact between particles increases the resistivity decreases. After [11, 14].

The results of preliminary research indicated the effect of particle size on ink conductivity is another aspect which is explained by percolation theory as seen in Figure 1.3. In this case the contact area between particles is dependent on particle size rather than the amount of binder separating the particles. However, it should be pointed out that despite being cured at the same temperature, the two inks depicted in Figure 1.3 are not the same and have unknown binder types, so it is unclear as to whether or not there is remaining binder affecting the electrical performance. Though there is some ambiguity associated with the behavior of the binder

material during the curing process, particles of greater size will have a greater contact area between one another as compared to smaller counterparts. Another factor controlling contact area could be related to the shape of the particles, for example flakes could lay upon one another better than spheroid particles. A bimodal distribution of particle size could also increase the contact area between the conductive particles as smaller particles could fill in voids which could exist between larger particles.

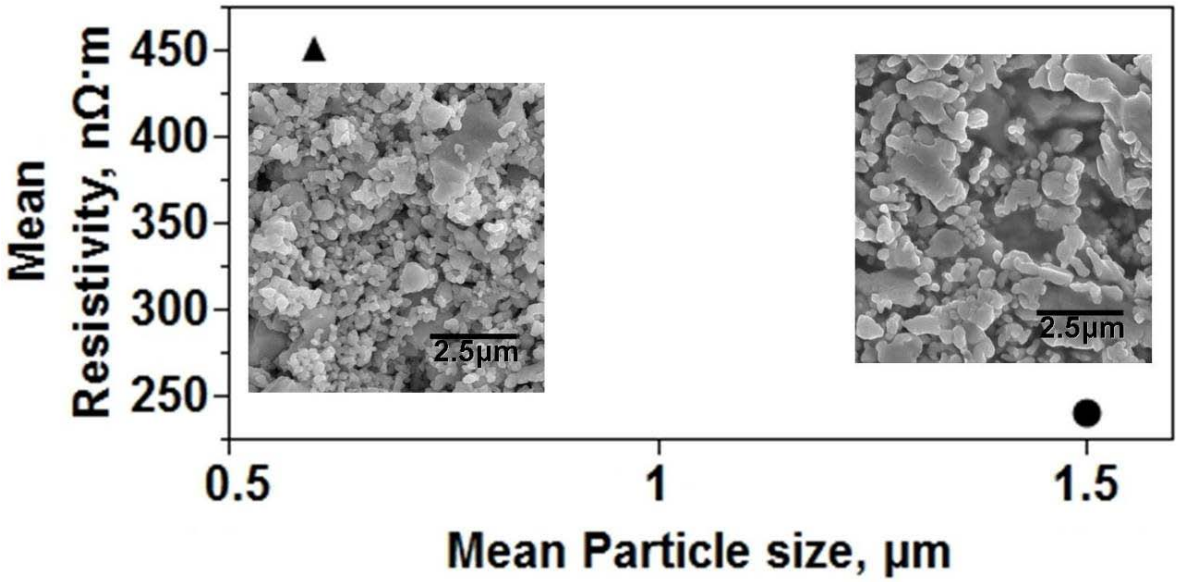

Figure 1.3: Relationship between the particle size and the resistivity of serpentine patterns printed with Ferro 3309F (triangle) and DuPont CB028 (circle) after curing at a temperature of 160°C for 1h. Extracted from data reported in [13].

Sintering

A necked microstructure resulting from the sintering of conductive particles comes about after the binder has been removed from the system. The key geometric feature in this microstructure is the neck which forms between the sintering particles. A schematic of the neck growth process is seen in Figure 1.4.

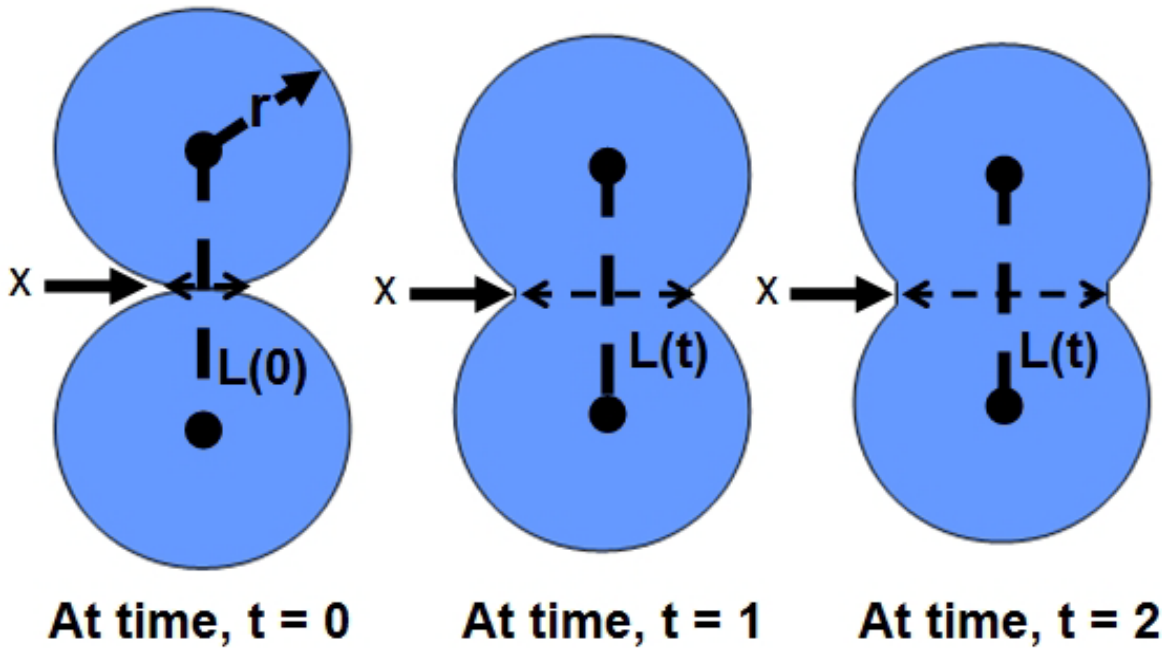

Figure 1.4: Representation of neck growth during sintering. As the neck grows, the neck diameter, x, increases, while the distance between the particle centers, L, decreases. Particles are of a radius, r. After [11,15].

A relationship between the neck geometry and resistivity has been mathematically expressed in [11] based on considering the neck growth is a function of time and results in a decrease in the distance, *L*, between the centers of two particles, resistivity is related to separation of the particles and the radius, *r*, of the particles at a given time by the following equation:

$$\rho(t) = \frac{2\rho_o}{\pi} \times \ln\left\{\frac{r + L(t)/2}{r - L(t)/2}\right\}. \tag{1.1}$$

Here ρ_o is the initial resistivity before necking occurs. The neck radius, *x*, comes into play by the relationship between the initial distance between particle centers and the distance between the particle centers at a specific time, which is expressed by the following equation [11]:

$$L(t) = L(0) \times \sqrt{1 - \left(\frac{x}{r}\right)^2}\ . \tag{1.2}$$

The transformation from sovereign particles to a networked necked structure is facilitated by diffusion mechanisms. The paths, over which diffusion will occur, are the surface, crystal

lattice, and the grain boundaries [11, 15]. The first diffusion mechanism to take effect is surface diffusion [11, 12] which is expected due to the fact the only interaction between non-sintered particles is through the contact area. The rate at which the neck will grow depends on the mechanism or mechanisms in play at the time [11, 15]. The different diffusion paths facilitating the transport of material during the sintering process are illustrated in Figure 1.5.

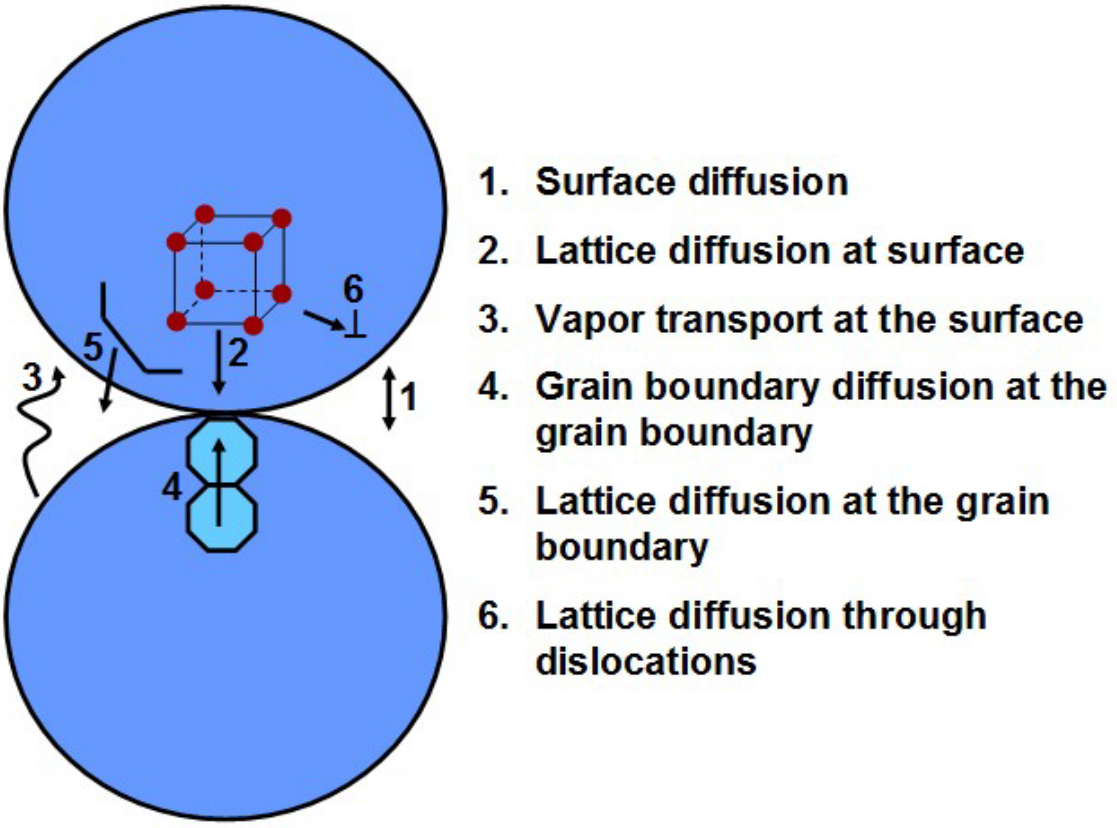

Figure 1.5: The different diffusion paths in play during the sintering process. Diagram after [11]; list of paths from [15].

The necking process will end when the limit to how large the neck radius can grow to is reached. This limit is defined by the following equation [15]:

$$x = \left(E_{Ad}/rG\right)^{1/3} r \tag{1.3}$$

where G is the shear modulus of the material the particles are composed of., E_{Ad} is the initial energy of adhesion between the two particles, which is related to the surface free energy of the particles F_s and the boundary free energy γ_{gb} at the point of contact between the particles by [15]:

$$E_{Ad} = 2F_s - \gamma_{gb}. \tag{1.4}$$

A graphical representation of Equation (1.4) is seen in Figure 1.6(a) for four conductors. As can be seen in the figure, aluminum has a nearly identical propensity to neck as silver. However, necking is not the dominant mechanism of conductivity as will be seen in the following explanation.

Assuming all particles are of the same size it is possible to predict the minimum resistivity which will occur once necking is completed. If Equation (1.3) is expressed in terms of *x/r* and consider that in this case, *x* is considered x_{max}, and we consider *L(0)* to be *2r* due to the geometry involved, Equation (1.2) can be rewritten in terms of the minimum distance between particle centers, L_{min}, as:

$$L_{\min} = 2r \times \sqrt{1 - \left(E_{Ad}/rG\right)^{2/3}} \tag{1.5}$$

Equation 1.1 can now be rewritten in terms of minimum resistivity, ρ_{min}, to describe the minimum resistivity attainable by necking:

$$\rho_{\min} = \frac{2\rho_o}{\pi} \times \ln\left\{\frac{r + L_{\min}/2}{r - L_{\min}/2}\right\} \tag{1.6}$$

The relationship presented in Equation (1.6) can be applied towards predicting the minimum resistivity achievable by sintering for nanoparticle based inks. A graphical representation of the model is seen in Figure 1.6(b) for four conducting metals with a maximum particle diameter of 100nm and a minimum particle diameter of 2nm. Note that for the four conductors modeled—aluminum, silver, copper and gold—silver is the metal which is capable of attaining the lowest resistivity. The low resistivity attributed to the sintering of silver nanoparticles is one reason for the popularity of silver as a loading material for conductive inks.

The second lowest resistivity attainable by the four conductors modeled is that of copper. Along with the lower price, the relatively low resistivity is a reason for the growing interest in the utilization of copper in the creation of nanoparticle loaded inks.

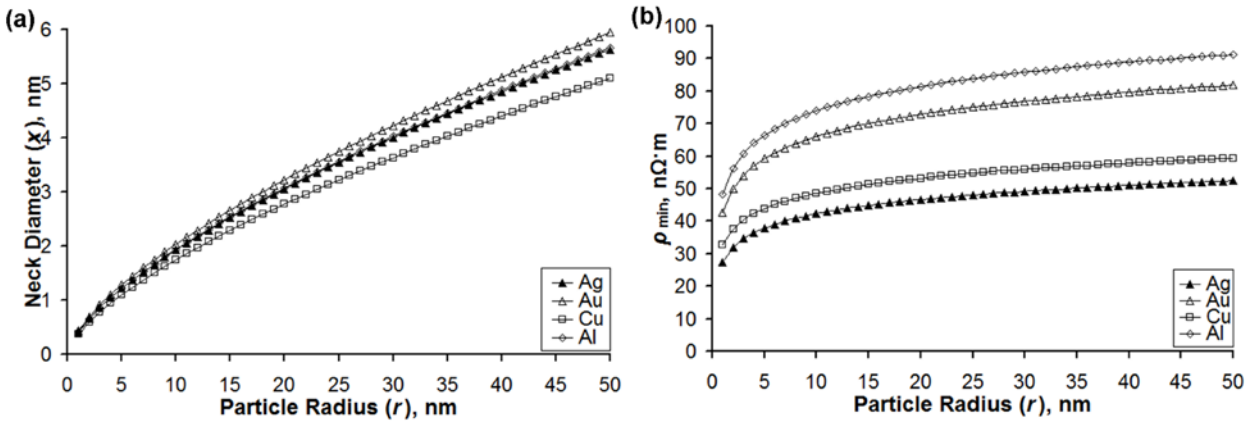

Figure 1.6: Graphical representation of the models derived in **(a)** Equation (1.4) and **(b)** Equation (1.6) for four conductors.

Grains

Given the necessary amount of thermal energy and time, the microstructure will eventually become that of a solid film consisting of grains and voids [12]. Though essentially a solid film, a printed line will not reach the resistivity of bulk silver due to the presence of voids. The voids exist because the resultant microstructure is caused by solid state diffusion and grain growth processes. The diffusion paths facilitating grain growth are the same as those facilitating necking [15].

A model exists relating the resistivity of a film consisting of grain size and voids. The key to this model is the understanding of the grain boundary acting as a barrier an electron must overcome during the passing of current through the film. Work involving silver films in a nanostructure form [16] led to the development of an equation relating resistivity, grain size, and porosity (density difference due to voids) which is expressed as [17]:

$$\rho = \rho_B \frac{\lambda_B}{\lambda} T^{*\left(\frac{\lambda}{d}\right)} \tag{1.7}$$

where d is the grain diameter, λ_B is the mean free path of the bulk material, λ is the mean free path in the material ρ_B is the resistivity of the bulk material and T^* is the electron transmission coefficient of the material. The above relationship takes into consideration the material density as there is a near-linear relationship between T^* and the density of "nanostructured" silver as was reported in [16].

A simpler model for describing the effect of grain size on the electrical conductivity of metals was described in the class notes for MASE 5344 (Interfacial Phenomena in Materials Systems, Fall 2010) and is the Hall-Petch like relationship between mean free path (MFP) and grain size:

$$\ell_C \cong \ell_O(1 - k/D) \tag{1.8}$$

Here, a larger grain diameter, D, corresponds to a larger mean free path, ℓ_C. The MFP of a metal is directly proportional to electrical conductivity, σ_C, as described by:

$$\sigma_C = \ell_C(n_C e^2 / m v_F) \tag{1.9}$$

where n_C, is the free electron density of the material, e, is the charge of the electron, m is the mass of an electron, and v_F, is the Fermi velocity of the electron. Figure 1.7 depicts the effect of grain size on MFP where essentially, the larger the grain size the better the electrical conductivity due to fewer grain boundaries being present which act as electron scattering points for the flow of electrons. As is seen in Figure 1.6 if the grain size were to be infinite the drift velocity of the electron, v_d, equals the Fermi velocity, v_F. The equation describing drift velocity is [18]:

$$v_d = \frac{e\tau}{m}E \tag{1.10}$$

where E is the applied electric field and τ is the mean time between collisions of electrons. The Fermi velocity of a material is related to MFP by τ by the following equation [19]:

$$\tau = \frac{\ell}{v_F} \tag{1.11}$$

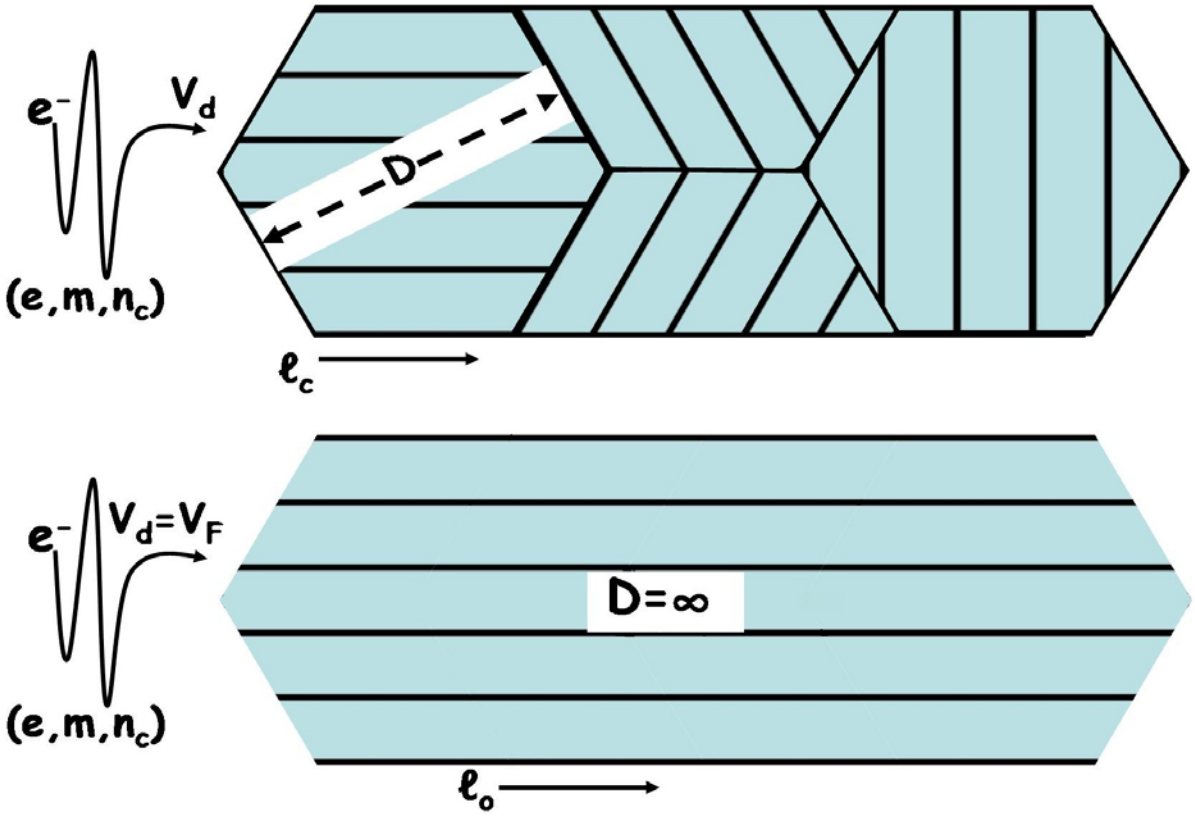

Figure 1.7: Illustration of the effect of grain size on mean free path. After class notes, MASE 5344 Interfacial Phenomena in Materials Systems, Fall 2010.

1.2.2 Examples of Microstructural Effect on Conductivity

The best way to illustrate the importance of microstructure is by the presentation of experimental results. Consider the microstructures seen in Figure 1.8 which are representative microstructures of printed conductive traces printed from a silver nanoparticle ink. The microstructural evolution of thermal curing was documented by thermally curing sample sets of printed lines at increasing temperatures. The microstructure of the of the printed lines cured at 100°C and 110°C are acting under the principle of percolation theory as the conduction is occurring through the particles touching each other. The difference in resistivity between 100°C and 110°C is a result of more binder being present within the lines cured at 100°C compared to those cured at 110°C. For the lines cured at 150°C, necking has begun which is pointed out by

the white arrows. Here the resistivity is describable by equations 1.1 and 1.6. A more densified microstructure is illustrated for the lines cured at 200°C and 250°C and thus the resistivity is lower than the beginning stages of necking.

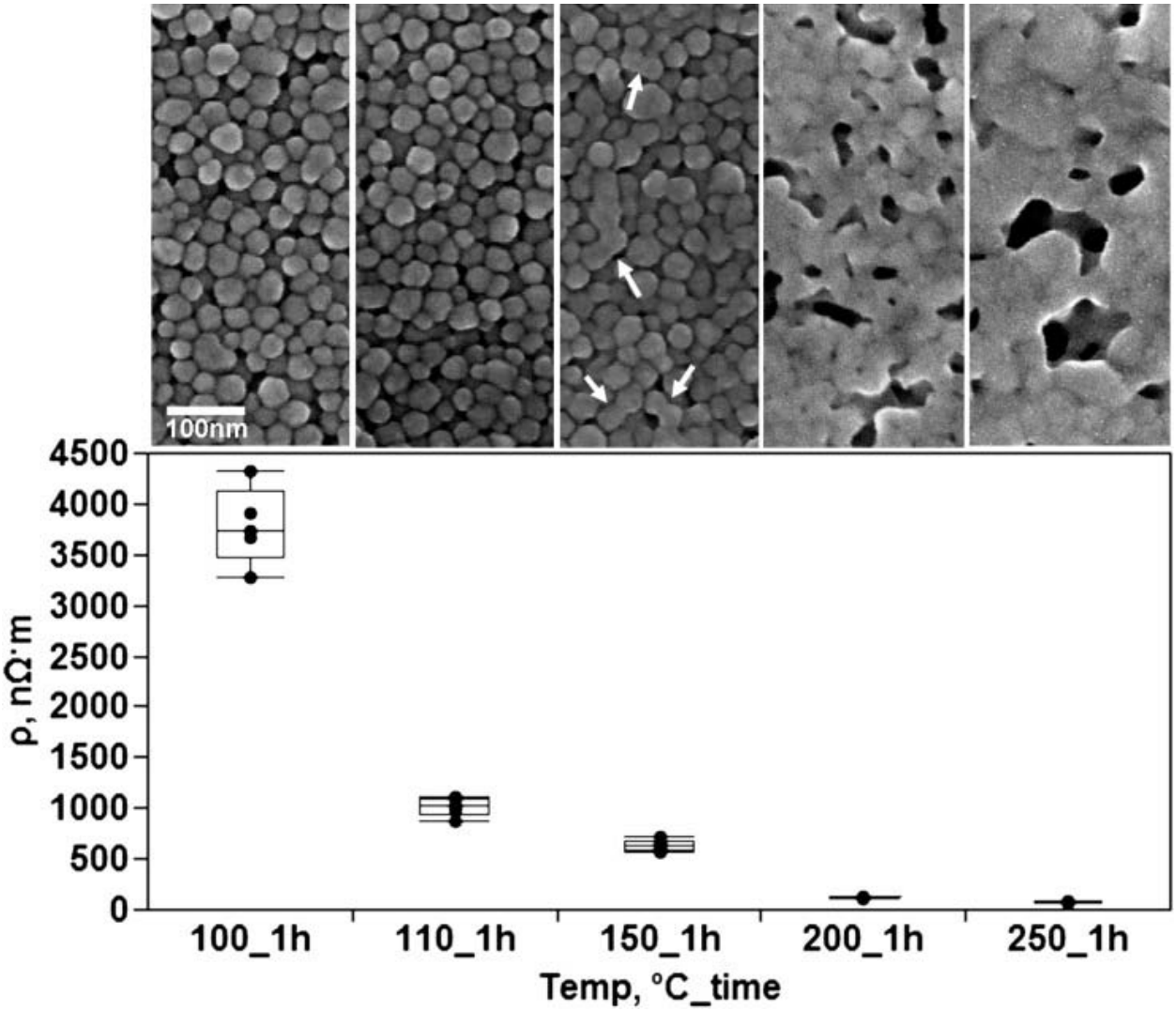

Figure 1.8: Microstructural evolution of silver nanoparticle ink cured at increasing temperatures along with the measured resistivity. Data from [13].

The relationship between microstructure and electrical performance is not limited to spherical particles or nanoparticle-based ink. Consider the inks illustrated in Figure 1.9. The graph illustrates the difference in resistivity while the overlaid micrographs demonstrate the clear

difference in microstructure. The lower resistivity sample set has a microstructure which is a film consisting of grains and pores while the other sample is of silver particles lying next to each other. Also notice the variability differences between the two microstructures.

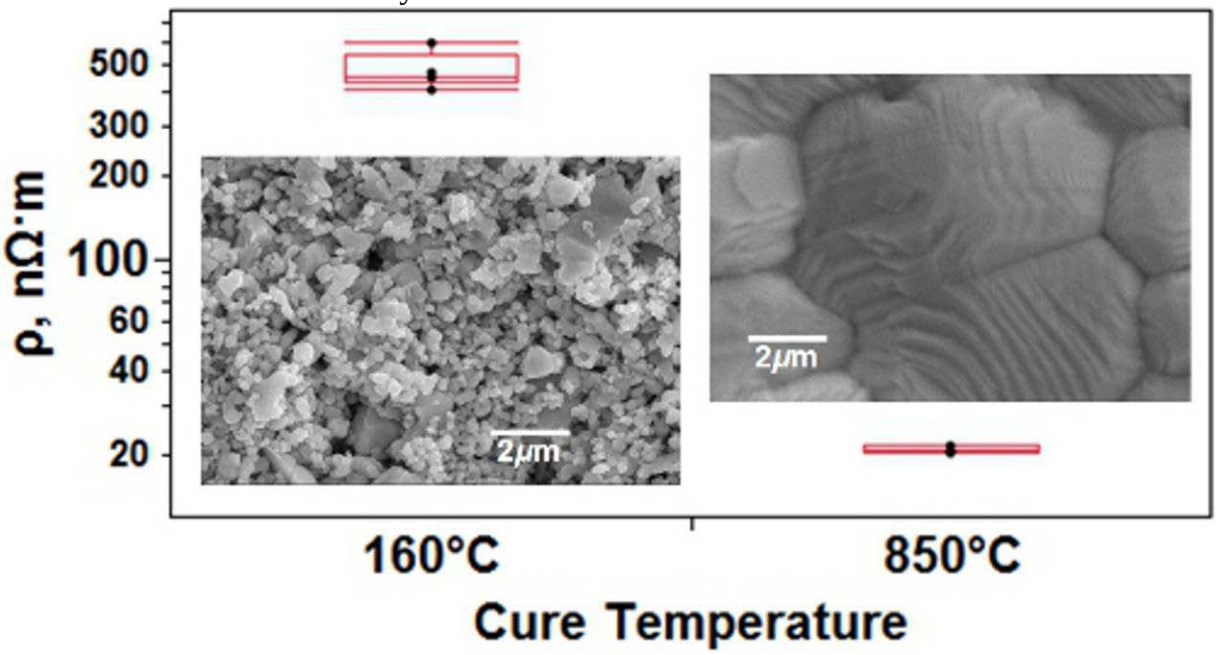

Figure 1.9: Illustration of the effect of microstructure on measured resistivity of conductive traces of Ferro 3309F sample set was subjected to a temperature of 850°C for 2 hours while the CB028 sample set was subjected to a temperature of 160°C for 1 hour. In both examples n=5. Data from [13].

The characteristics associated with ink deposition also play a role in the microstructural evolution which occurs in a thermal curing process. Roberson *et al*. [13] demonstrated a decrease in resistivity for inkjet-printed lines when the lines were printed multiple times. The expectation is that resistivity should remain constant for lines cured at a given temperature as the value of resistivity takes into account dimensional aspects of the conductive trace. As seen in Figure 1.10, increasing the number of layers printed (creating thicker lines by printing the same line multiple times on itself) led to sintered particles with more pronounced necking than the particles observed in lines printed only once. A more detailed characterization of the effect of the number of layers printed on the measured resistivity of the conductive trace can be found in Chapter 3.

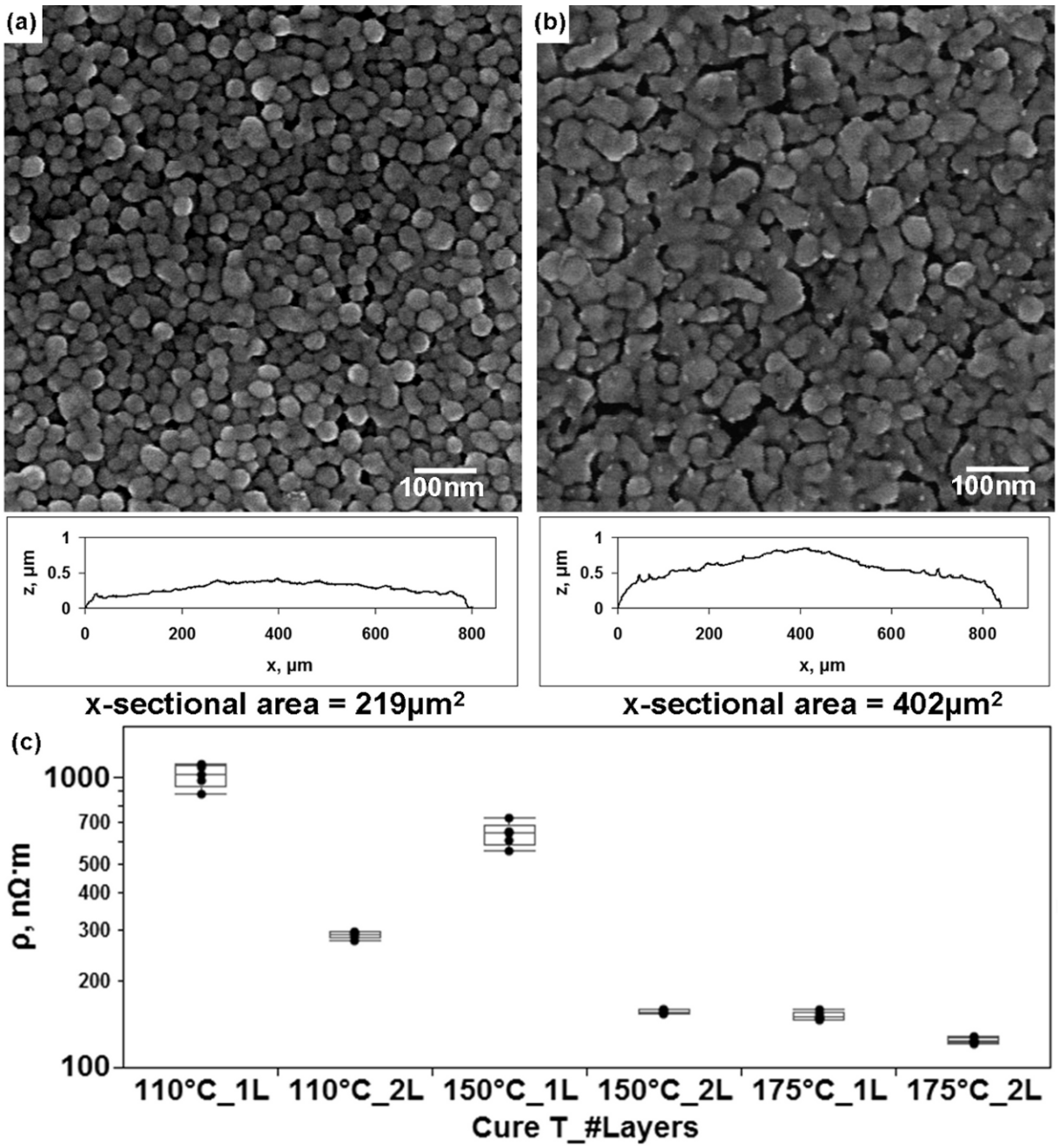

Figure 1.10: Comparison of the microstructures of printed lines of CCI-300 cured at 150°C for 1h between **(a)** 1 printed layer with the measured profile and cross sectional areas below and **(b)** two printed layers with the measured profile and cross sectional areas below. **(c)** Graphical results comparing the measured resistivity of lines printed in one and two layers and thermally processed at given temperatures for 1h. Sample size n=5 for all sets.

The entire curing process is represented in Figure 1.11 starting from particles separated by binder, then transitioning to particles conducting through percolation, then sintering, and,

finally ending with a thin film consisting of grains and voids. As illustrated above, when dealing with conductive inks, the microstructure resulting from different curing regimens arises from complex physical interactions due to the application of thermal energy. Consideration of the microstructure present after specific curing regimens must be made if conductive ink is to be used properly and to its full potential. The goal of any curing process is to achieve a microstructure which is most conducive to conductivity. Pertinent to the work presented in this dissertation, achieving a microstructure analogous to that attained by thermal curing at a high temperature—200°C and above—without actually subjecting the bulk substrate to these temperatures is the goal of this work.

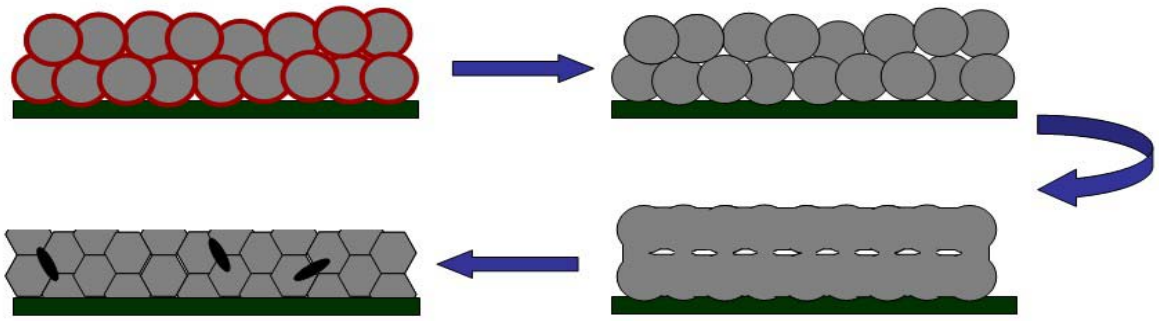

Figure 1.11: Depiction of the microstructural changes which can occur during thermally processing conductive ink. After [12].

1.3 Printing Methodologies

The work conducted in this dissertation deals primarily with two specific printing techniques; direct print micro dispense, and inkjet printing. Both techniques are non-contact printing techniques where the printable material is the only item to contact the substrate. Inkjet printing was carried out with a Dimatix 2800-Series Materials Printer (Fujifilm Dimatix, Inc, Santa Clara, CA, USA) which is shown in Figure 1.12. Direct print micro dispensing was performed with an nScrypt 3D 450 system (nScrypt, Inc., Orlando, Florida, USA) and example of which is seen in Figure 1.13.

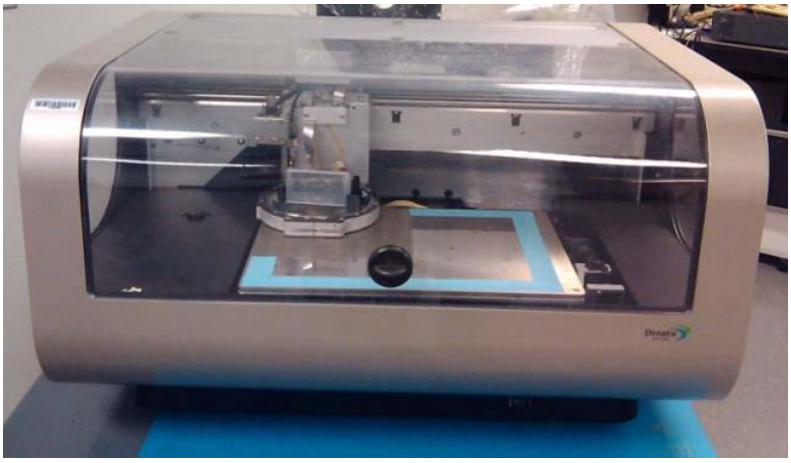

Figure 1.12: The Fujifilm Dimatix 2800-Series Materials Printer used in this study.

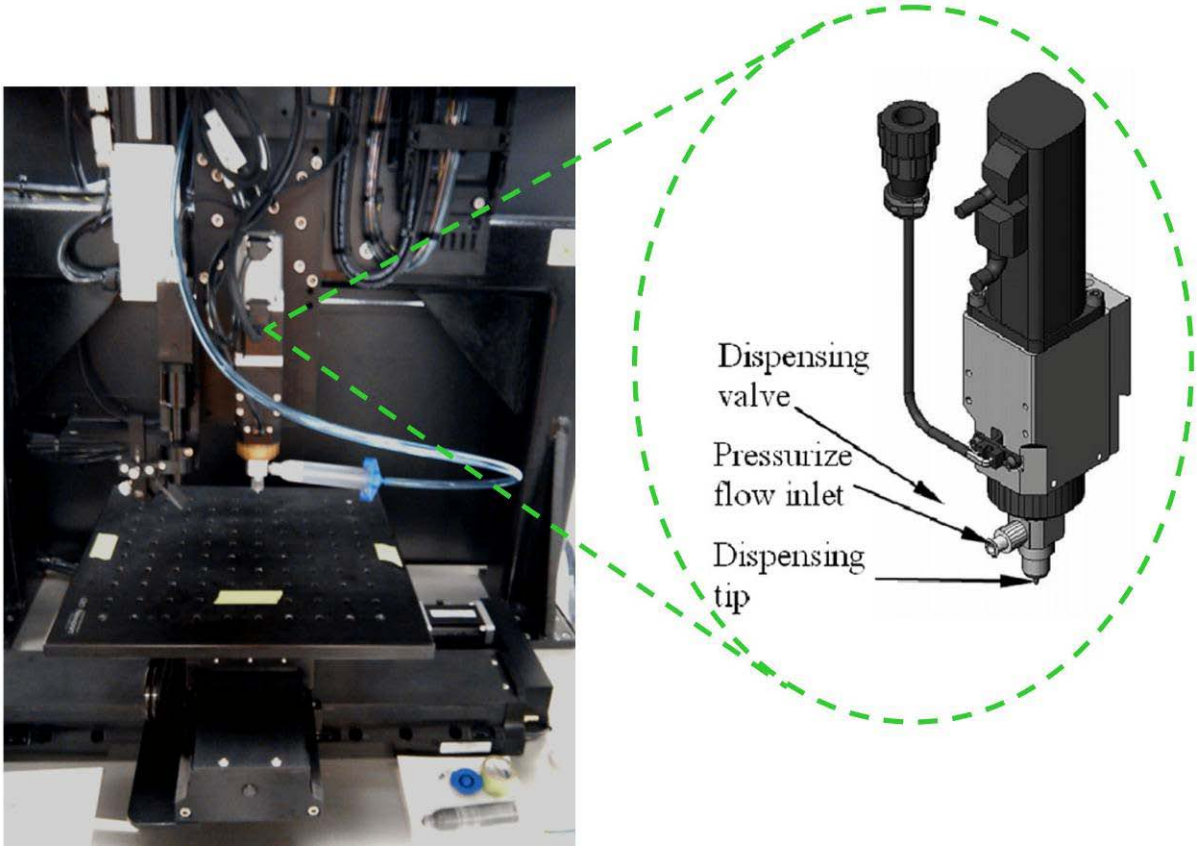

Figure 1.13: The nScrypt Direct Write Microdispense system with inset describing components of the SmartPump™ system. Inset from [22].

Inkjet printing is limited to nanoparticle based inks such as the silver loaded Cabot CCI-300 (Cabot Corporation, Albuquerque, NM, USA), due to the orifice size of the nozzle, which in the case of the cartridge used in this study, (DMC-11610) is 21μm [20]. Inkjet printing systems fall into two categories—drop on demand (DOD) and continuous—defined by the way the ink exits the nozzle [21]. In DOD systems ink droplets are ejected from the nozzle by either a piezoelectric actuator [12, 21] or a thermally controlled system which relies of the vaporization of a small amount of ink to drive a droplet from the nozzle [21]. In a continuous inkjet system, a piezoelectric driven actuator drives a stream of ink from a nozzle which is then subjected to an electric field which causes droplets to form [21]. The Dimatix 2800-Series Materials Printer used in this work is a DOD inkjet system.

The nScrypt direct print system falls into the category of a filament-based direct write system [21] where media is extruded through either a pen-like or syringe tip. Though the printable material is not sprayed from the orifice as is the case with the inkjet technique, the tip does not touch the substrate. Rather, a filament of material is created between the opening of the dispensing tip and the substrate. The nScrypt system has the ability to print a wide range of viscosities; 1 to 1,000,000 cP (.001 to 1,000 Pa·s) [21-23] compared to viscosities of 0.04 and lower for inkjet printing [21]. The minimum advertised printable feature size for nScrypt is 50μm [23] while the minimum theoretical feature size limit for inkjet is 1μm [13, 24, 25].

Gravure printing is another method used in the creation of printed microelectronics and has been demonstrated as a technique for printing RF antennas and polymer field-effect transistors [26, 27]. A schematic of this printing technique is seen in Figure 1.13. Gravure printing is an ancient printing technique in which an engraved drum is coated with a printing media. As seen in Figure 1.14, the drum is then rolled onto the substrate and the image of the drum is transferred to the substrate. The feature size is seemingly dictated by capability of the drum making process and feature sizes as small as 100μm have been reported [26].

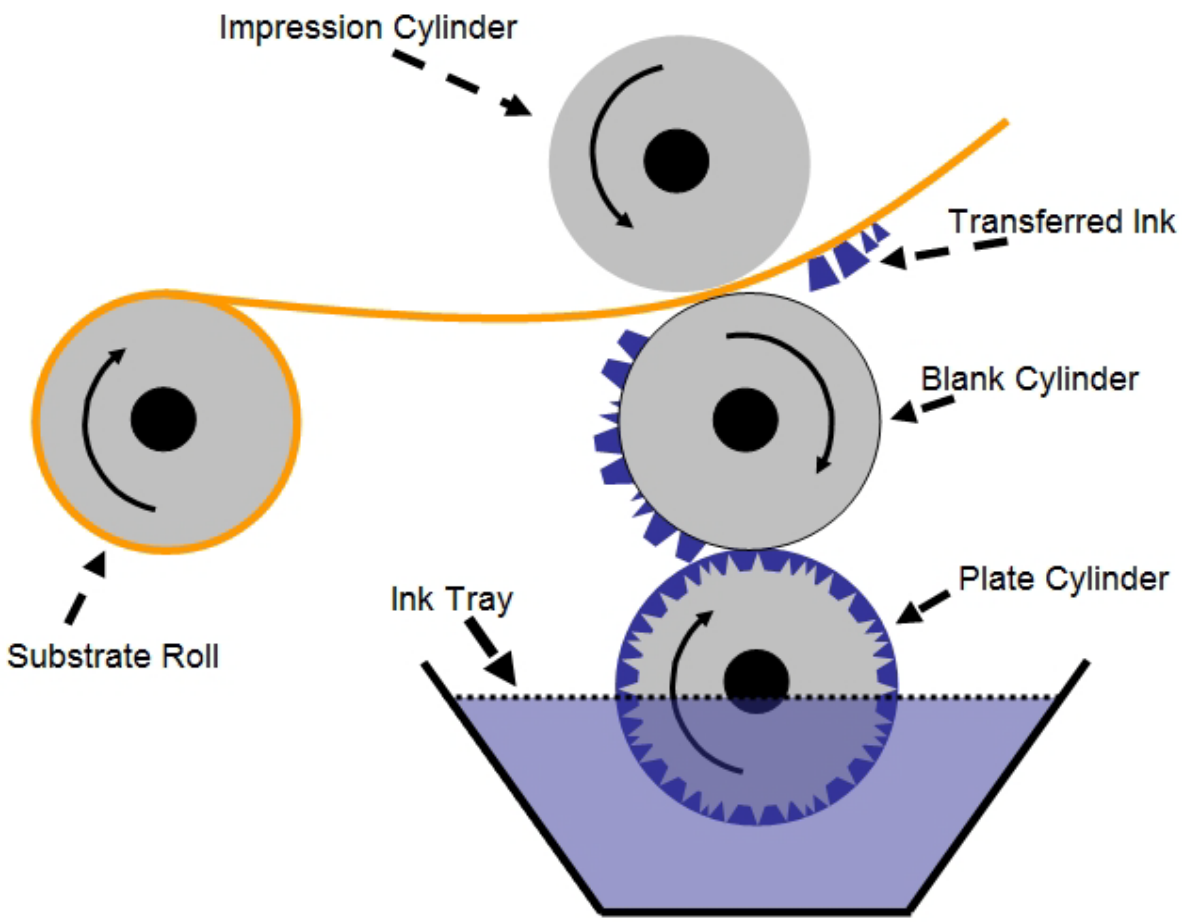

Figure 1.14: Schematic of the Gravure printing process. After [28].

Nanoscale feature size has been achieved by coating an atomic force microscope (AFM) tip with ink by dipping the tip into ink. Dip Pen Nanolithography is (DPN) the term used to describe this printing technique [21, 25] and a commercial system (NSCRIPTOR™) has been developed by NanoInk (NanoInk, Skokie, IL) where lines as small as 760nm in width have been demonstrated [25]. A schematic of the DPN process is seen in Figure 1.15. DPN demonstrates the capability of direct write technology to print submicron features and is important to the promotion of the growth of non-lithographic production of conductive traces.

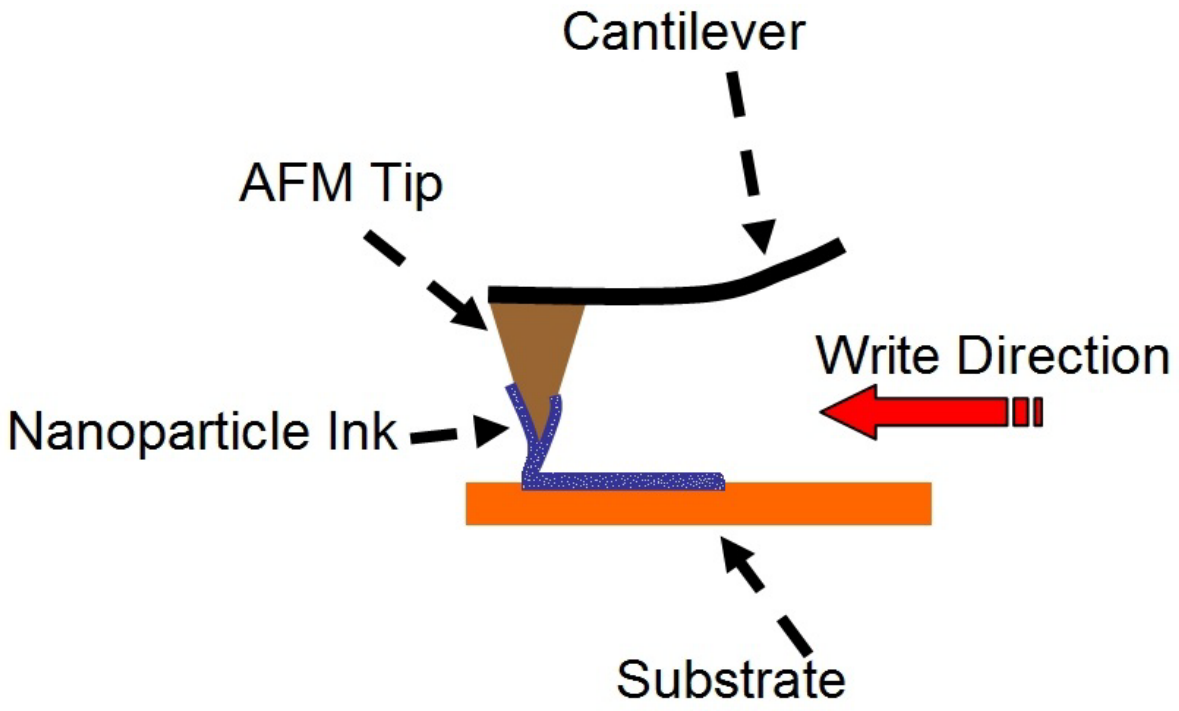

Figure 1.15: Schematic of the DPN technique. Here a conductive trace is created after an AFM tip was coated with a silver-loaded nanoparticle ink. After [25].

1.4 Examples of Non-thermal Curing Techniques

The need for an alternative to thermally curing conductive ink has not gone unnoticed by researchers. Novel techniques have been demonstrated to create a desirable microstructure without the use of thermal processing. These techniques, namely the use of microwaves and lasers, are a demonstration of the use energy sources other than thermal to cure a printed conductive ink trace.

1.4.1 Laser Curing

Characterization of laser curing of nanoparticle silver ink at different wavelengths reported by Maekawa *et al.* [29] demonstrated a sintered microstructure for each of the four wavelengths tested (1064nm, 980nm, 532nm, 488nm). The larger wavelengths produced a less porous structure, however the smaller wavelengths produced conductive traces with better

adhesion to the substrate. The smaller wavelength samples also produced adhesion greater to those which were thermally cured. Increasing the laser power was found to have the effect of creating conductive traces with lower resistivity. The thermally cured samples had lower electrical resistivity, however this was attributed to the time difference between curing methods—around 2 seconds for the laser curing and an hour for the thermal curing.

In another study comparing laser curing to a standard thermal process reported by Kim *et al.* [30] characterized the effects of curing a nanoparticle silver ink with a single wavelength (532nm) and was able to produce conductive of a sintered structure. This study also found a decrease in resistivity with an increase in laser power, but also characterized the effect of time and found a decrease in resistivity with an increase in curing time. Though the resistivity was found to not be as low as thermally cured comparisons, the maximum laser curing time was 60 seconds compared to the thermal cure time of 30 minutes.

Lopes [31] has shown the number of laser passes (times the laser traces the printed line) to have an effect on the resultant resistance. Experiments were the laser was directed 1.) directly on the ink trace, 2.) on the edge of the printed trace, and 3.) on the substrate all demonstrated a drop in measured resistance with and increase in laser passes. The maximum amount of laser passes explored in this experiment was twelve.

The method of laser curing mentioned above presents two key points to consider when searching for an alternative to thermal curing. One, the time involved to cure the conductive trace was almost instantaneous compared to the hour necessary to thermally cure the ink tested. Two, the testing of the physical properties of the conductive trace—in this case adhesion, and electrical properties—compared to the benchmark thermal processing is paramount in the determination of the viability of the alternative curing process in question. Moreover the laser curing method has the advantage over thermal curing in that the curing process is localized to the conductive trace minimally affecting the substrate.

1.4.2 Microwave Sintering

Microwaves have also been utilized as an alternative to thermal energy in the processing of conductive ink. The creation of a sintered microstructure via the application of microwaves to ink-jet printed traces of nanoparticle-based silver ink has been demonstrated by Perelaer *et al*. [32] where the ability to create a conducting microstructure by exposing printed lines to microwave radiation for 4 minutes was demonstrated. Microwave processing is an attractive alternative to thermal processing of conductive traces printed on polymeric substrate due to the fact the polymeric substrates will not absorb enough energy to be harmed and also due to the fact he curing time is relatively short. Another study conducted by Perelaer *et al.* [33] found that printing antenna shaped conductive traces and subjecting these traces to a short thermal cure to dry the ink increased the conductivity of the printed traces, which may be looked upon as a drawback to utilizing a microwave-based process.

The two alternative methods to thermally curing conductive ink presented above demonstrate a key paradigm to keep in mind: the localization of the application of energy needed to cure or process conductive ink. Laser curing is localized because a beam is focused on the printed line. Microwave sintering is localized because more microwave energy is absorbed by the metallic line than the polymeric substrate, though the substrate is also subjected to the microwave energy.

Another way to consider the processes conductive ink can be classified into categories by considering how they work and how they are applied. The categories are: *globally extrinsic*, *locally extrinsic*, and *globally intrinsic*. As seen in Table 1.1, thermal processing of conductive ink is classified as *globally extrinsic* because both the ink and the substrate are subject to the external element causing the ink to cure. Laser curing falls into the *locally extrinsic* category because only the ink is affected by a focused laser beam imposing energy onto the printed line. Microwave sintering is *globally intrinsic* because the printed line and substrate are subjected to the microwave radiation, but the effect of this microwave radiation is determined by absorption of energy which is an inherent material property.

Table 1.1: Categorization of described methods of curing particle-based conductive ink.

Globally Extrinsic	*Locally Extrinsic*	*Globally Intrinsic*	*Locally Intrinsic*
Thermal External heat energy applied to both substrate and printed line	**Laser Cure** Localized photonic energy applied directly to printed line	**Microwave** Microwave energy applied to both substrate and printed line, but intrinsic material properties determine effect	**Ohmic** Electric current applied directly to printed line, intrinsic property of resistance determines effect

Admittedly, there are some grey areas to this classification, namely the fact that nanoparticle ink will sinter at a lower temperature than a flake-based counterpart due to the scaling effect of heat transfer [11, 12, 32]. Also, it has been found that nanoparticle-based ink absorbs the most photonic energy at around 412–420nm [29, 33]—which could potentially be one reason Maekawa *et al.* [29] achieved the best results curing conductive lines at the smallest wavelength tested, 488nm. The fact is all curing methods succeed or fail due to some intrinsic material property of either the ink or substrate, but for the sake of categorization, the curing methods have been separated as explained above.

1.5 The Proposed Curing Method

The proposed curing method is the utilization of ohmic heating to cure or enhance the conductivity of a printed trace. A full characterization of ohmic curing is discussed in great detail in Chapter 4, falls into a fourth category, *locally intrinsic*. The ohmic curing method relies on a physical property of the ink as the key enabler for the curing process, namely the resistance of the printed line. This is a simple method which has the advantages over the state of the art of curing methods in that it is relatively fast, localized, and does not require complex equipment. Moreover the opportunity exists for easy integration into existing printing equipment.

Ohmic heating (also referred to as resistance heating) is a concept utilized practically every day in daily activities. The hot plate on a coffee maker utilizes resistance heating to keep the carafe warm. An electric heater utilizes resistance heating to generate heat to keep us warm

in the winter. An electric clothes dryer utilizes resistance heating to dry our clothes. A hair dryer utilizes resistance heating to dry our hair. The list is seemingly endless.

As illustrated in Section 1.2, the microstructures within printed conductive traces play a key role in the measured resistance. Any electronic circuit will transfer heat when active as originally described by Joule in the following equation [34]:

$$Q = I^2 Rt \tag{1.12}$$

where Q is the heat transferred in joules I, is the current applied to the electric circuit, R is the resistance, of an electric circuit and t is the time the circuit is active. As current is applied to the conductive ink printed line, the heat transferred by ohmic heating mechanisms will cause binder material to bake off. If enough heat is transferred, the microstructural changes described in Section 1.2 may occur.

The property of resistance of the printed line is the most important factor to consider when evaluating a curing process. In most cases, the printed conductive line acts as an interconnect between devices. Assuming the use of an ink with conductive particles in a binder, the total resistance is given as [35]:

$$R_{total} = R_{btw\ particles} + R_{btw\ particles\ and\ device} + R_{particles} \tag{1.13}$$

In the case of utilizing electrical resistance to initiate a curing process in the scenario above, the resistance which plays the greatest role is potentially the resistance between the particles. The resistance of the particles themselves will not change nor should the resistance of the connection between the device and the printed line. As illustrated in Section 1.2, the resistance between particles is controlled by contact area either controlled by the amount of binder or the geometry of a neck during sintering.

Considering the categorization above, an important parameter is the initial resistance of the printed line which is an intrinsic property. The application of current to the printed trace is a localized process. This is this is an attractive alternative to thermally curing conductive ink

when utilizing polymeric substrates as the bulk substrate is not subjected to the localized heat transferred by the resistance heating mechanisms. This is also a process extremely applicable to the creation of 3D microelectronics due to need to cure conductive traces in three dimensions as illustrated in Figure 1.16.

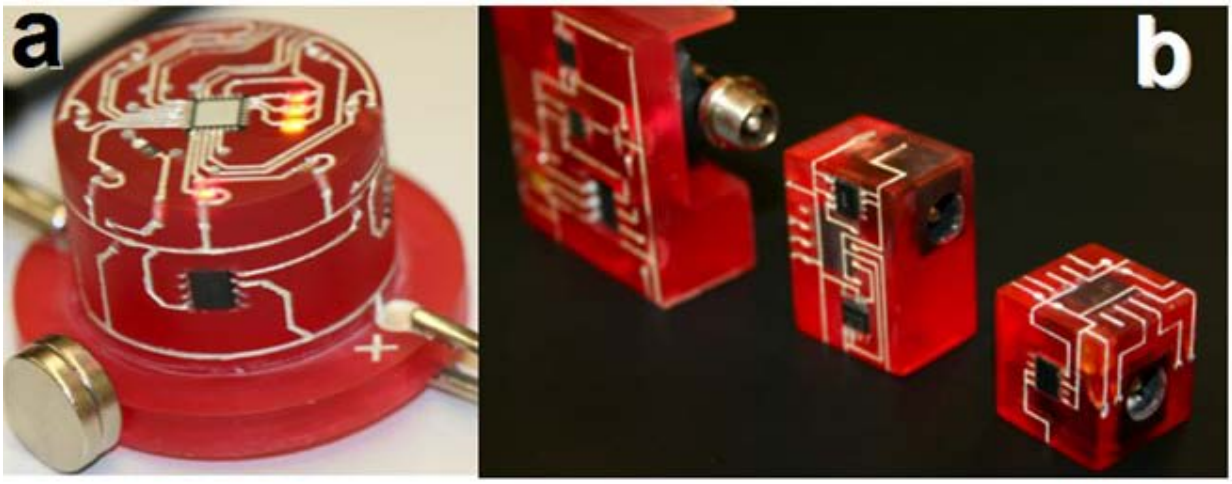

Figure 1.16: Examples of structural 3D microelectronics, **(a)** multi-axis magnetometer and **(b)** examples of the shrinking in form factor arising from the generational process evolution of a magnetometer. These devices contain conductive lines printed from conductive ink which could all have been cured via resistance-based curing. Part **(b)** from [36].

1.6 The Creation of 3D Structural Electronics

The components seen in Figure 1.16 are prime examples of the capability of combining the two technologies of direct printing and additive manufacturing (AM). AM is also sometimes referred to as a rapid prototyping (RP) technique as well as three dimensional printing (3DP). Lopes [31] demonstrated AM/DP system integration between a nScrypt direct write microdispense component and a 3D Systems (3D Systems Inc., Rock Hill, SC) SLA-250/50 stereolithography (SL) machine capable of creating 3D structural electronics similar to those seen in Figure 1.16. Examples of structural electronics created from the use of SL/DP technology integration are a GPS-enabled wireless motion sensor as reported by Navarette *et al.*, [37] and a LM555 temperature sensor as demonstrated by Lopes *et al.* [38].

The AM method of SL starts by the conversion of CAD data into a “slice” file. The file is then used to create a solid form by building up material layer by layer. The layering process

occurs by the curing (polymerizing) of individual layers of a photocurable resin upon one another with a UV laser until a 3D object is created. [39-42] As seen in Figure 1.17, a platform lowers after each layer is cured allowing for more material to be cured by the UV laser.

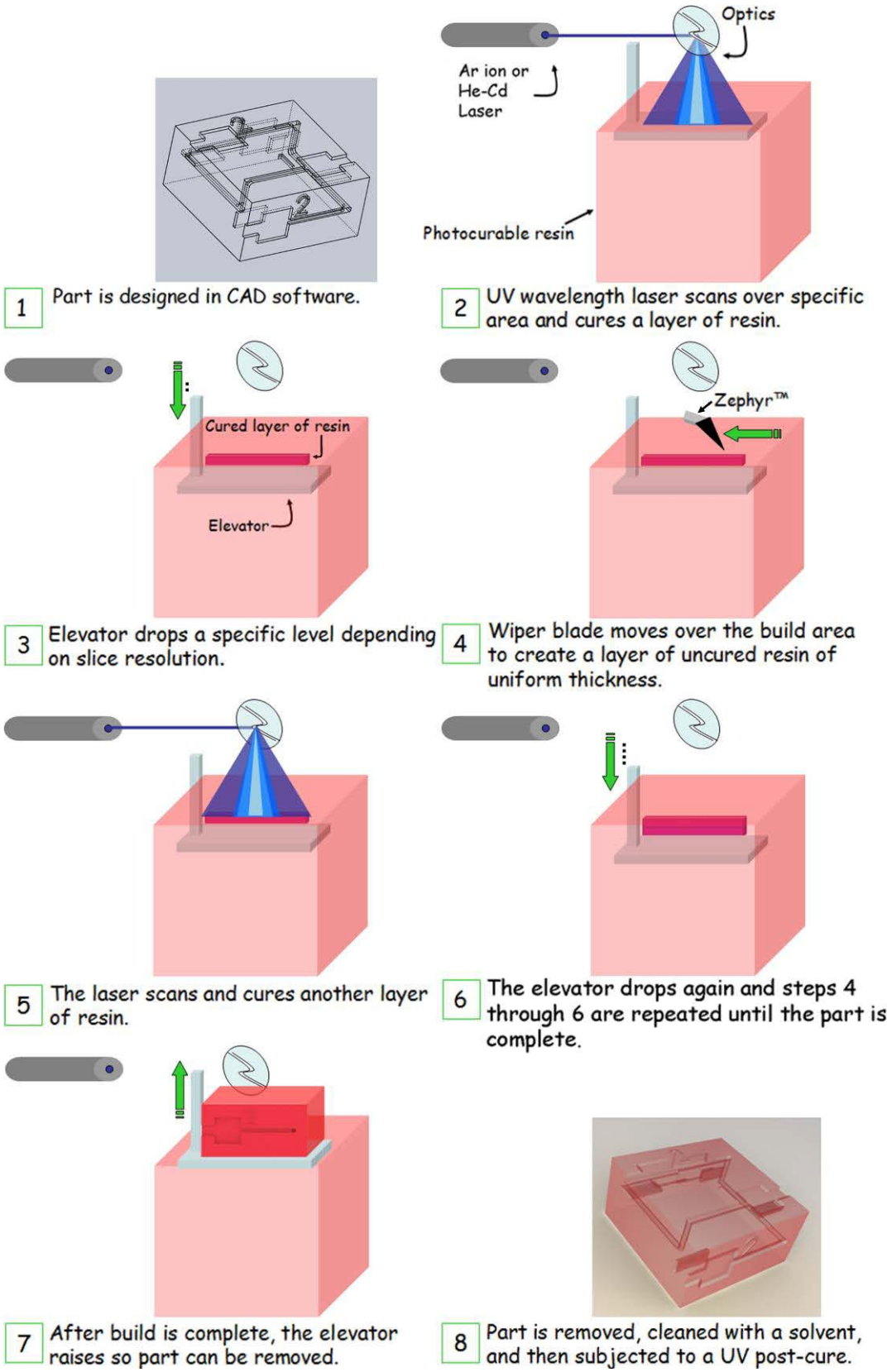

Figure 1.17: Simplified depiction of the SL process. Adapted from [39-42].

The use of AM techniques such as SL to create 3D substrates essentially turns the circuit board of a microelectronic gadget into the gadget itself and turns the concept of form factor into an element limited only by ones imagination and capability of using a CAD software such as SolidWorks® (Dassault Systemès SolidWorks Corp., Concord, MA). Also pertinent to microelectronics manufacturing, the use of AM techniques can also be used to enhance the metallization process when DP techniques are used. As was illustrated in Figure 1.1, DP has the ability to create conductive paths in fewer, more efficient steps that a typical metallization process. Another metallization process is the damascene process—depicted in Figure 1.18—where the substrate is altered to guide the metallization process. When AM techniques are used to create the substrate, a damascene-like structure can be built in which aids the metallization. Moreover, a dual-damascene structure consisting of vias and interconnects can be created within an AM-built component as seen in Figure 1.19. Even more profound is that the via/interconnect system can be created in three dimensions.

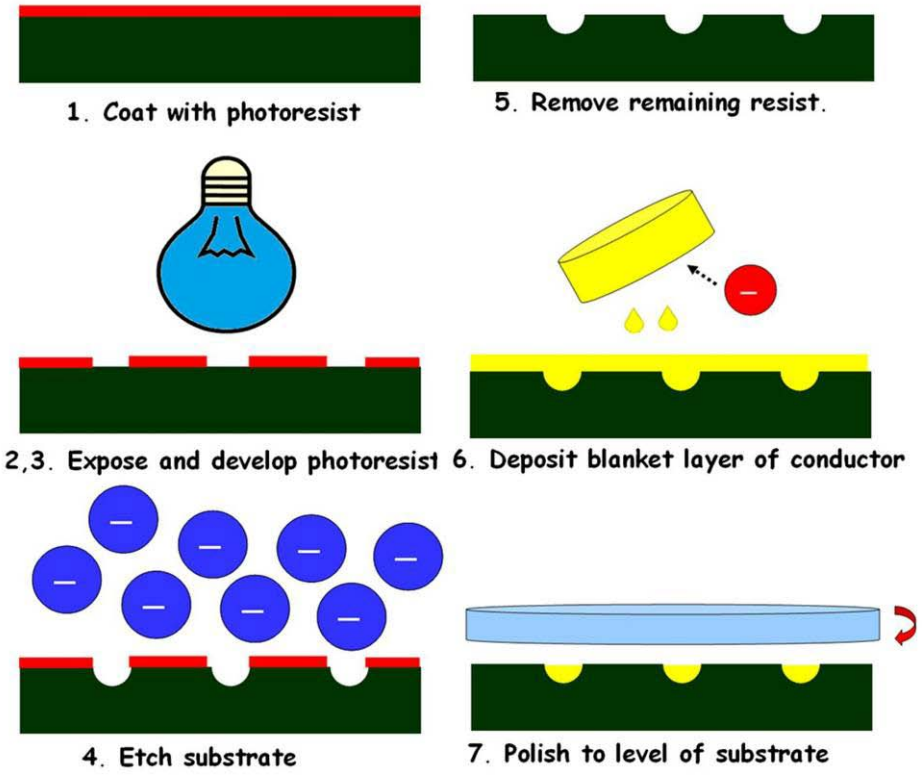

Figure 1.18: A simple depiction of the damascene process of metallization. Integration of AM and DP techniques offers a simpler method to achieve a similar end result.

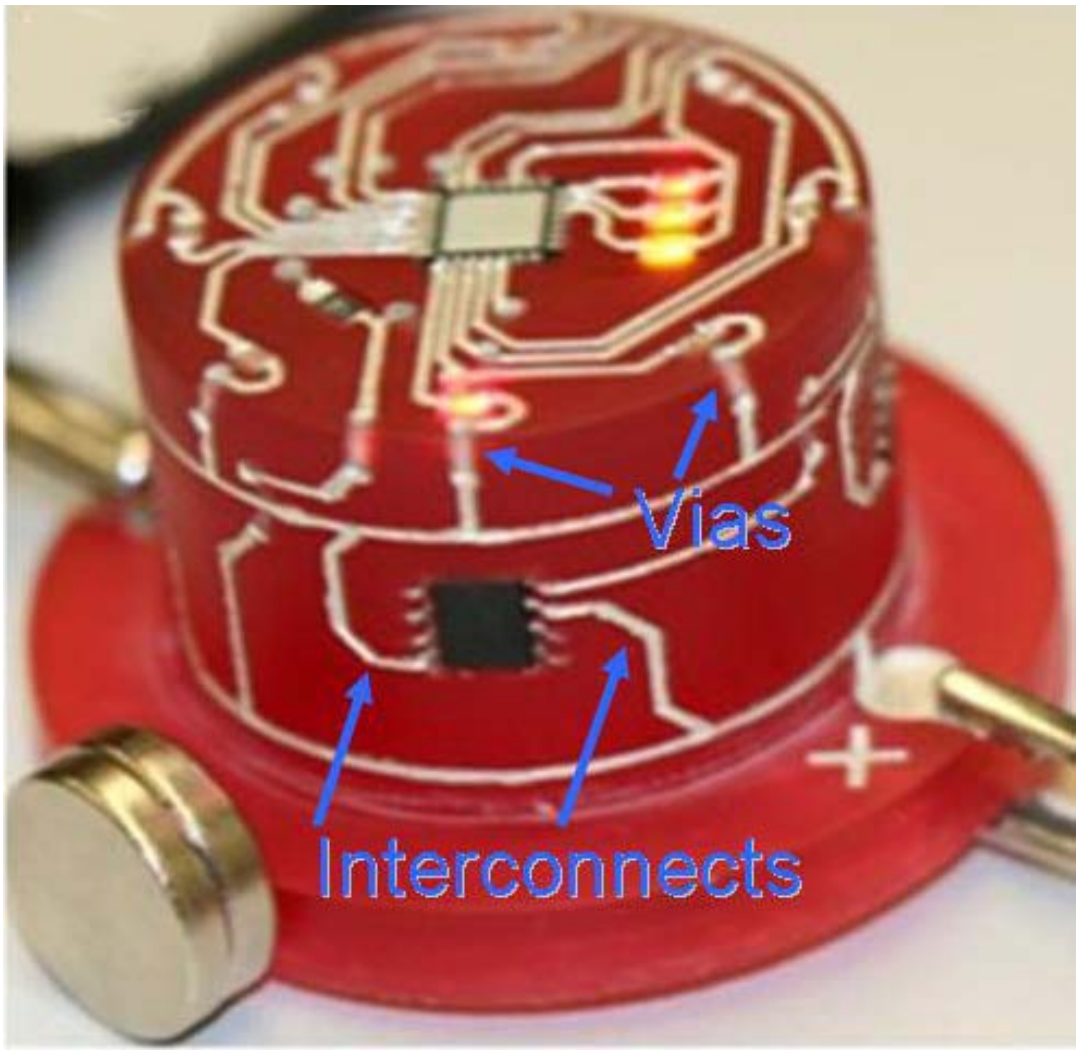

Figure 1.19: Example of a 3D dual-damascene metallization which is made possible by the combination of AM and DP techniques.

As compared to other AM techniques, SL produces components with a smoother surface finish [40]. The layer-by-layer build nature of SL is a key enabler for the creation of 3D electronics as it makes possible the stopping of the build process to insert electrical components and interconnects, and then continue the build process until the component is complete [31, 38].

Though the building of electrical components is not explored in this dissertation, the application of curing techniques was explored for interconnects created in 3D substrates. The

equipment used to create the substrates was a 3D Systems Viper™ SLA®. The SL machine used to create 3D substrates is seen in Figure 1.20.

Figure 1.20: The 3D Systems Viper™ SLA® system used to create 3D substrates tested in this study.

1.7 References

[1] J. Hu, "Overview of flexible electronics from ITRI's viewpoint," in *2010 28th VLSI Test Symposium (VTS)*, Santa Cruz, CA, USA, 2010, pp. 84-84.

[2] M. F. A. M. van Hest *et al.*, "Direct-write contacts: Metallization and contact formation," in *33rd IEEE Photovoltaic Specialists Conference, 2008. PVSC '08*, 2008, pp. 1-3.

[3] J.-W. Kim *et al.*, "Characterization of direct patterned Ag circuits for RF application," *Microelectronic Engineering*, vol. 87, no. 3, pp. 379-382, Mar. 2010.

[4] R. O. Kadara, N. Jenkinson, B. Li, K. H. Church, and C. E. Banks, "Manufacturing electrochemical platforms: Direct-write dispensing versus screen printing," *Electrochemistry Communications*, vol. 10, no. 10, pp. 1517-1519, Oct. 2008.
[5] D. Tobjörk, N. J. Kaihovirta, T. Mäkelä, F. S. Pettersson, and R. Österbacka, "All-printed low-voltage organic transistors," *Organic Electronics*, vol. 9, no. 6, pp. 931-935, Dec. 2008.
[6] *Cabot Conductive Ink CCI-300 Data Sheet*, Cabot Printed Electronic Materials, Albuquerque, NM, 2009, p. 2.
[7] *DuPont CB100 Conductive Via Plug Paste Technical Data Sheet*, Du Pont, Wilmington, DE, 2009, p. 2.
[8] *DuPont CB028 Silver Conductor Technical Data Sheet*, Du Pont, Wilmington, DE, 2009, p. 1.
[9] S. Merilampi, T. Laine-Ma, and P. Ruuskänen, "The characterization of electrically conductive silver ink patterns on flexible substrates," *Microelectronics Reliability*, vol. 49, no. 7, pp. 782-790, Jul. 2009.
[10] R. D. Mancosu, J. A. Q. Quintero, and R. E. S. Azevedo, "Sintering, in different temperatures, of traces of silver printed in flexible surfaces," in *Thermal, Mechanical & Multi-Physics Simulation, and Experiments in Microelectronics and Microsystems (EuroSimE), 2010 11th International Conference on*, 2010, pp. 1-5.
[11] J. R. Greer and R. A. Street, "Thermal cure effects on electrical performance of nanoparticle silver inks," *Acta Materialia*, vol. 55, no. 18, pp. 6345-6349, Oct. 2007.
[12] D. Kim and J. Moon, "Highly Conductive Ink Jet Printed Films of Nanosilver Particles for Printable Electronics," *Electrochemical and Solid-State Letters*, vol. 8, no. 11, p. J30-J33, Nov. 2005.
[13] D. A. Roberson, R. B. Wicker, L. E. Murr, K. Church, and E. MacDonald, "Microstructural and Process Characterization of Conductive Traces Printed from Ag Particulate Inks," *Materials*, vol. 4, no. 6, pp. 963-979, May. 2011.
[14] R. F. Saraf, J. M. Roldan, R. Jagannathan, C. Sambucetti, J. Marino, and C. Jahnes, "Polymer/metal composite for interconnection technology," in *Electronic Components and Technology Conference, 1995. Proceedings., 45th*, 1995, pp. 1051-1053.
[15] L.E. Murr, "Properties of Interfaces," in *Interfacial Phenomena in Metals and Alloys*, Massachusetts: Addison-Wesley, 1975, pp. 297-299.
[16] X. Y. Qin, W. Zhang, L. D. Zhang, L. D. Jiang, X. J. Liu, and D. Jin, "Low-temperature resistance and its temperature dependence in nanostructured silver," *Physical Review B*, vol. 56, no. 16, p. 10596, Oct. 1997.
[17] C. Huang, M. F. Becker, J. W. Keto, and D. Kovar, "Annealing of nanostructured silver films produced by supersonic deposition of nanoparticles," *Journal of Applied Physics*, vol. 102, no. 5, p. 054308:1-054308:8, 2007.
[18] S. O. Kasap, "Electrical and Thermal Conduction in Solids," in *Principles of Electrical Engineering Materials and Devices*, New York, NY: Irwin McGraw Hill, 1997, p. 103.
[19] A. Beiser, "The Solid State," in *Concepts of Modern Physics*, 5th ed, New York: McGraw Hill, 1995, p. 347
[20] *Materials Printer, Cartridges & Printheads DMP-3000, DMC-11601/11610, SX3, SE3, SE-DPN, D-128/1 DPN and D-128/10 DPN Data Sheet*, Fujifilm Dimatix, Inc., Santa Clara, CA, 2008, p. 2.
[21] Y. Zhang, C. Liu, and D. Whalley, "Direct-write techniques for maskless production of

microelectronics: A review of current state-of-the-art technologies," in *Electronic Packaging Technology & High Density Packaging, 2009. ICEPT-HDP '09. International Conference on*, 2009, pp. 497-503.
[22] B. Li, P. A. Clark, and K. H. Church, "Robust Direct-Write Dispensing Tool and Solutions for Micro/Meso-Scale Manufacturing and Packaging," *ASME Conference Proceedings*, vol. 2007, no. 42908, pp. 715-721, Jan. 2007.
[23] nScrypt Corporate web site. "World-wide Leader in Micro to Pico-liter Dispensing Systems with our Patented Micro Dispense Pump™." Internet: www.nscryptinc.com/direct-print-smartpump. [July 21, 2011].
[24] J. Stringer and B. Derby, "Limits to feature size and resolution in ink jet printing," *Journal of the European Ceramic Society*, vol. 29, no. 5, pp. 913-918, Mar. 2009.
[25] H.-T. Wang *et al.*, "Toward conductive traces: Dip Pen Nanolithography® of silver nanoparticle-based inks," *Applied Physics Letters*, vol. 93, no. 14, p. 143105:1-143105:3, 2008.
[26] M. Pudas, N. Halonen, P. Granat, and J. Vähäkangas, "Gravure printing of conductive particulate polymer inks on flexible substrates," *Progress in Organic Coatings*, vol. 54, no. 4, pp. 310-316, Dec. 2005.
[27] M. M. Voigt *et al.*, "Polymer Field-Effect Transistors Fabricated by the Sequential Gravure Printing of Polythiophene, Two Insulator Layers, and a Metal Ink Gate," *Advanced Functional Materials*, vol. 20, no. 2, pp. 239-246, Jan. 2010.
[28] H. W. Kang, H. J. Sung, T.-M. Lee, D.-S. Kim, and C.-J. Kim, "Liquid transfer between two separating plates for micro-gravure-offset printing," *Journal of Micromechanics and Microengineering*, vol. 19, no. 1, pp. 015025-015034, Jan. 2009.
[29] K. Maekawa *et al.*, "Influence of wavelength on laser sintering characteristics of Ag nanoparticles," in *Electronic Components and Technology Conference, 2009. ECTC 2009. 59th*, 2009, pp. 1579-1584.
[30] M.-K. Kim, *et al.*, "Laser sintering of the printed silver ink," in *IEEE International Symposium on Assembly and Manufacturing, 2009. ISAM 2009*, 2009, pp. 155-158.
[31] A. J. Lopes, "Hybrid manufacturing: Integrating stereolithography and direct print technologies," Ph.D. dissertation, Dept. Mat. Sci. and Eng., The Univeristy of Texas at El Paso, El Paso, TX, 2010.
[32] B. K. Park, D. Kim, S. Jeong, J. Moon, and J. S. Kim, "Direct writing of copper conductive patterns by ink-jet printing," *Thin Solid Films*, vol. 515, no. 19, pp. 7706-7711, Jul. 2007.
[33] L. Mo, *et al.*, "Preparation and Conductive Mechanism of the Ink-Jet Printed Nanosilver Films for Flexible Display," in *2nd International Congress on Image and Signal Processing, 2009. CISP '09*, 2009, pp. 1-5.
[34] J. C. Maxwell, "Electric Current," in *An elementary treatise on electricity*, Oxford: Clarendon Press, 1888, p. 100.
[35] K.-S. Moon *et al.*, "Thermal behavior of silver nanoparticles for low-temperature interconnect applications," *Journal of Electronic Materials*, vol. 34, no. 2, pp. 168-175, Feb. 2005.
[36] S. Castillo, D. Muse, F. Medina, E. MacDonald, R. Wicker, "Electronics Integration in Conformal Substrates with Additive Layered Manufacturing," in *Proceedings of the 2009 Solid Freeform Fabrication Symposium*, Austin, Texas, pp. 730-737, 2009
[37] M. Navarette, A. Lopes, J. Acuna, R. Estrada, E. MacDonald, J. Palmer, R. Wicker, "Integrated Layered Manufacturing of a Novel Wireless Motion Sensor System with GPS,"

in *Proceedings of the 2009 Solid Freeform Fabrication Symposium,* Austin, Texas, pp. 575-585, 2007.

[38] A.J. Lopes, M. Navarrete, F. Medina, J.A. Palmer, E. MacDonald, R.B. Wicker, "Expanding Rapid Prototyping for Electronic Systems Integration of Arbitrary Form," in *Proceedings of the 2006 Solid Freeform Fabrication,* Austin, Texas, pp. 644-655, 2006.

[39] R. I. Olivas, "Conformal electronics manufacturing through additive manufacturing and micro-dispensing," M.S. thesis, Dept. of Electrical and Computer Eng., The University of Texas at El Paso, El Paso, TX, 2011.

[40] D. T. Pham and R. S. Gault, "A comparison of rapid prototyping technologies," *International Journal of Machine Tools and Manufacture,* vol. 38, no. 10-11, pp. 1257-1287, Oct. 1998.

[41] M. N. Cooke, J. P. Fisher, D. Dean, C. Rimnac, and A. G. Mikos, "Use of stereolithography to manufacture critical‐sized 3D biodegradable scaffolds for bone ingrowth," *Journal of Biomedical Materials Research Part B: Applied Biomaterials*, vol. 64, no. 2, pp. 65-69, Feb. 2003.

[42] K. Arcaute Cantu, "Stereolithography of poly (ethylene glycol) hydrogels with application in tissue engineering as peripheral nerve regeneration scaffolds" Ph.D. dissertation, Dept. Mat. Sci. and Eng., The Univeristy of Texas at El Paso, El Paso, TX, 2008.

CHAPTER 2: RESEARCH OBJECTIVES AND PRESENTED PUBLISHED PAPERS

2.1 Research Objectives

Printed electronics is an emerging technology which is dependent on the capability of a conductive ink or paste to achieve optimum electrical performance. The predominant goal of this research was to develop a method to improve the electrical conductivity (minimize the electrical resistivity) of printed conductive traces on various polymeric substrates in a way which would not damage the substrate. The ability to apply the curing technique to multiple ink and substrate types also needed to be demonstrated. At the same time, research complementary to the area of printed electronics manufacturing was also performed. Overall, the research objectives of this dissertation are:

1. Characterize the effects of thermal curing of various ink types printed using different printing methods.
2. Characterize the ohmic curing process for various ink types.
3. Failure analysis of a direct print component.
4. Demonstrate the application of the ohmic curing process for interconnects used in 3D structural electronics.

The basis of the first objective serves a dual purpose in that it provides research which is complementary to the area of printed electronics, as well as establishing a baseline by which the ohmic curing process can be rated against. The first objective is covered in Chapter 3 and Chapter 7. The second objective, captured in Chapter 4, is a microstructural and process characterization of the ohmic curing process. The third objective is research complimentary to the area of printed electronics as it covers a failure investigation of a critical component of a

direct print system. The third objective is covered in Chapter 5. Finally the fourth objective, seen in Chapter 6, demonstrates the versatility of the ohmic curing process.

2.2 Published Works

The bulk of this dissertation is composed of published works. The Citation's and abstracts for each published work along with the corresponding chapter are as follows:

Chapter 3

The material in Chapter 3 is from the article in the journal *Materials* cited as follows:

D. A. Roberson, R. B. Wicker, L. E. Murr, K. Church, and E. MacDonald, "Microstructural and Process Characterization of Conductive Traces Printed from Ag Particulate Inks," *Materials*, vol. 4, no. 6, pp. 963-979, May. 2011.

Permission to use the article cited above in this dissertation has been granted by the publisher as documented in Appendix A.

Abstract

Conductive inks are key enablers for the use of printing techniques in the fabrication of electronic systems. Focus on the understanding of aspects controlling the electrical performance of conductive ink is paramount. A comparison was made between microparticle Ag inks and an Ag nanoparticle ink. The microstructures resulting from thermal cure processes were characterized morphologically and also in terms of their effect on the resistivity of printed traces. For microparticle inks, the variability of resistivity measurements between samples as defined by coefficient of variation (CV) was greater than 0.1 when the resistivity was 10 to 50 times that of bulk Ag. When the resistivity was lower (~1.4 times that of bulk Ag) the CV of sample sets was less than 0.1. In the case of the nanoparticle ink, resistivity was found to decrease by a factor ranging from 1.2 to 1.5 after doubling the amount of layers printed prior to curing though it was expected to remain the same. Increasing the amount of layers printed also enhanced the sintering process.

Chapter 4

The material in Chapter 4 has been published in *Journal of Electronic Materials* under the following citation:

D. A. Roberson, R. B. Wicker, E. MacDonald, "Ohmic Curing of Printed Conductive Traces," *Journal of Electronic Materials*, In Revision, 2012

Permission to use the material in Chapter 4 is in Appendix B.

Abstract

Ohmic heating was demonstrated as a novel curing method (or curing enhancement) useful in decreasing the resistivity while 1) only locally heating the substrate and 2) curing in a matter of seconds compared to the range of thirty minutes to an hour required by traditional oven curing. In one experiment traces composed of microparticle ink, which required initial air-drying as a pre-process step, the application of an ohmic curing cycle resulted in a resistivity of 80nΩ·m, roughly 6 times that of bulk silver. In a second experiment employing nanoparticle inks, which required an initial thermal cure as a pre-process, a resistivity of 43nΩm, roughly 3 times that of bulk silver was attained after the application of an ohmic curing cycle. Electrical characterization of the ohmic curing process was performed in real time to understand the impact of cycling and duration on the resulting conductivity. Finally, the effect of printed trace length on the ohmic curing process was explored and found to have a near linear relationship with the reduction in resistance when applied electrical current was normalized to measured resistance. The microstructural changes which occurred as a result of ohmic curing such as particle sintering and grain growth were characterized by scanning electron microscopy (SEM). The results presented in this work demonstrate the use of ohmic heating to rapidly improve the electrical performance of printed conductive traces and the potential of ohmic curing to overcome temperature limitations imposed upon a thermal curing process by substrate material properties or other sources.

Chapter 5

The material found in Chapter 5 has been published in *Journal of Failure Analysis and Prevention* under the following citation:

D. A. Roberson, E. MacDonald, K. Church, and R. B. Wicker, "Failure Investigation of Direct Write Pen Tips," *Journal of Failure Analysis and Prevention*, vol. 10, no. 6, pp. 504-507, Aug. 2010.

Permission to use the article cited above in this dissertation has been granted by the publisher as documented in Appendix C.

Chapter 7

The material in Chapter 7 is from the following citation:

D. A. Roberson, R. B. Wicker, and E. MacDonald, "Microstructural characterization of electrically failed conductive traces printed from Ag nanoparticle inks," Materials Letters, vol. 76, no. 0, pp. 51–54, Jun. 2012.

Permission to use this material can be found in Appendix D.

Abstract

Conductive traces printed from nanoparticle loaded silver inks failed due to the application of excessive electrical current. A non-homogeneous microstructure was observed in the vicinity of the failed region consisting of sintered particles, grains and melted particles indicating a significant amount of heat was transferred to the conductive trace, in some cases, resulting in substrate damage. A simple physical model describing the failure mechanisms is proposed.

CHAPTER 3: MICROSTRUCTURAL AND PROCESS CHARACTERIZATION OF CONDUCTIVE TRACES PRINTED FROM AG PARTICULATE INKS

3.1 Introduction

The creation of conductive paths in electronic systems has traditionally involved the addition and subtraction of conductive material by means of deposition, mask, and etch processing [1, 2]. Printing techniques, such as rotogravure, screen printing, inkjet, and direct write micro dispense have been proven as viable alternative methods for creating conductive paths and have the additional benefit of creating these paths in a simple two step process involving only printing and curing [3–6]. Conductor loaded inks allow printing technologies to be applied in the creation of electronic systems. Beyond the creation of conductive paths for use as interconnects, conductive inks have been utilized in the creation of electronic components such as transistors, RF antennas, and glucose sensors [7–9] among others.

The thermal cure process produces microstructural changes in particle-based conductive inks (of both the micro and nano scale), which impacts the overall electrical properties of a printed conductive trace. In the case of inks where the particle size is of the micron scale, low temperature curing (between 100°C and 200°C for inks designed to work in this temperature range) in which the amount of material suspending the conductive particles will decrease, resulting in particles conducting through physical contact in a process known as percolation [3, 10–12]. This mechanism has been demonstrated by Saraf *et al.* [12] for an Ag microflake conductive ink. In [12], a model was developed which demonstrated a relationship between resistivity and the relative volume fraction of the binder material separating the conductive particles where higher curing temperatures lowered the amount of binder in the ink system and conductivity increased. For nanoparticle inks, the full microstructural evolution which occurs during thermal processing has also been well characterized in which sintering is the mechanism for creating a semisolid film [13–15]. In this case, semisolid films can be created after curing at relatively low temperatures (<300°C) due to the effect of particle size on melting temperature.

The relationship between particle size and melting temperature has been modeled for Au [16] and Ag [17, 18] nanoparticles and a depression of melting temperature is observed when the particle size is at or below the nano-regime. The relationship between size and physical properties is sometimes referred to as the "scaling law" [19] and many examples exist in nanoscale literature.

The allowable curing temperature range is largely dictated by the substrate choice, which is in turn dependent on the particular electronics application. For example, applications requiring flexible substrates could employ the use of a polymeric material as a substrate. The glass transition temperature of polymers in many cases will overlap with or be below the manufacturer recommended curing parameters. On the other hand, an application in which flexibility is not needed could use a rigid substrate, such as ceramic, which can withstand temperatures higher than the melting point of the printed conductor. The ability to cure the printed conductor near the melting temperature of the conductive particles allows the electrical performance of these conductors to be improved dramatically. Understanding the effect of microstructure on electrical performance is important when selecting a conductive ink for utilizing printing technologies in the production of electronic systems especially when polymeric substrates are used due to the corresponding temperature limits. In this paper, a comparison is made between micro and nanoparticle loaded conductive inks. The microstructural changes which occur as a result of thermally curing these two ink types are documented. Two printing techniques are utilized, inkjetting of nanoparticle loaded inks and direct write micro dispensing of microparticle loaded inks.

3.2 Experimental

3.2.1 Ag Microparticle Inks on Flexible and Rigid Substrates

For the characterization of microparticle inks, two substrates were used. The first substrate was a flexible DuPont Kapton® substrate (DuPont, Wilmington, DE, USA) while the second was a rigid ceramic 96% alumina substrate. The ceramic substrate has the benefit of

being able to withstand high temperatures, and these high temperatures substantially improve the electrical conductivity of the ink by permitting particle sintering. Conversely, the Kapton® substrate has the desirable property of being flexible, which allows conductive lines printed on this substrate to be used in conformal or flexible applications, and in general, increases the application potential. However, the drawback of Kapton® is that thermal processing is typically restricted to temperatures below the glass transition temperature of approximately 360°C [20], around 100°C below that required for the sintering of Ag particles of sizes in the micro regime.

For experiments involving microparticle inks, printing was performed via the direct write micro dispensing technique with an nScrypt 3D 450 system (nScrypt, Inc., Orlando, Florida, USA). The patterns shown in Figure 3.1 were printed for the experiments. Table 3.1 summarizes the experimental parameters for all inks used in this paper. The first ink type was Ferro 3309F conductive ink (Ferro Corporation, Cleveland, OH, USA) which was designed for use on alumina ceramic substrates and has a recommended maximum cure temperature of 850°C [21] as used in commercial Low Temperature Co-Fired Ceramics (LTCC) technology. The Ferro 3309F ink was printed on a rigid ceramic 96% alumina substrate in the pattern seen in Figure 3.1(a) and then subjected to a curing cycle starting at110°C for 20min and then increasing the temperature to 850°C and maintaining the temperature at 850°C for 10min. The total cure cycle, including the temperature ramp, lasted 2h.

The second conductive ink used, DuPont CB028 (DuPont, Wilmington, DE, USA), has a lower recommended curing temperature of 160°C [22] and is therefore often targeted for use in flexible applications that require a low maximum processing temperature. The DuPont CB028 ink was printed on DuPont Kapton® polyimide substrates in the pattern displayed in Figure 3.1(a) and then thermally cured at 160°C for 1h. To further compare the effects of processing temperature, a second set of Ferro 3309F was printed on the same type of polyimide substrate and cured at 160°C for 1h, although this is a significant departure from the manufacturer's recommendation.

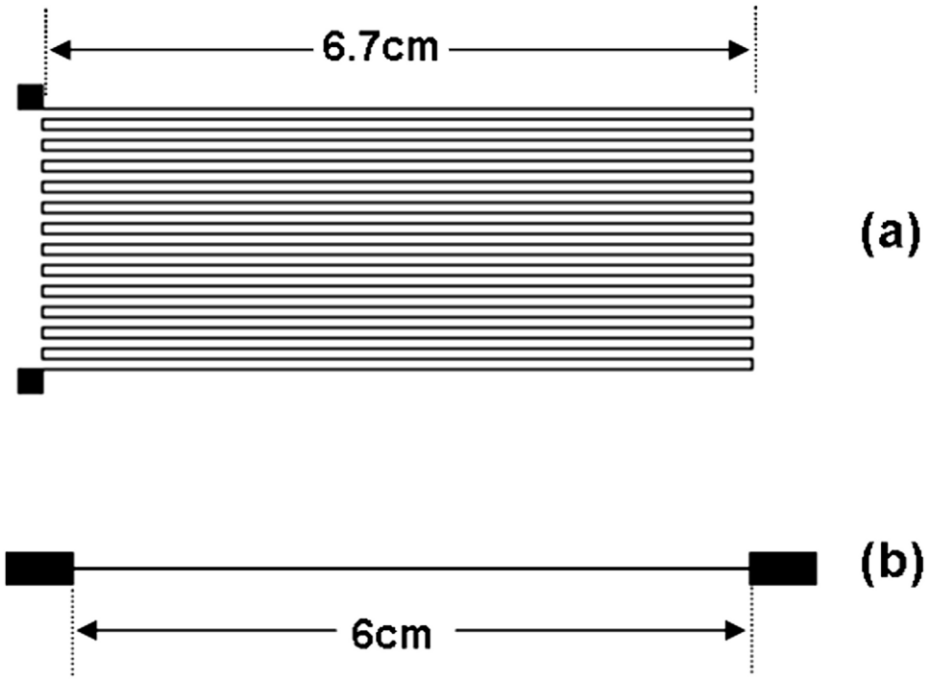

Figure 3.1: The **(a)** serpentine pattern and **(b)** straight line pattern used in the testing of Ag particle loaded inks. The target line width for microparticle inks was 250μm while the target line width for nanoparticle inks was 850μm.

Table 3.1: The inks, print methods, substrates, test patterns, and curing parameters for experiments performed in this study.

Ink	Print Method	Substrate	Test Pattern	Cure Parameters
Ferro 3309F	Direct write	Alumina	Serpentine	Cycled to 850°C max
		Kapton®	Serpentine	160°C 1h
DuPont CB028	Direct write	Kapton®	Serpentine	160°C 1h
Ercon E1660	Direct write	Kapton®	Line	Air Dried
			Line	138°C 1h
Cabot CCI-300	Inkjet	Kapton®	Line	100°C 1h
			Line	110°C 1h
			Line	150°C 1h
			Line	160°C 1h
			Line	175°C 1h
			Line	200°C 1h
			Line	250°C 1h, 24h

A third microparticle loaded ink, Ercon E1660 (Ercon Incorporated, Wareham, MA USA), was printed via direct write micro dispense on a Kapton® substrate in the pattern depicted in Figure 3.1(b). Ercon E1660 is designed for use on both rigid and flexible substrates and has a recommended curing temperature of 121°C [23]. Two cure methods were employed: (1) Air drying and (2) Curing at 138°C for 1h. The temperature of 138°C was utilized based on a previous performance characterization of this ink by Navarrete *et al.* [24]. The size distribution of the particles within the ink was measured from SEM micrographs for the Ercon E1660 as well as the first two inks discussed previously. As seen in Figure 3.2, the E1660 is loaded with Ag particles, which are roughly twice as large as the particles in the DuPont ink and roughly 10 times as large as the particles in the Ferro ink.

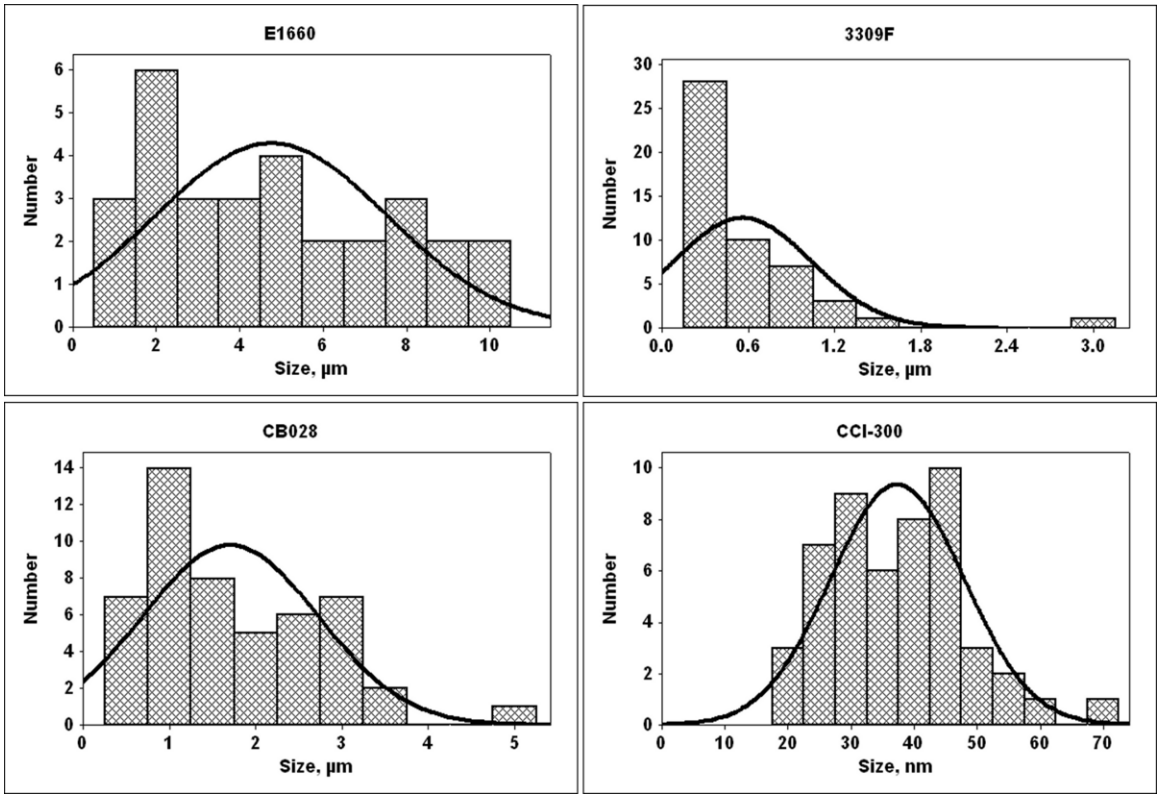

Figure 3.2: Measured size distributions of the conductive particles used in all experiments. Measurements were made from SEM micrographs.

Resistivity of the printed traces was calculated based on dimensional measurements of the printed patterns and the measured resistance. The equation used to calculate resistivity, ρ, is:

$$\rho = R\frac{A}{l} \tag{3.1}$$

where R is measured resistance, A is the cross-sectional area of the printed line, and l is the length of the printed line. For each ink and substrate combination, multiple samples were printed and the resistance was measured using a Keithley Model 2000 multimeter (Keithley Instruments, Inc., Cleveland, OH, USA). Cross-sectional areas of the printed lines were calculated by first measuring the line thickness with a KLA-Tencor Alpha Step IQ stylus profilometer (KLA-Tencor, Milpitas, CA, USA.) operating with a resolution of 20nm. An outline representing the cross section of the printed line was generated by plotting x *vs*. z where the thickness was taken to be along the z-axis and the width to be along the x-axis. The cross-sectional area was approximated by calculating the area beneath the plotted curve utilizing a Riemann sum-type approach:

$$Area = \sum_{i=1}^{n} z_i \Delta x_i \tag{3.2}$$

In this case, Δx is 1μm. An example of the graphical representation of the cross section of a printed line is seen in Figure 3.1. Validation of the profilometer method was made by examining SEM cross sections of a printed line of Ferro 3309F on an alumina substrate and comparing the thickness of the printed line to the measured profile as seen in Figure 3.3 Resistivity was then calculated based on the known length of 1.8m for the serpentine patterns and 6cm for the straight line patterns seen in Figure 3.1(a) and (b) respectively. Comparing random measurements among all of the printed samples revealed a variation in measured cross section to be roughly 10%.

Specimen preparation for scanning electron microscope (SEM) microanalysis of the printed lines entailed the use of a surgical scalpel to section the polymeric substrates and the use of a glass cutter to section the ceramic substrates. The samples were then subjected to Au

sputtering for 30s with a Gatan Model 682 Precision Etching Coating System (Gatan, Inc., Pleasanton, CA, USA) to reduce charge effects in the SEM. SEM was performed on all samples in a top down fashion using a Hitachi S-4800 Ultra-high Resolution Field Emission Scanning Electron Microscope (Hitachi High-Technologies Corporation, Tokyo, Japan) utilizing a 20keV accelerating voltage.

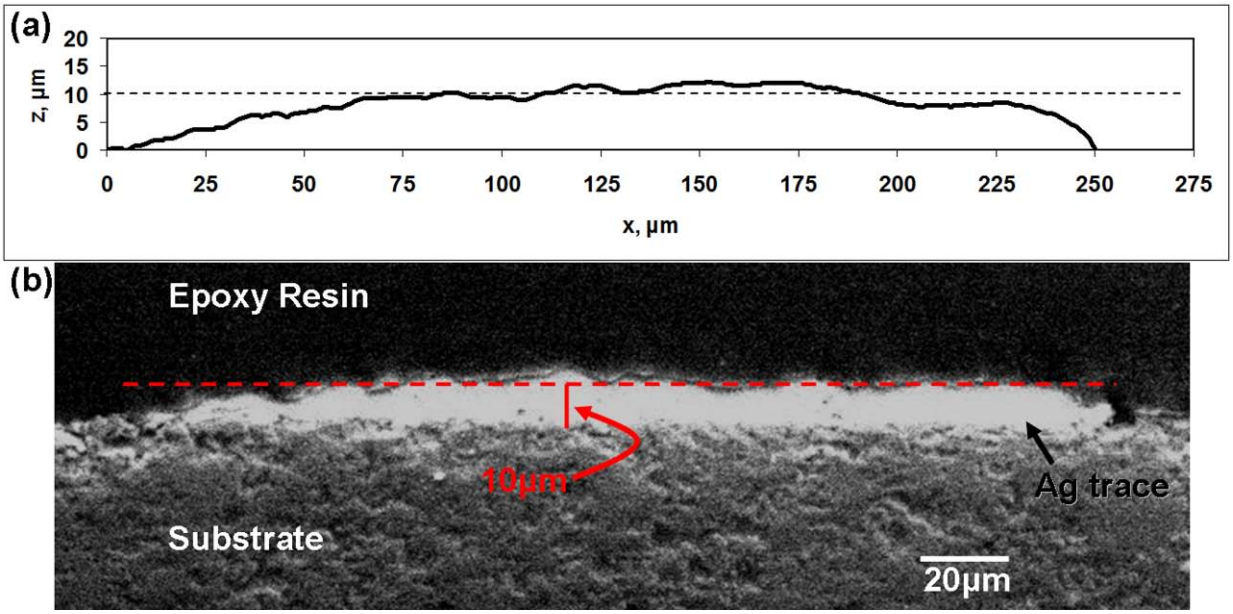

Figure 3.3: (a) Example of a randomly measured profile of a printed trace of Ferro 3309F on a ceramic substrate and **(b)** SEM micrograph of a random cross section of a printed trace of Ferro 3309F on a ceramic substrate.

3.2.2 Ag Nanoparticle Ink on Flexible Substrates

An alternative to using microparticle-based inks in applications where the cure process is controlled by the thermal constraints of a polymeric substrate is to use a nanoparticle-based ink and take advantage of the reduced sintering temperature found in the nano regime. In order to explore this option, the 6cm long pattern seen in Figure 3.1(b) was utilized in the characterization of a commercially available Ag nanoparticle ink, Cabot CCI-300, (Cabot Corporation, Albuquerque, NM, USA). The test pattern was inkjet printed on a Kapton® substrate with a Dimatix 2800-Series Materials Printer (Fujifilm Dimatix, Inc, Santa Clara, CA, USA). One layer (single print) was printed at 1270 DPI. In order to improve the wetting

characteristics of the ink substrate interface, the Kapton® substrate was first cleaned with UV-Ozone for 10min with a Jelight UVO Cleaner Model 342A (Jelight Company, Inc, Irvine, CA, USA). Sample sets of five were oven cured for 1h at each of the following temperatures: 100°C, 110°C, 150°C, 160°C, 175°C, 200°C, and 250°C. SEM microanalysis in a top down fashion was performed as described previously. Resistivity was determined based on the technique outlined previously for microparticle inks.

3.3 Results and Discussion

3.3.1 Ag Microparticle Inks on Flexible and Rigid Substrates

Using the resistance and dimensional measurements of the printed lines, resistivity for the inks was calculated and the graphical results are seen in Figure 3.4. Comparing the measured results to the bulk resistivity of Ag, 14.6nΩ•m [25], allows for the results of the cure experiments to be benchmarked. The Ferro 3309F patterns cured at 850°C on ceramic substrates produced resistivity values calculated to be 21nΩ•m ±5.7nΩ•m while the resistivity for the patterns printed on Kapton® using the same ink cured at 160°C was calculated to be 480nΩ•m ±74nΩ•m. The resistivity of the DuPont CB028 ink samples printed on Kapton® and cured at 160°C was calculated to be 239nΩ•m ±57nΩ•m. The Ercon E1660 samples in the air dried condition had a resistivity of 405nΩ•m ±45nΩ•m while samples of the same ink cured at 138°C for 1h had a resistivity of 103nΩ•m ±14nΩ•m. The three inks printed on Kapton® were roughly an order of magnitude less conductive than the patterns printed on ceramic due to the ability of the ceramic substrate to withstand the higher curing temperature. The DuPont ink cured at 160°C is roughly two times more conductive than the Ferro ink cured at the same temperature. Utilizing the Ferro 3309F processed at this temperature is not the manufacturer intended application as the Ferro 3309F ink was optimized for 850°C. The air drying of the E1660 samples produced a resistivity on par with the 3309F cured at 160°C while the Ercon E1660 cured at 138°C produced the most conductive trace for the inks printed on Kapton®. This significantly better performance is potentially due to the average particle size being the largest among the inks tested. The

implication made here is that percolation theory should also be characterized in terms of particle size in addition to the amount of binder material separating the conductive particles. However, the larger particle size restricts the minimum feature size that can be printed.

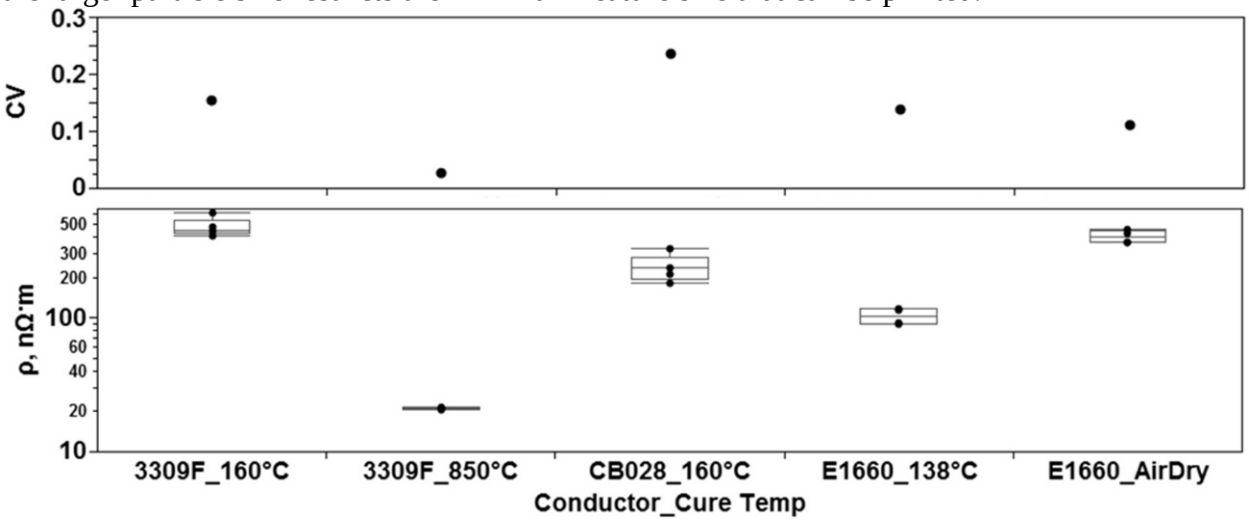

Figure 3.4: Graphical results of the measured resistivity for the thermal cure experiments involving flake-based inks. Note the variation of the sample set is greater for patterns with a higher resistivity.

Based on the comparison of the measured results to the bulk resistivity of Ag, a conclusion can be drawn that the Ferro 3309F printed on ceramic has created a conductive path with a conductivity approaching bulk Ag (67% of bulk Ag) due to the higher temperatures involved in the curing process. A conclusion can also be drawn that as the Ferro is intended for LTCC processing which will create a microstructure favorable to conductivity—in this case, grains.

Microstructural characterization reveals differences in the governing factors controlling conductivity, namely conduction through physical contact between particles vs. conduction in a grainy film. In the case of both DuPont CB028 and Ercon E1660, the microstructure is that of individual particles conducting as a result of the particles physically touching one another as seen in Figure 3.5. The decrease in resistivity between air dried samples and thermally cured samples of both DuPont CB028 and Ercon E1660 is in agreement with the results noted by Saraf *et al.* [12] which showed an increase in conductivity for higher curing temperatures compared to lower

curing temperatures for a microparticle based ink. In the case of Ferro 3309F, the thermal processing at 850°C changed the microstructure of the ink printed on ceramic to a semi-porous film as seen in Figure 3.6(b), with a grain diameter of ~5μm as determined by the linear intercept method. The differences between both high and low temperature curing of the Ferro 3309F ink are clearly illustrated in Figure 3.6. After low temperature curing, the morphology is that of slightly sintered particles mixed with larger particles as seen in Figure 3.6(a). The key aspect of this microstructure is particles and sintered groups of particles touching each other. Conversely, after the high temperature curing, the transformation from particles of a sub-micron size to a near solid form composed of faceted grains on the order of ~5μm in diameter is indicative of a solid state grain growth process via grain boundary diffusion, a process well-characterized in the sintering of Ag and other materials [26, 27]. The ability of the alumina ceramic substrate to withstand the temperature required to initiate this solid state growth process has enabled the transformation from particle to a near-solid porous film and consequently, these films provide the best conductivity which is approaching that of bulk Ag—14.6nΩ•m [25]

The impact of grain size and porosity on the resistivity of a printed conductive trace has been characterized in literature [28, 29]. The key aspects of these models are that microstructures consisting of large grains are more conductive than microstructures consisting of small grains and that less porosity is more favorable to conductivity. Consequently, the resistivity of the Ferro 3309F ink processed at higher temperatures is governed by the grain size and the amount of pores in the film. By contrast, the lower temperature thermal processing of the DuPont CB028, Ercon E1660, and Ferro3309F inks printed on Kapton® did not result in the creation of a film and therefore the resistivity is higher due to the dependence of resistivity on the amount of physical contact between the Ag particles. The difference between the two main factors controlling resistivity (contact area *vs.* grain size) is graphically represented in Figure 3.4. A difference exists not only in resistivity between the printed lines cured at high and low temperatures, but also in the distribution of the data. Figure 3.4 illustrates a higher variability

(defined by the coefficient of variation, CV) associated with the previously mentioned percolation theory mechanism.

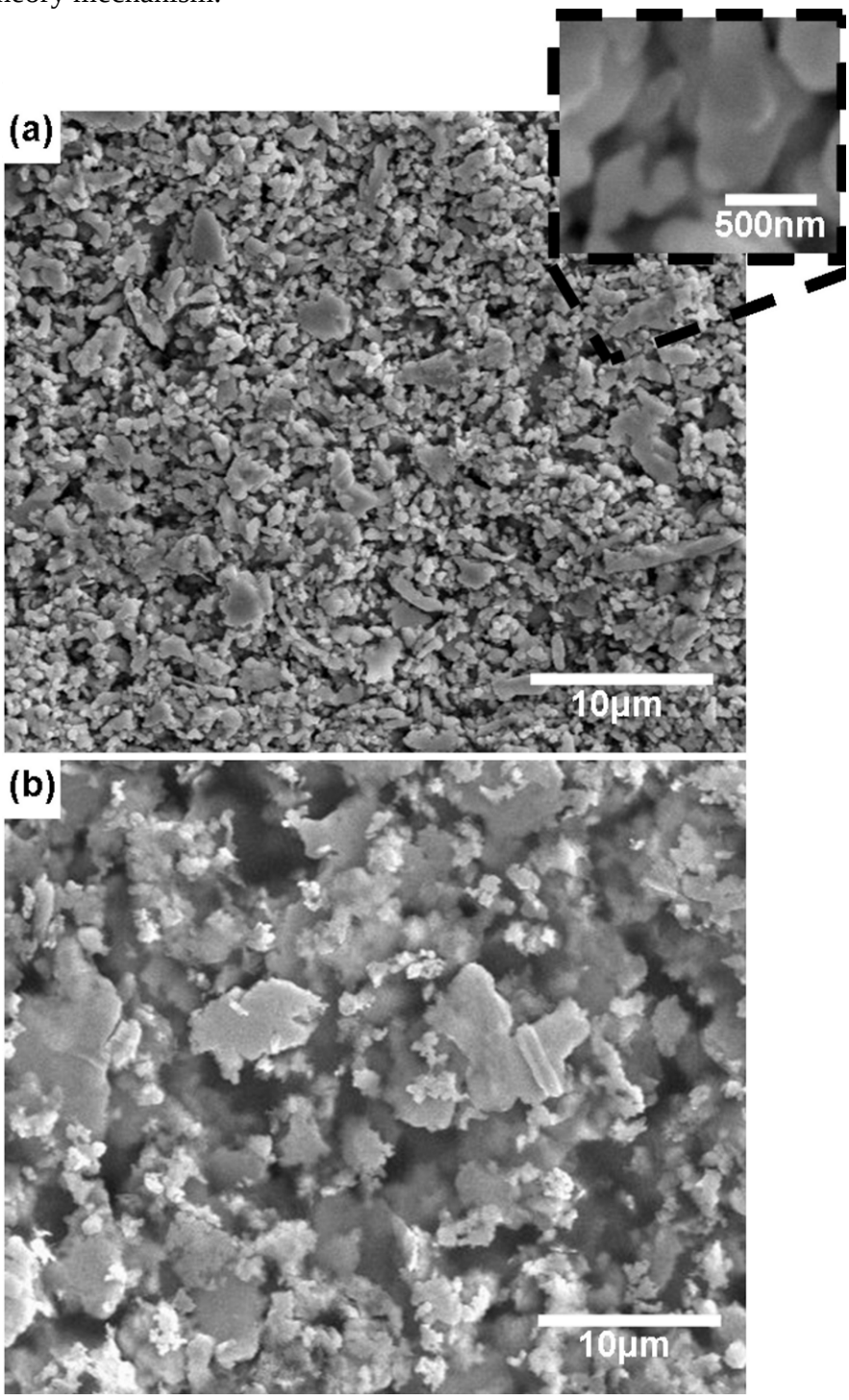

Figure 3.5: (a) SEM micrograph of DuPont CB028 ink after thermally curing for 1h at 160°C and **(b)** Ercon E1660 after thermally curing for 1h at 138°C.

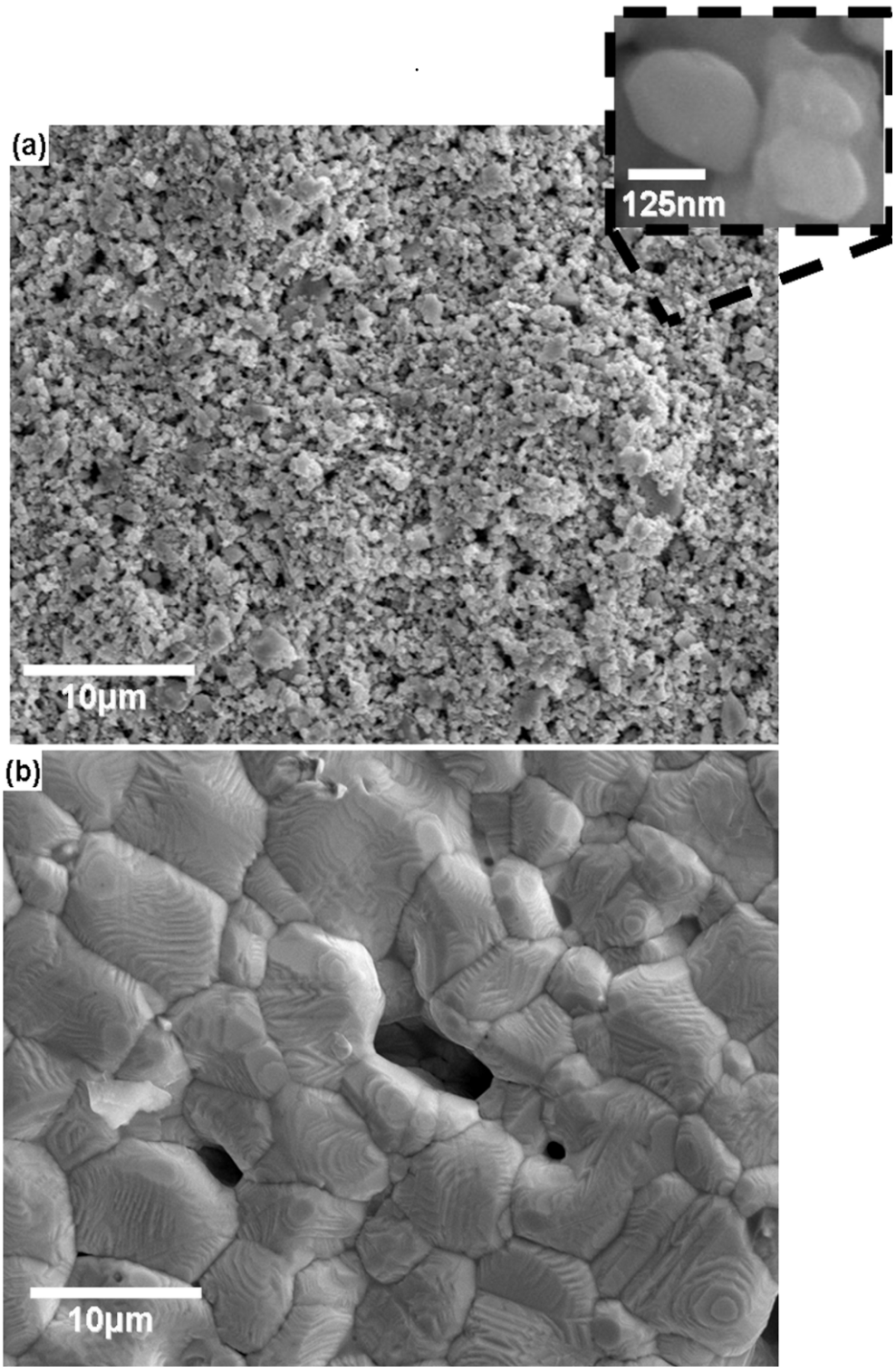

Figure 3.6: SEM Micrographs of Ferro 3309F **(a)** after thermally curing for 1h at 160°C and **(b)** after a 2h thermal cure cycle which peaked at 850°C for 10min. Note the extreme difference in microstructure.

3.3.2 Ag Nanoparticle Loaded Conductor on Flexible Substrate

The microstructural evolution, which occurs with an increase in processing temperature, is illustrated in Figure 3.7 for the Cabot CCI-300 lines printed on Kapton® substrates. The graphical results of the corresponding resistivity (ρ) measurements for each curing temperature are also seen in Figure 3.7. Curing temperatures of 100°C and 110°C resulted in a microstructure consisting of unaltered Ag particles. The method of conduction at these two temperatures is percolation and it is assumed that curing at 110°C removed more solvent, which increased the amount of contact between the particles and thus, the conductivity. The assumption based on the observed decrease in resistivity is consistent with the previously mentioned percolation theory and the results noted in [12] and [13]. At 150°C the microstructure is that of slightly necked particles—examples of which are indicated by white arrows. At 160°C and 175°C the sintering process is more pronounced as indicated by the neck growth. A relationship between conductivity and the neck diameter of sintering particles has been documented in [13] where conductivity increases as the neck diameter grows. Curing at 200°C and 250°C resulted in a film-like microstructure consisting of fully sintered particles and voids which can only occur at these processing temperatures.

Analyzing the variability in resistance measurements of the nanoparticle loaded ink does not reveal as clear of a relationship between method of conduction and variability as the results of the microparticle loaded inks did. One reason for this may be the non-homogenous nature of the inkjet printing process. When comparing the microstructure of the edge of the printed line with the center of the printed line, a difference between the degree of sintering is observed as seen in Figure 3.8. One reason for this occurrence may be due to the particles being less densely packed on the edge of the printed line. Sintering is governed by various diffusion processes beginning with surface diffusion [13] which has to rely on the amount of contact between the particles.

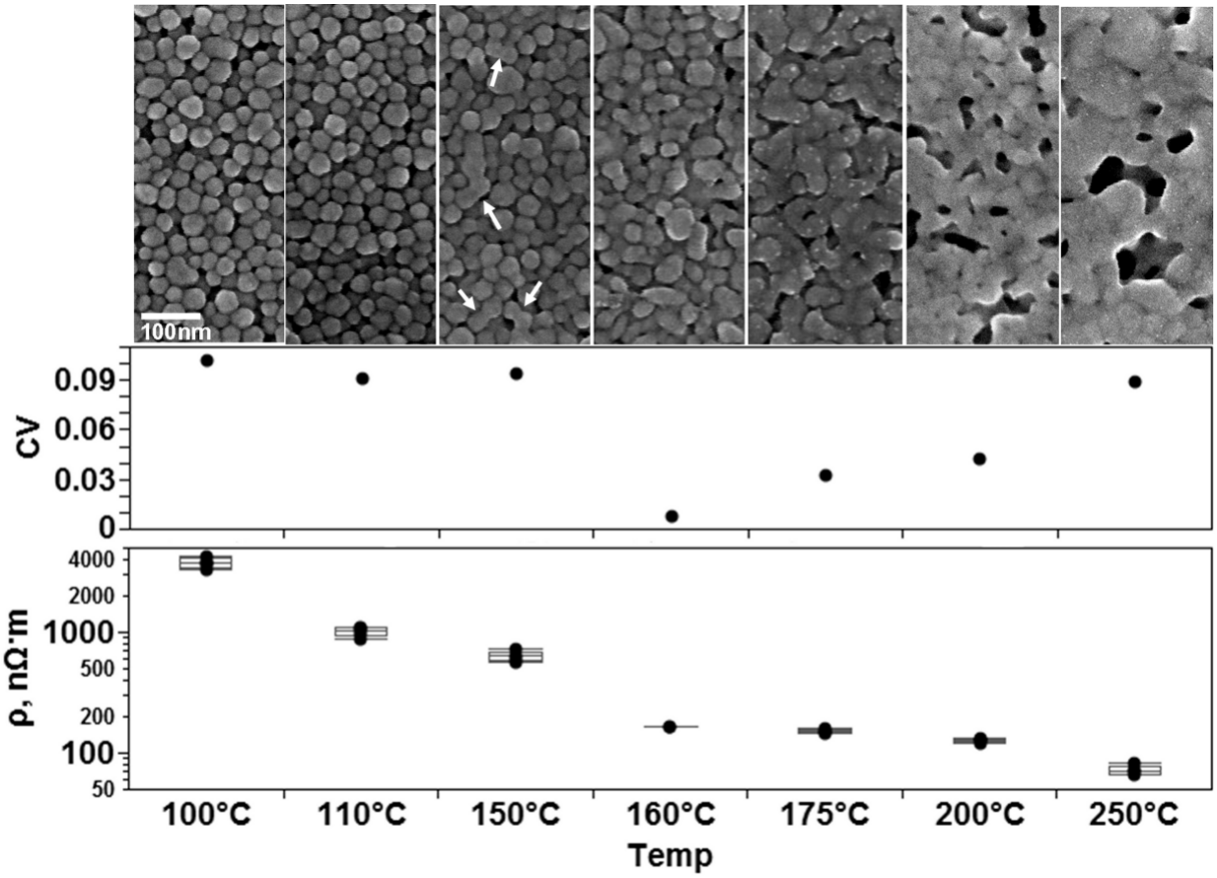

Figure 3.7: SEM micrographs of the microstructures resulting from thermally curing printed traces of Cabot CCI-300 conductive ink for 1h at the indicated temperatures. All images are at the same magnification. The corresponding graphical results of measured resistivity (ρ) are below the micrographs. The relationship between variation and method of conduction is not as clear as in the case of microparticle based ink. Sample size n=5 for all sets.

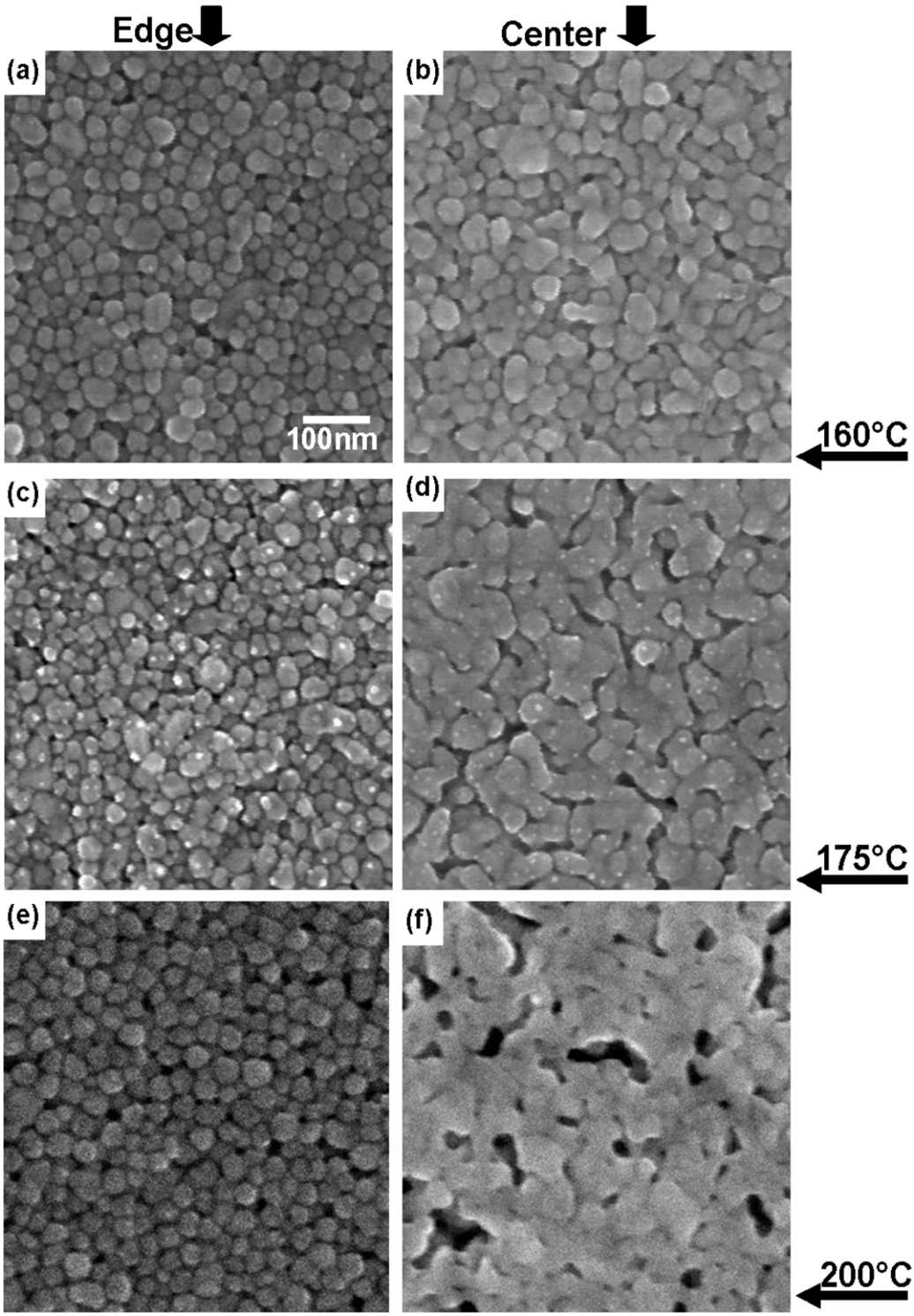

Figure 3.8: SEM micrographs of CCI-300 printed lines comparing **(a)** the edge of a printed line with **(b)** the center of a printed line cured at 160°C, **(c)** the edge and **(d)** the center of a line cured at 170°C, **(e)** the edge and **(f)** the center of a line cured at 200°C. All lines were printed in one layer and cured for 1h. All images are the same magnification.

To further explore the effect of particle contact area on the resulting microstructure, printing the pattern in multiple times was explored. Printing the same pattern with two or more layers—essentially printing the pattern multiple times on itself—results in a decrease in resistivity though expectation is that resistivity should be the same between one and multiple layers as the ratio of area over length should normalize the measurements. All samples were printed at the same time and then thermally cured at the same time for the given cure temperature. Analyzing the microstructural differences between lines printed in one and multiple layers may explain the drop in resistivity. Comparing the microstructures (Figure 3.9) of lines printed in one layer with lines printed in multiple layers and then cured at 110°C shows the microstructure to remain largely the same between printing in one, two and five layers. Examining the microstructures of lines printed at 150°C for 1h reveals the sintering process to be enhanced as a function of the number of layers printed.

The fact the necking process is more evolved at the same processing temperature is consistent with the notion of the dense packing model controlling the amount of sintering and also follows observations made on the edge of the printed lines in the previous experiment. Also seen in Figure 3.9 is a graphical representation of the effect of increasing the number of printed layers on the resistivity. It is notable here that the resistivity of lines cured at 110°C and 150°C decreases by a factor of 1.2 and 1.5 respectively between one and two layers of printing. The conclusion can be made that printing more layers results in a higher amount of contact between particles. The basis for this reasoning is that two phenomena are enhanced when increasing the amount of printed layers. The first phenomenon is conduction through percolation which increases as the amount of contact area grows. The increase in conductivity for lines cured at 110°C can only be explained by greater contact area between particles. Also governed by contact area are the diffusion mechanisms driving neck growth which was enhanced by increasing the number of printed layers for lines cured at 150°C as seen in Figure 3.9.

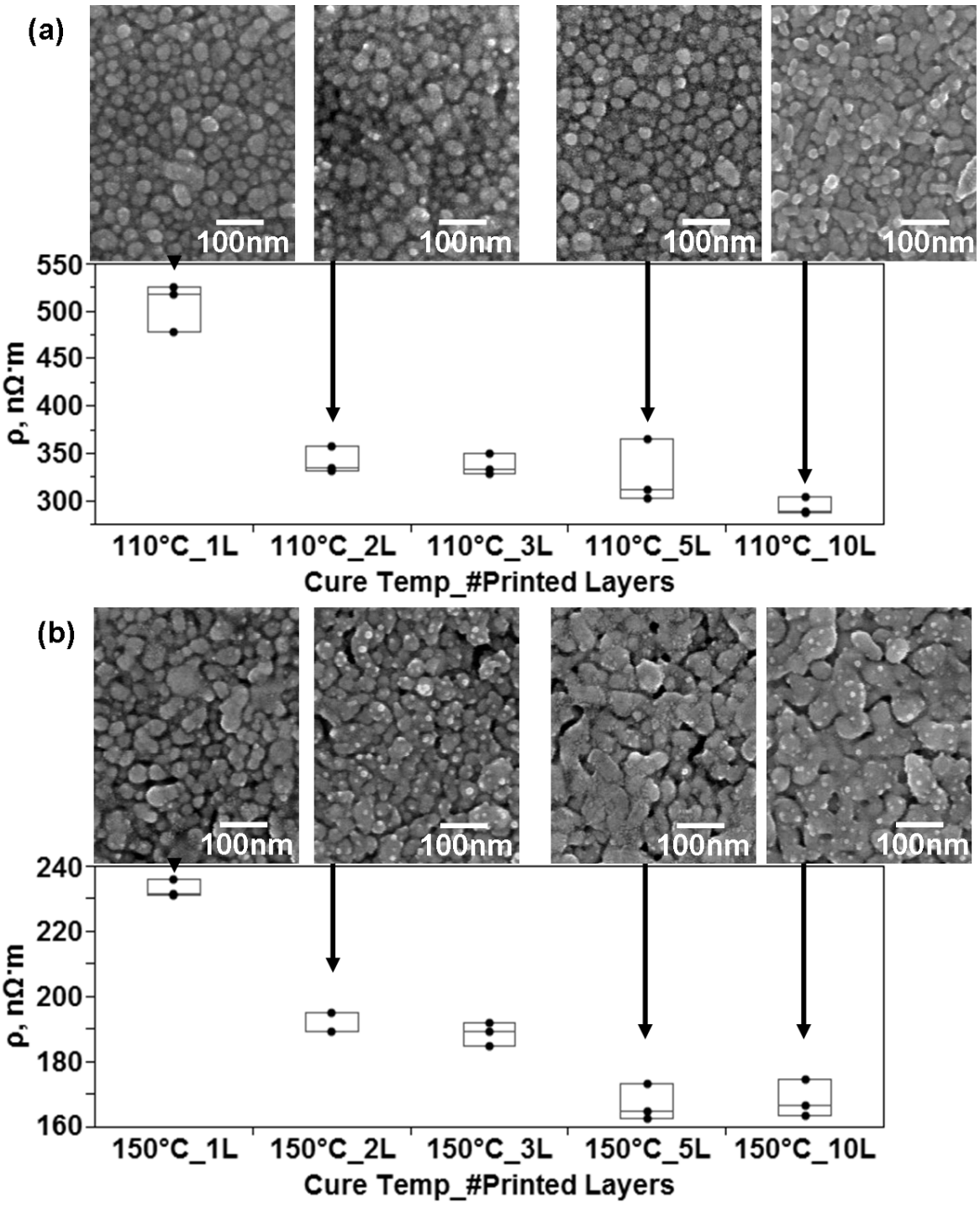

Figure 3.9: Comparison of the microstructures and resistivity measurements of printed lines of CCI-300 resulting form a difference in the amount of layers printed prior to printing for **(a)** lines cured for 1h at 110°C and **(b)** lines cured for 1h at 150°C. Note the drop in resistivity when the amount of layers is increased to 2.

Comparing the microstructure of the fully sintered film to that of the Ferro 3309F ink cured at 850°C reveals limitations of utilizing nanoparticle ink. Despite being fully sintered at 250°C, there is no grain growth occurring at this processing temperature. Increasing the cure time to 24h did not result in grain coarsening as is illustrated in Figure 3.10. Conversely, the higher thermal processing of the conductive ink printed on ceramic substrates resulted in coarse faceted grains. The grainy microstructure is pertinent to electrical performance due to the previously discussed relationship between grain size and resistivity. Though the capability of the nanoparticles to sinter at a depressed temperature offers the ability to process at a relatively low temperature, once the sintering process is complete, the resultant film would need a higher temperature processing for the creation of coarse grains to occur. A general rule of thumb for temperatures needed to induce grain growth in metals is roughly half the melting temperature of the given metal. In the case of silver, a temperature of around 460°C would be required to coarsen the grains. Furthermore, longer curing times appear to have an adverse effect on the electrical performance in terms of measured resistance as seen in Figure 3.10 that is potentially the result of oxidation as the thermal curing did not take place in an inert environment. According to the manufacturer specification sheet for Cabot CCI-300 ink [30], the maximum cure temperature is 350°C, however electrical characterization data on the same data sheet showed no improvement to electrical resistivity for curing temperatures above 250°C.

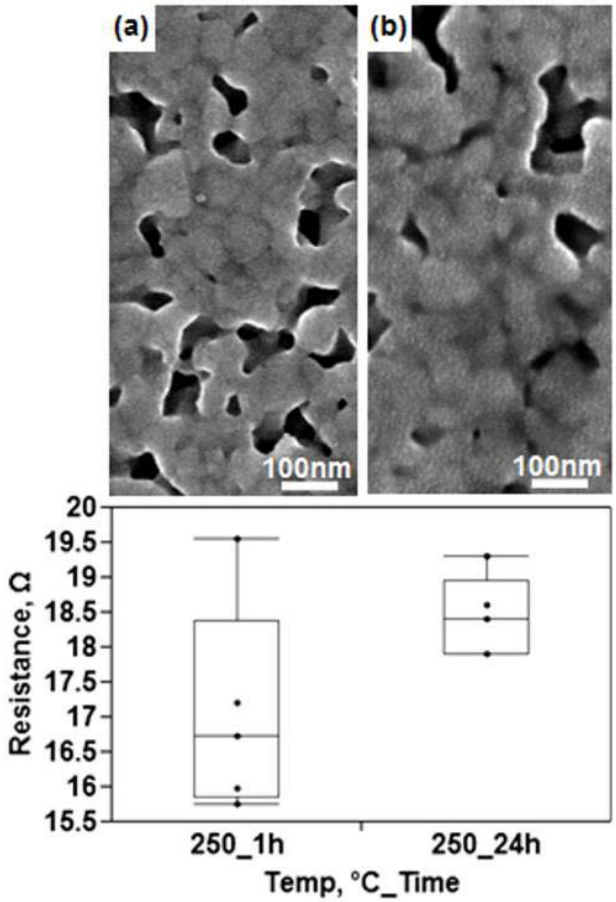

Figure 3.10: SEM micrographs of Cabot CCI-300 cured at 250°C for **(a)** 1h and **(b)** 24h along with corresponding graph of resistance measurements.

Analysis of the data from all the experiments performed in this study reveals two trends. The first trend was observed from examining the variability of the resistivity of the printed samples. As the microstructure becomes more conductive, there is less variability. In the case of microparticle loaded inks, conduction through percolation yields a more variable situation than conduction through grainy film. The trend of a decrease in variability as the resistivity lowers is also observable in the processing of printed lines composed of nanoparticle loaded ink though not as pronounced as the trend observed in the microparticle loaded ink experiments. The second observable trend is a decrease in resistivity in inkjet printed lines when the pattern is printed two or more times prior to the application of the thermal curing process. Figure 3.11 is a

graphical representation of the resistivity for some experiments in this study and allows for a comparison between the electrical performance of microparticle and nanoparticle loaded inks.

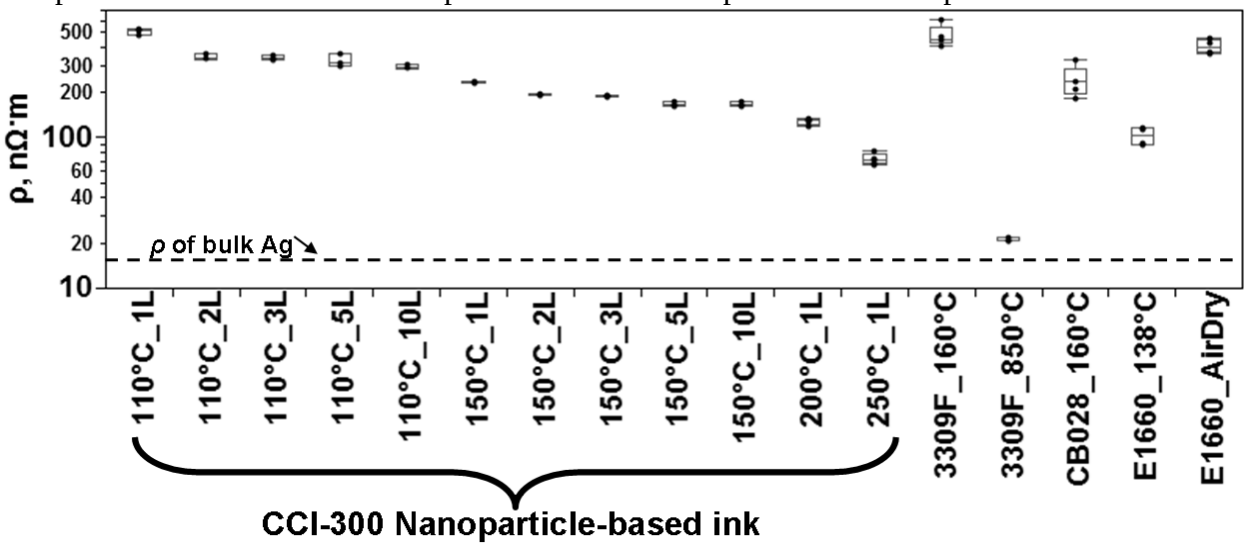

Figure 3.11: Comparison of resistivity (ρ) measurements for experiments conducted in this study.

When deciding which ink type to use, the electrical performance is only one parameter to consider along with the recommended curing temperature. From the graph in Figure 3.11, the electrical performance in terms of resistivity of the Ercon E1660 is comparable to the nanoparticle loaded ink tested in this study. However, in terms of the micro (or nano) constituents of the ink, the minimum feature size is limited by the large particle size within the ink—as large as 10μm in diameter according to the measured size distribution in Figure 3.2. Obviously, if submicron features are desired, the ink utilized would have to be composed of submicron particles though a printing technique other than inkjet would be needed as the minimum feature size of this process is greater than 1μm [31, 32].

3.4 Conclusions

The microstructures, which arise as a result of the thermal processing of Ag particle loaded inks, play a role in the overall electrical performance of printed conductive traces. The key enabler for the most conductive microstructure observed in the experiments performed in

this paper was high temperature processing (greater than half the melting temperature of the conductive particles) of the printed traces. The thermal processing in this temperature regime can only be withstood by rigid ceramic substrates. The dominant characteristic of this microstructure are grains of 5μm in diameter.

An observable trend in the decrease in sample set variability with an increase in conductivity exists in the processing of microparticle loaded conductors that corresponds with a microstructural change incurred by the thermal processing of printed traces. The trend is not as clear when examining the resistivity of lines created from the inkjet printing of nanoparticle loaded ink due to the lack of homogeneity of the microstructure at the edge of the printed lines.

Despite the fact lines created via inkjet printing of Ag nanoparticle loaded ink have the ability to attain a more conductive microstructure due to the ability of the nanoparticles to undergo sintering at low temperatures, lines created with Ag microparticle based inks (particles on the order of 5μm) will have a similar resistivity. In the case of nanoparticle loaded inks, once a sintered film is attained, temperatures on the order of 460°C would be required to obtain a coarse grain structure.

A profound nuance of inkjet printed traces is that the number of layers printed before curing results in a decrease in the measured resistivity of the conductive trace. The reduction in resistivity may be due to the densification of the packing of the nanoparticles resulting from the additional of layers. The densification results in a higher contact area between the individual particles which will enhance conduction through percolation when sintering has not occurred. The sintering process is enhanced by increasing the amount of layers printed which may also be due to more contact between the Ag nanoparticles which would enhance the diffusion mechanisms driving the sintering process.

3.5 References

[1] B. K. Park, D. Kim, S. Jeong, J. Moon, and J. S. Kim, “Direct writing of copper conductive

patterns by ink-jet printing," *Thin Solid Films*, vol. 515, no. 19, pp. 7706-7711, Jul. 2007.
[2] Y. Zhang, C. Liu, and D. Whalley, "Direct-write techniques for maskless production of microelectronics: A review of current state-of-the-art technologies," in *Electronic Packaging Technology & High Density Packaging, 2009. ICEPT-HDP '09. International Conference on*, 2009, pp. 497-503.
[3] M. Pudas, N. Halonen, P. Granat, and J. Vähäkangas, "Gravure printing of conductive particulate polymer inks on flexible substrates," *Progress in Organic Coatings*, vol. 54, no. 4, pp. 310-316, Dec. 2005.
[4] S. Merilampi, T. Laine-Ma, and P. Ruuskänen, "The characterization of electrically conductive silver ink patterns on flexible substrates," *Microelectronics Reliability*, vol. 49, no. 7, pp. 782-790, Jul. 2009.
[5] H.-H. Lee, K.-S. Chou, and K.-C. Huang, "Inkjet printing of nanosized silver colloids," *Nanotechnology*, vol. 16, no. 10, pp. 2436-2441, Oct. 2005.
[6] B. Li, P. A. Clark, and K. H. Church, "Robust Direct-Write Dispensing Tool and Solutions for Micro/Meso-Scale Manufacturing and Packaging," *ASME Conference Proceedings*, vol. 2007, no. 42908, pp. 715-721, Jan. 2007.
[7] D. Tobjörk, N. J. Kaihovirta, T. Mäkelä, F. S. Pettersson, and R. Österbacka, "All-printed low-voltage organic transistors," *Organic Electronics*, vol. 9, no. 6, pp. 931-935, Dec. 2008.
[8] J.-W. Kim *et al.*, "Characterization of direct patterned Ag circuits for RF application," *Microelectronic Engineering*, vol. 87, no. 3, pp. 379-382, Mar. 2010.
[9] R. O. Kadara, N. Jenkinson, B. Li, K. H. Church, and C. E. Banks, "Manufacturing electrochemical platforms: Direct-write dispensing versus screen printing," *Electrochemistry Communications*, vol. 10, no. 10, pp. 1517-1519, Oct. 2008.
[10] S. Kirkpatrick, "Percolation and Conduction," *Reviews of Modern Physics*, vol. 45, no. 4, p. 574, Oct. 1973.
[11] V. K. S. Shante and S. Kirkpatrick, "An introduction to percolation theory," *Advances in Physics*, vol. 20, no. 85, p. 325, 1971.
[12] R. F. Saraf, J. M. Roldan, R. Jagannathan, C. Sambucetti, J. Marino, and C. Jahnes, "Polymer/metal composite for interconnection technology," in *Electronic Components and Technology Conference, 1995. Proceedings., 45th*, 1995, pp. 1051-1053.
[13] J. R. Greer and R. A. Street, "Thermal cure effects on electrical performance of nanoparticle silver inks," *Acta Materialia*, vol. 55, no. 18, pp. 6345-6349, Oct. 2007.
[14] D. Kim and J. Moon, "Highly Conductive Ink Jet Printed Films of Nanosilver Particles for Printable Electronics," *Electrochemical and Solid-State Letters*, vol. 8, no. 11, p. J30-J33, Nov. 2005.
[15] R. D. Mancosu, J. A. Q. Quintero, and R. E. S. Azevedo, "Sintering, in different temperatures, of traces of silver printed in flexible surfaces," in *Thermal, Mechanical & Multi-Physics Simulation, and Experiments in Microelectronics and Microsystems (EuroSimE), 2010 11th International Conference on*, 2010, pp. 1-5.
[16] P. Buffat and J.-P. Borel, "Size effect on the melting temperature of gold particles," *Physical Review A*, vol. 13, no. 6, p. 2287, Jun. 1976.
[17] S. Zhao, S. Wang, and H. Ye, "Size-Dependent Melting Properties of Free Silver Nanoclusters," *Journal of the Physical Society of Japan*, vol. 70, pp. 2953-2957, 2001.
[18] C. C. Yang and S. Li, "Size-Dependent Phase Stability of Silver Nanocrystals," *The Journal of Physical Chemistry C*, vol. 112, no. 42, pp. 16400-16404, Oct. 2008.

[19] J. Wang, H. L. Duan, Z. P. Huang, and B. L. Karihaloo, "A scaling law for properties of nano-structured materials," *Proceedings of the Royal Society A: Mathematical, Physical and Engineering Science*, vol. 462, no. 2069, pp. 1355 -1363, May. 2006.

[20]. *DuPont Kapton® HN polyimide film Technical Data Sheet*, DuPont, Wilmington, DE, 2011, p. 3.

[21] *Ferro 3309F Silver Conductor Technical Data Sheet*, Ferro Corporation, Cleveland, OH, 2001, p. 1.

[22] *DuPont CB028 Silver Conductor Technical Data Sheet*, Du Pont, Wilmington, DE, 2009, p. 1.

[23] *Ercon E1660; Technical Data Sheet*, Ercon Incorporated, Wareham, MA, 2007, p. 1.

[24] M. Navarette, A. Lopes, J. Acuna, R. Estrada, E. MacDonald, J. Palmer, R. Wicker, "Integrated Layered Manufacturing of a Novel Wireless Motion Sensor System with GPS," in *Proceedings of the 2009 Solid Freeform Fabrication Symposium*, Austin, Texas, pp. 575-585, 2007.

[25] S. O. Kasap, "Electrical and Thermal Conduction in Solids," in *Principles of Electrical Engineering Materials and Devices*, New York, NY: Irwin McGraw Hill, 1997, p. 113.

[26] D. Bregiroux, F. Audubert, and D. Bernache-Assollant, "Densification and grain growth during solid state sintering of LaPO4," *Ceramics International*, vol. 35, no. 3, pp. 1115-1120, Apr. 2009.

[27] A. D. Albert, M. F. Becker, J. W. Keto, and D. Kovar, "Low temperature, pressure-assisted sintering of nanoparticulate silver films," *Acta Materialia*, vol. 56, no. 8, pp. 1820-1829, May. 2008.

[28] X. Y. Qin, W. Zhang, L. D. Zhang, L. D. Jiang, X. J. Liu, and D. Jin, "Low-temperature resistance and its temperature dependence in nanostructured silver," *Physical Review B*, vol. 56, no. 16, pp. 10596-10604, Oct. 1997.

[29] C. Huang, M. F. Becker, J. W. Keto, and D. Kovar, "Annealing of nanostructured silver films produced by supersonic deposition of nanoparticles," *Journal of Applied Physics*, vol. 102, no. 5, p. 054308:1-054308:8, 2007.

[30] *Cabot Conductive Ink CCI-300 Data Sheet*, Cabot Printed Electronic Materials, Albuquerque, NM, 2009, p. 2.

[31] J. Stringer and B. Derby, "Limits to feature size and resolution in ink jet printing," *Journal of the European Ceramic Society*, vol. 29, no. 5, pp. 913-918, Mar. 2009.

[32] H.-T. Wang *et al.*, "Toward conductive traces: Dip Pen Nanolithography® of silver nanoparticle-based inks," *Applied Physics Letters*, vol. 93, no. 14, p. 143105:1-143105:3, 2008.

CHAPTER 4: OHMIC CURING OF PRINTED CONDUCTIVE TRACES

4.1 Introduction

The use of conductive ink in the production of electronic systems allows for printing methods, such as inkjet, direct print and rotogravure to be utilized in place of traditional metallization processes. The ability to produce working components created solely from printing methods has been demonstrated for RFIDs [1] and more complex semiconductor devices such as junction transistors [2]. Fabrication of electronic systems through the exclusive use of printing techniques is an attractive manufacturing method as the number of processing steps required to produce electronics is less than either semiconductor or printed circuit board technologies. These traditional technologies use many complex processes including deposition, lithography and etch—all of which introduce inherent waste. Additionally, printing technologies can be performed in ambient conditions with no requirement for vacuum or clean-room processing; the removal of which substantially reduces both cost and complexity.

As compared to traditional deposition techniques, conductive traces created from printed ink suffer from lower conductivity due to dependence on thermal cure processes. The lower conductivity places importance on the characterization of new cure processing techniques designed to enhance the electrical performance of printed conductive traces. The utilization of conductive inks opens the door to applications requiring the use of polymeric substrates, which provide physical flexibility but at the expense of placing temperature limitations on thermal processes used to convert the ink into a conductive state. The process of applying thermal energy in the curing of conductive ink has been well characterized [3–5] where increasing the curing temperature increases the conductivity of the printed trace. The key drawbacks to thermally curing conductive inks are time and the limitations to maximum cure temperature imposed by the substrate in question, particularly if polymeric substrates are to be used which are currently garnering significant interest in the context of the emerging field of flexible electronics.

The exploration into multiple curing methods of particle based conductive inks has proven the viability applying different forms of energy—photonic and microwave for instance—in order to achieve a microstructure (namely sintering of the conductive particles) favorable to electrical conductivity. One example is the utilization of lasers in which it has been found that increasing laser power and exposure time produces printed conductive traces with lower resistance—analogous to the time and temperature relationship in the thermal cure process [6,7]. Laser frequency has also been found to have an influence on the laser curing process [8]. One disadvantage of using lasers is that curing time is proportional with the total length and width of the traces to be cured [8]. Microwaves have also been proven as a viable option in curing printed conductive traces, though pre-drying and the shape of the printed pattern have a strong effect on the effectiveness of the processing [9,10]. In the examples of the use of lasers and microwaves where nanoparticle inks were used, the resulting microstructure was sintered particles. Furthermore, both of the above methods produce a conductive trace with equivalent electrical performance when compared to thermal curing, but in a fraction of the time.

The study in this paper presents a simple method of curing via the application of electrical current across a conductive trace to produce ohmic heating in order to cure traces printed from ink. The scientific goal of this study is to explore the exploitation of an intrinsic property—in this case the resistance of the printed trace—in order to improve the electrical properties of a printed conductive trace. The novelty of the ohmic curing method is that instead of applying external thermal, microwave or photonic energy to the conductive trace (which is then transferred into heat), heat is transferred within the trace upon the application of electrical current due to the resistance of the trace itself. The conversion of a gold particle suspension from a non-conducting state to a conducting state through the application of voltage has been demonstrated and electrically characterized by Sivaramakrishnan *et al.* [11] where the particles were angstrom-scale. Creating a sintered microstructure from deposited silver nanoparticles through the application of voltage across a short path has been demonstrated as a viable method for creating “wire-like” structures in lieu of printing by Mattila *et al.* [12]. The technique of

"electrical sintering" of printed traces composed of silver nanoparticle ink where traces of up to 5mm in length were shown to have undergone sintering upon the application of DC voltage was demonstrated by Allen *et al.* [13]. While these approaches are good examples of clever methods to rapidly create sintered structures capable of acting as a conductive path, no characterization of the use of ohmic heating as a curing method for printed conductive traces has been previously performed over a broad range of ink types and initial conditions.

Contrary to prior work which demonstrates sintering only, the work presented here deals with curing, sintering, improving the conductivity of pre-sintered traces, as well as demonstrating the phenomena of grain growth. All the while demonstrating the use of ohmic heating to improve the conductivity of printed traces composed of micro and nano particle loaded conductive inks. Sintering is not the end goal, but rather, the decrease of the electrical resistivity of a printed trace is. Two printing techniques were utilized; direct print and inkjet. The advantage ohmic curing has over conventional thermal curing in an oven is the conductive trace essentially acts as a heating element localizing the transferred heat to the area around the conductive trace and thus allows for a wider range of substrate materials. Furthermore, ohmic curing can be implemented in a fraction of the time of traditional oven curing. A potential drawback to ohmic curing is that physical contact must be established at both ends of the trace with an electrical current source. However, the application of electric current via conventional integrated circuit test equipment and a bed of nail fixture could be reasonably utilized to perform ohmic curing in a manufacturing setting.

Experiments were carried out to characterize the ohmic curing process and it should be noted that in order for ohmic curing to occur, the traces must first be in a relatively conductive state. For this reason, all experiments involve some pre-processing to establish an initial level of conductance prior to the application of electrical current. The first two experiments involved two microparticle conductive inks, which only required air-drying to provide sufficient conductance prior to the application of ohmic curing. Results of ohmic curing, in the form of resistivity measurements, were compared to the results of conductive traces cured to the ink

manufacturer specifications in an oven. Experiments three and four involved two different nanoparticle inks thermally cured to a temperature which was limited to the maximum allowable by a polycarbonate substrate (glass transition temperature, T_g, of 150°C) [14] to demonstrate the use of ohmic curing as a post cure process to overcome thermal limitations imposed by the substrate and also to demonstrate the ability of ohmic curing to improve the conductivity in printed traces which have already undergone a sintering process. In order to understand the influence of time and cycling on ohmic curing, computer automated experiments were carried out on one of the two nanoparticle inks and measured in real time. Scanning electron microscopy (SEM) was used to characterize the microstructural changes in each experiment resulting from the curing of the printed traces. Finally, a sixth experiment involving the variation of the length of the printed trace was carried out in order to discover the effect of length on the ohmic curing process.

4.2 Experimental

For all experiments, applied electric current was supplied by a Kepco model ABC 25-4DM programmable power supply (Kepco, Inc, Flushing, NY, USA). Resistance measurements were taken with a Fluke model 289 True RMS multimeter (Fluke Corporation, Everett, WA, USA). The probes used to measure the resistance and apply electrical current were copper toothless alligator clips model number 7236K51 available from McMaster-Carr (McMaster-Carr, Elmhurst, Il, USA) measuring 1.5mm wide. Contact resistance was determined to be negligible by printing the pattern seen in Figure 4.1(b) in lengths varying from 1cm to 5cm and subjecting the patterns to three different cure temperatures, 110°C, 150°C and 200°C to enable testing on different cure conditions. The resistance of these three sample sets was measured and plotted against the length of the printed line. Linear regression shows convergence near zero (Fig. 4.1(c)) meaning the contact resistance is negligible.

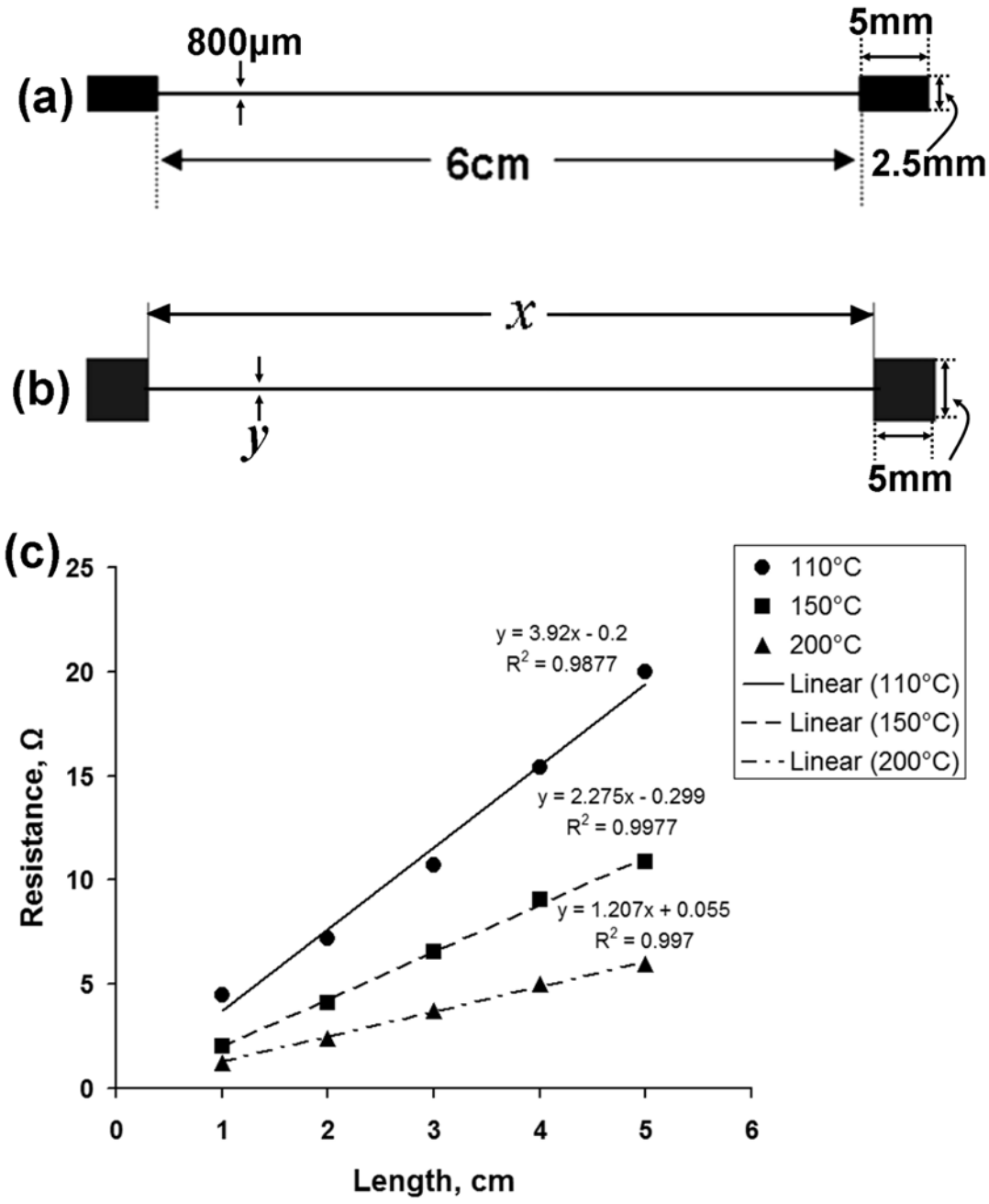

Figure 4.1: Test patterns used in this study **(a)** pattern used in experiments three and four, **(b)** pattern used in all other experiments where x = 6cm and y = 250µm for the microparticle inks used in experiments one and two, x = 5cm and y = 800µm for real time measurement experiments and x varied between 1 and 10cm in the length study. The linear interpolation of the measured resistance values **(c)** of a thermally cured length study show the contact resistance between the test pad and probes to be negligible.

The procedure for determining volume resistivity can be found in Roberson *et al.* [15] and entails the use of a stylus profilometer to measure the cross sectional area of the printed conductive trace to calculate the resistivity based on the following equation:

$$\rho = R\frac{A}{l} \tag{4.1}$$

where ρ is resistivity, R is the measured resistance of the conductive trace, A is the cross-sectional area of the conductive trace and l is the length of the conductive trace. SEM microanalysis was performed on samples from each experiment with a Hitachi S-4800 Ultra-high Resolution Field Emission Scanning Electron Microscope (Hitachi High-Technologies Corporation, Tokyo, Japan) utilizing a 20keV accelerating voltage. In order to reduce the effects of charging due to the polymeric substrate, all samples were treated to Au/Pd sputtering for 30s with a Gatan Model 682 Precision Etching Coating System (Gatan, Inc., Pleasanton, CA, USA). The microparticle inks used in this study were able to achieve conductivity through air drying at room temperature. Reliable conductivity through air-drying could not be achieved for the nanoparticle inks used in this study so each experiment having to do with nanoparticle ink involved some initial thermal cure. Thermal curing was performed in a VWR Signature™ Horizontal Air Flow Oven model 1370FM (VWR International, West Chester, PA, USA).

Microparticle Inks

A simple "dog bone" test pattern (Figure 1(b)) in the form of a 6mm long straight line measuring 250μm in width with two test pads on either end was utilized in experiments involving microparticle inks. The patterns were created via a direct print technique using an nScrypt 3Dn 450 micro-dispensing system (nScrypt, Inc., Orlando, Florida, USA). The first ink used was DuPont CB028 Silver Conductor, (DuPont, Wilmington, DE, USA). The size of the silver particles in this ink has been measured to be 1.7μm ± 1μm.[15] DuPont Kapton® polyimide film was utilized as a substrate material. The thickness of the lines printed from this ink was ~5.5μm. The printed patterns were allowed to dry at room temperature for seven days as

this ink type was able to achieve conductivity in an air-dried state. Though the drying time may seem excessive, the point of this experiment was to demonstrate the use of ohmic curing as a complete replacement for thermal curing. Initial resistance measurements were taken with a multimeter.

The samples were then divided into sets of five for three ohmic cure experiments and one thermal cure experiment. The thermal cure experiment was intended to act as a benchmark for the ohmic cure experiments. The parameters for the thermal processing of the benchmark sample set, 160°C for 1h were based on the manufacturer recommended curing parameters [16]. For the three ohmic cure experiments, electric current was applied to the conductive trace by placing positive and negative probes on the pad structures at each end of the printed lines. A trial and error process was used to determine the experimental parameters—in this case, time and current density—for each sample set. The three ohmic curing experiments were performed under the following parameters: 1) current density of 0.35mA/μm^2 for 1min, 2) current density of 0.35mA/μm^2 for 30s and 3) current density of 0.5mA/μm^2 for 30s. The method used to evaluate the ohmic cure experiments was comparing the resistivity measured after pre-processing with the resulting measured resistivity of the three ohmic cure experiments and the thermally cured benchmark experiment.

The second microparticle silver ink used was Ercon E1660 (Ercon Incorporated, Wareham, MA USA). The composition of this ink is 68 wt% silver loading in a modified polyester binder [17]. The size of the silver particles in this ink has been measured to be 4.8μm ± 2.8μm [15]. The thickness of the lines printed from this ink was measured to be ~5.7μm. As was the case in experiments involving DuPont CB028, test patterns were printed via direct print on a Kapton® substrate and allowed to air dry for 7 days. Four samples were thermally cured at 138°C for 30min based on optimum curing parameters for this ink found in literature [8,18]. Trial and error led to the experimental parameters for ohmic curing cycles of 0.30mA/μm^2 to be applied for 30s. Reduction in resistance over the initial air dried state was compared between thermal and ohmic cured samples.

Pre-cured Nanoparticle Inks

To explore the effectiveness of ohmic curing on lines printed from low viscosity inks, the inkjet process was used to create conductive traces from nanoparticle inks. Experiments were designed around the thermal constraint of a polycarbonate substrate which has a T_g of 150°C [14]. These experiments had the intent of examining the effect of utilizing ohmic curing in combination with another curing method—in this case, thermal curing with a restrictive temperature limit. The first ink used was a commercially available silver/copper nanoparticle ink from Cima NanoTech, IJ242-54, (Cima NanoTech, St. Paul, MN, USA). The composition of this ink is 50 wt% conductor loading in an ethylene glycol butyl ether acetate binder while the size of the conducting particles is 50nm [19]. The "dogbone" pattern seen in Figure 1(a) was printed on DuPont Kapton® polyimide film with a Dimatix 2800-Series Materials Printer (Fujifilm Dimatix, Inc, Santa Clara, CA, USA). The substrates were first treated with UV-ozone by a UVO Cleaner Model 342A (Jelight Company, Inc, Irvine, CA, USA) for 5min to ensure a clean surface and to aid in the ink adhesion. The thickness of the lines printed from this ink was measured to be ~350nm. All patterns were initially thermally cured at 150°C (the T_g of polycarbonate) for 20h. The resistance of the printed lines was then measured with a multimeter. Two sample sets were selected for additional ohmic curing. A trial and error process led to the selection of the experimental parameters applied to these sample sets of five samples: the application of a current density of $0.40 mA/\mu m^2$ for 30s and another with the same current density but for only a 3s duration. To understand how the application of ohmic curing compared to curing lines at a higher unrestricted curing temperature, a third sample set of five samples received no ohmic curing but instead was subjected to an additional thermal cure cycle of 250°C for 1h which is the maximum temperature specified by the manufacturer [19]. Again, this temperature would preclude the use of a polycarbonate substrate but was included for completeness. The measured resistance was then compared between the three curing experiments.

The same experiment with the thermal constraint of 150°C was repeated using a second commercially available nanoparticle ink, Cabot CCI-300 silver conductive ink (Cabot Corporation, Albuquerque, NM, USA). The composition of this ink is 19 to 21 wt% conductor loading in an alcohol-based binder [20]. The size of the silver particles has been measured to be 37nm ± 10nm [15]. The test pattern was printed with a Dimatix 2800-Series Materials Printer on DuPont Kapton® polyimide film and the thickness of the printed lines measured to be ~600nm. Prior to printing, the substrates were treated with UV-ozone for 10min by a UVO Cleaner Model 342A. The printed lines were thermally cured at 150°C for 20h. Resistance measurements were then taken. Two sample sets of five samples were subjected to additional ohmic curing cycles. Trial and error led to two experiments to be carried out with the following parameters: 1) an applied current density of 1.2mA/μm^2 for 30s and 2) an applied current density of 1.7mA/μm^2 for 30s. The applied current densities were much higher compared to the Cima NanoTech IJ242-54 ink because the initial resistance values were lower for the traces printed from the Cabot CCI-300 ink and therefore a higher current density was required to produce an equivalent level of ohmic heating. As was done with the experiment involving the Cima NanoTech IJ242-54 ink, an additional sample set of five samples was not processed by ohmic curing but instead to an unrestricted thermal curing cycle of 250°C for 1h to act as a comparison between curing at a higher thermal temperature and the ohmic curing process.

Real-time Measurement Experiments

Real-time measurements of electrical parameters were obtained by connecting the power supply to a personal computer (PC) by way of a National Instruments SC-2345 Signal Conditioning Connector Block (National Instruments, Austin, TX, USA). The pattern in Figure 1(b) was printed via inkjet in a 5cm long length using Cabot CCI-300 conductive ink. The Patterns were first oven dried for 1h at 110°C and then subjected to ohmic curing. Cabot CCI-300 was chosen for these experiments due to the low resistance values attained after drying the ink at 110°C. The curing temperature of 110°C was chosen as this temperature was discovered

to be the maximum curing temperature which will not result in the sintering of the particles. The unsintered state was desired as a starting point because the goal of this experiment was to characterize the ohmic curing process from the lowest conductive state possible from a microstructural point of view to observe the effects of ohmic curing. This is similar to work performed by Allen *et al.* [13] where the application of voltage was intended to induce the sintering of silver nanoparticles. Three experiments were performed and current density was applied using two procedures in order to characterize the curing process. The first procedure was the application of static current densities of $0.33mA/\mu m^2$ and $0.66mA/\mu m^2$ in multiple cycles of 10s. The second procedure included ramping the current density from $0.33mA/\mu m^2$ to $0.66mA/\mu m^2$ in multiple cycles of 20s.

The Effect of Length on the Ohmic Curing Process

The pattern in Figure 1(b) was printed in 1cm increments from 1cm to 10cm again utilizing Cabot CCI-300 ink in order to understand the effect of length on the ohmic curing process. As was the case in the real-time measurement experiments, the conductive traces were first dried at 110°C for 1h. The maximum applied current value of 500mA which was applied to the 5cm lines used in the real-time measurement experiments was used as a baseline for scaling the electrical current applied to the traces used in the length study. The duration of the ohmic curing cycles was 10s and the sample size for each line length was four.

4.3 Results and Discussion

Microparticle Inks

The numerical results of the ohmic experiments performed on the direct print DuPont CB028 lines are listed in Table 4.1. In terms of resistivity, the application of a current density of $0.35mA/\mu m^2$ for 1min and 30s had similar results as samples which were cured for 1h at 160°C as all three experiments resulted in a resistivity of ~125nΩ•m which is roughly 9 times the resistivity of bulk silver—14.6nΩ•m [21]. The similar results suggest the ohmic curing process is able to produce electrical performance on par with recommended thermal processing

parameters while completely avoiding oven curing. Samples processed with an application of a current density of 0.5mA/μm^2 resulted in a resistivity of 80nΩ•m (~36% less than the thermally cured samples) and implies the potential of ohmic curing to create traces with higher conductivity than thermally cured traces when the temperature is restricted based on the application. In terms of the microstructure (Figs. 2(a) and (b)) there were no visible signs of melting or particle sintering. The comparison made in the SEM micrographs in Figures 2(a) and 2(b) is between a sample from the highest current density experiment (0.5mA/μm^2) and a thermally cured sample, respectively. There were no apparent differences in microstructure between the samples cured by ohmic curing sample and the thermally cured samples.

Table 4.1: The critical electrical and thermal parameters and sample sizes (N) for experiments one through four.

Ink type	***Initial Pre Process***	***Mean Resistivity After Pre Process, nΩ·m***	***Applied Current Density, mA/μm^2***	***Applied Current, mA***	***Duration of Current application, s***	***Mean Resistivity after ohmic curing, nΩ·m***	***Mean Resistivity of thermal behcnmark samples, nΩ·m***
Ag Microparticle CB028	Air dried at room temp. for 7 days.	253 ± 31	0.35	500	30	129 ± 11 N = 5	130 ± 11 N = 5 160°C for 1h
Ag Microparticle CB028	Air dried at room temp. for 7 days.	253 ± 31	0.35	500	60	119 ± 10 N = 5	
Ag Microparticle CB028	Air dried at room temp. for 7 days.	253 ± 31	0.50	750	30	76 ± 1.2 N = 5	
Ag Microparticle E1660	Air dried at room temp. for 7 days.	406 ± 45	0.30	500	30	143 ± 33 N = 6	103 ± 14 N = 4 138°C for 30min
Ag/Cu Nanoparticle IJ242-54	Oven cured at 150°C for 20h	2612 ± 229	0.40	150	30	358 ± 24 N = 5	746 ± 124 N = 5 250°C for 1h
Ag/Cu Nanoparticle IJ242-54	Oven cured at 150°C for 20h	2612 ± 229	0.40	150	3	336 N = 1	
Ag Nanoparticle CCI-300	Oven cured at 150°C for 20h	89 ± 6	1.20	500	30	69 ± 4 N = 5	42 ± 1.5 N = 5 250°C for 1h
Ag Nanoparticle CCI-300	Oven cured at 150°C for 20h	89 ± 6	1.70	750	30	40 ± 0.4 N = 5	

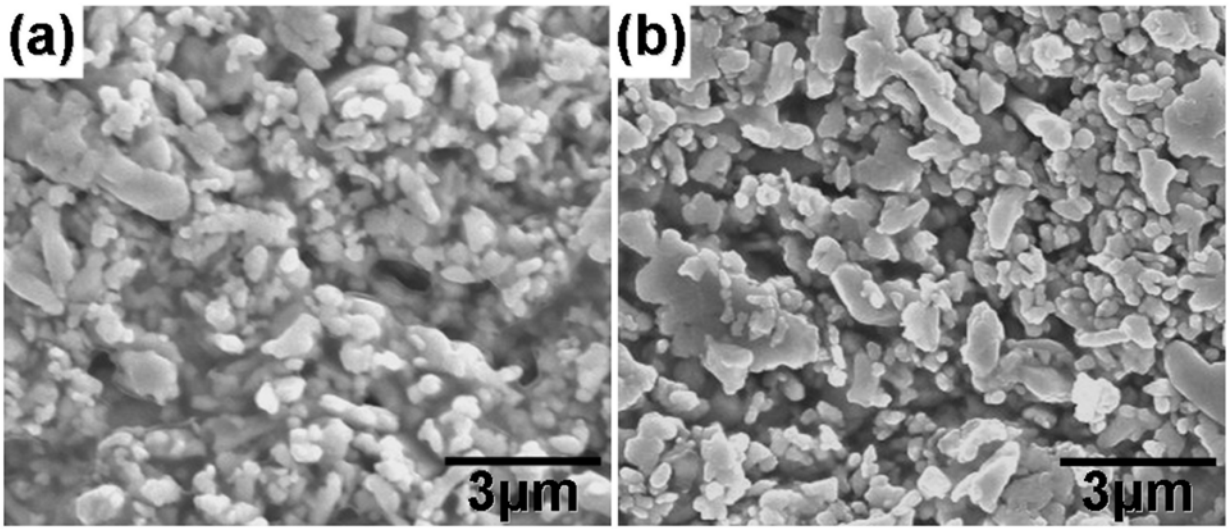

Figure 4.2: SEM Micrographs of **(a)** DuPont CB028 ink processed by the application of a current density of 0.5mA/μm^2 for 30s and **(b)** CB028 ink thermally cured for 1h at 160°C.

Results for experiments involving the second microparticle ink, Ercon E1660, are shown in Figure 4.3 and it can be seen that in terms of resulting resistivity, ohmic curing matched the results of thermally curing for only a few samples. Further investigation revealed the samples, which did not respond as well to the ohmic curing process, to have a line with variation—defined by the coefficient of variation (CV) of eight random width measurements) of 10% or more whereas lines which responded well to the ohmic curing process possessed a line width variation of 4%. Also observed on the poor performing samples was localized discoloration within the printed trace. Analysis via SEM reveals the discolored region to have undergone melting as seen in Figure 4.3(c). The localized discoloration was not observed on lines with low line width variation and no microstructural change was observed as seen by the comparison made between a thermally cured sample and a sample that underwent ohmic curing in Figures 4.3(a) and (b) respectively. It must be pointed out that sensitivity to line width variation is a potential drawback to the ohmic curing process. However, despite the non-homogeneous microstructure, the average resistivity dropped from 400 to 164nΩ•m for the ohmic cured lines with high line

width variation compared to 100nΩ•m for the lines with low line width variation. The variation in measured line width for the other experiments in this study were 5% and below.

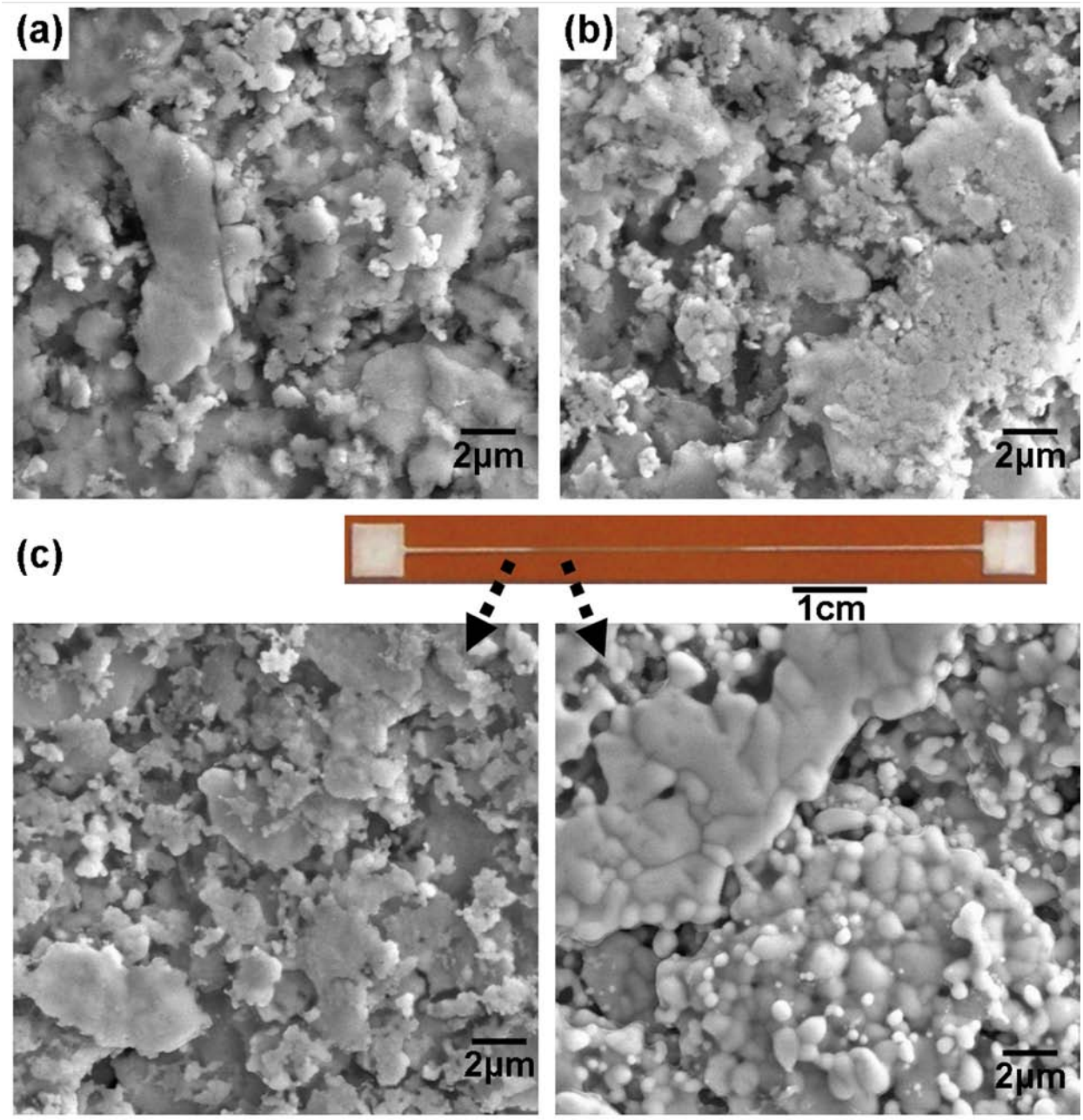

Figure 4.3: SEM micrographs illustrating the microstructure of Ercon E1660 lines **(a)** after air drying for 7 days **(b)** an additional thermal cure cycle of 138°C for 30min and **(c)** a line subjected to an ohmic cure cycle with a current density of 0.30mA/μm^2 for 30s. Note that the discoloration seen in **(c)** corresponds to localized melting observed on samples with high line width variation.

Pre-cured Nanoparticle Inks

The application of ohmic curing after the initial pre-cure at 150°C for 20h to inkjet printed lines of Cima NanoTech IJ242-54 resulted in an average decrease in measured resistivity from 2772nΩ•m to 300nΩ•m. The additional unrestricted thermal cycle of 250°C, reduced the measured resistivity to an average of 622nΩ•m and was therefore less effective than ohmic curing. The numerical results of these experiments are listed in Table 4.1. The microstructural differences which resulted from the different processing methods are apparent in Figure 4.4(a). There was little change in the microstructure of the ink particles after an additional higher temperature thermal cure cycle, but after the application of a current density of 0.40mA/μm^2 for 30s, a non-homogenous microstructure consisting of grains and sintered particles was observed. During the application of current, a color change was noted within the printed line. For one sample, the application of current was discontinued once the color change was noticed, which in this case was 3s. The color change is observable in Figure 4.4(b) and it is notable that the change in color is only over the entire length of the trace area and not in the contact pad area. Also, based on the results depicted in Figure 4.3, we have learned that color change means a microstructural change has occurred meaning the energy converted by resistance heating during the ohmic curing process is limited to the conductive trace. The difference in microstructure between the test pad and the cured conductive trace is observable by comparing Figures 4.4(c) and (d).

The numerical data in Table 4.1 show that the 3s ohmic cure experiment yielded results similar to the 30s cure experiment based on comparing the resistivity. Furthermore, a similar microstructural change was observed for the 3s sample as seen in Figure 4.4(d). As stated earlier, the color change observed in the samples cured by ohmic heating is the result of the microstructural change which occurred as a result of the curing process. No color change was observed on the samples subjected to the additional thermal cure cycle of 250°C for 1h as there was no microstructural change as seen in Figure 4.4(c).

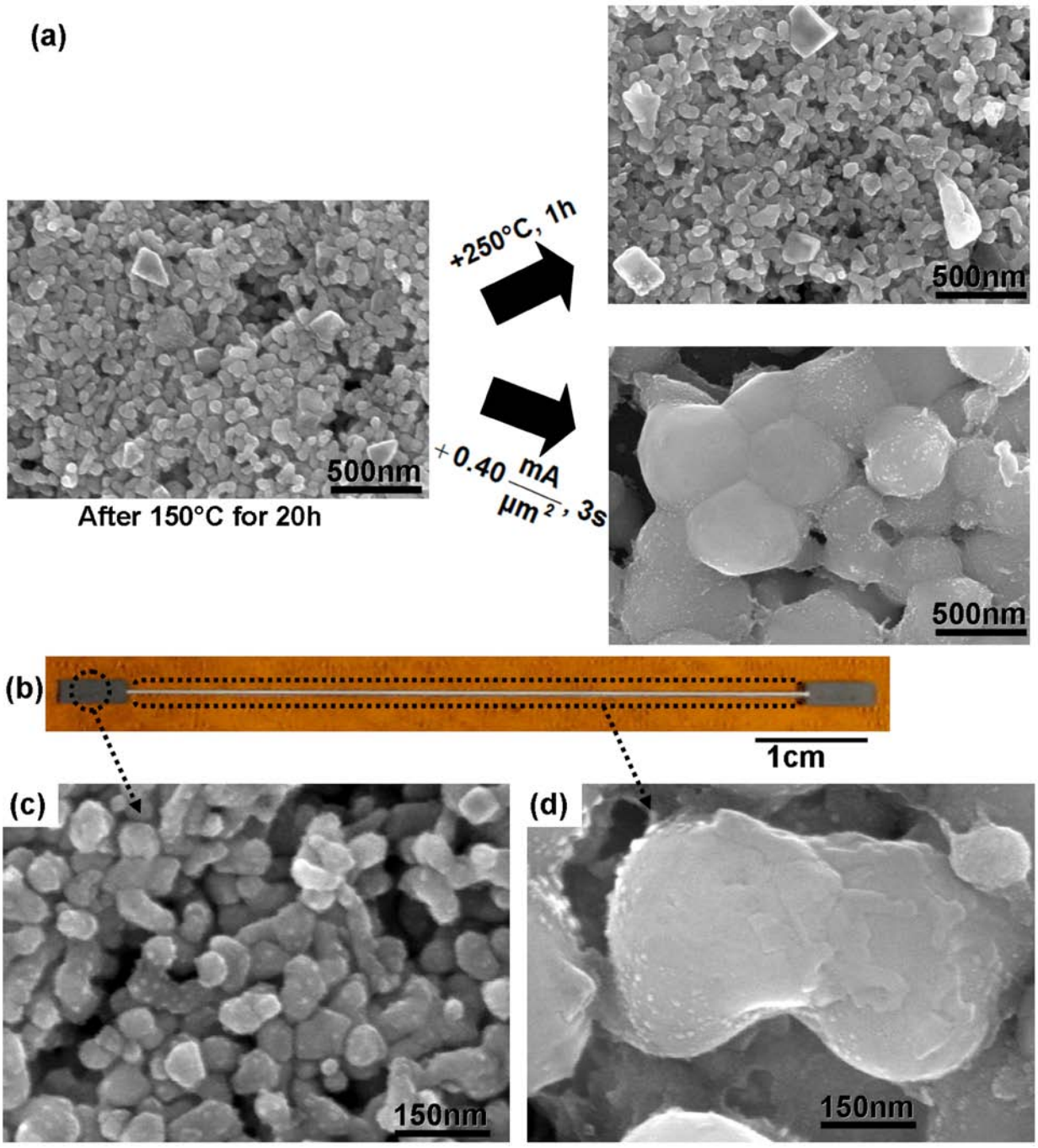

Figure 4.4: The change in microstructure **(a)** which occurs as a result of an additional thermal cycle of 250°C for 1h compared to a 3s ohmic curing cycle with a current density of 0.40mA/μm^2 for Cima NanoTech ink printed lines. The color change **(b)** was observed in as little as 3s and limited only to the conductive trace and not observed on thermally cured samples. SEM micrographs showing the microstructural difference between **(c)** the test pad and **(d)** the conductive trace after the application of a current density of 0.40mA/μm^2 for 30s.

The application of ohmic curing to printed lines of Cabot CCI-300 nanoparticle ink after initially curing the lines for 20h at 150°C also resulted in a decrease in measured resistance of the printed traces. After the initial pre cure, the measured resistivity of the printed lines averaged 83nΩ•m. The numerical results of the additional ohmic cure cycles are listed in Table 4.1 and show that for an applied current density of 1.2mA/μm^2 for 30s, the measured resistivity of the printed lines is reduced to an average of 65nΩ•m for the sample set of five. Increasing the current density to 1.7mA/μm^2 resulted in an average drop in measured resistivity to 43nΩ•m, roughly 3 times the resistivity of bulk silver. The application of 1.7mA/μm^2 for 30s resulted in a similar drop in measured resistivity as the application of an additional cure cycle of 250°C for 1h and demonstrates the use of ohmic curing in conjunction with an initial low temperature thermal curing cycle to achieve an electrical performance which could only be achieved by thermally curing at a higher temperature. Additionally, according to the manufacturer, the minimum resistivity attainable for CCI-300 based on thermal curing is 40nΩ•m [21]. The microstructural changes are seen in Figure 4.5 and it was observed that the initial thermal cure cycle of 150°C created a sintered state. The application of additional ohmic curing cycles resulted in the densification of the microstructure as did the application of an additional thermal cure cycle.

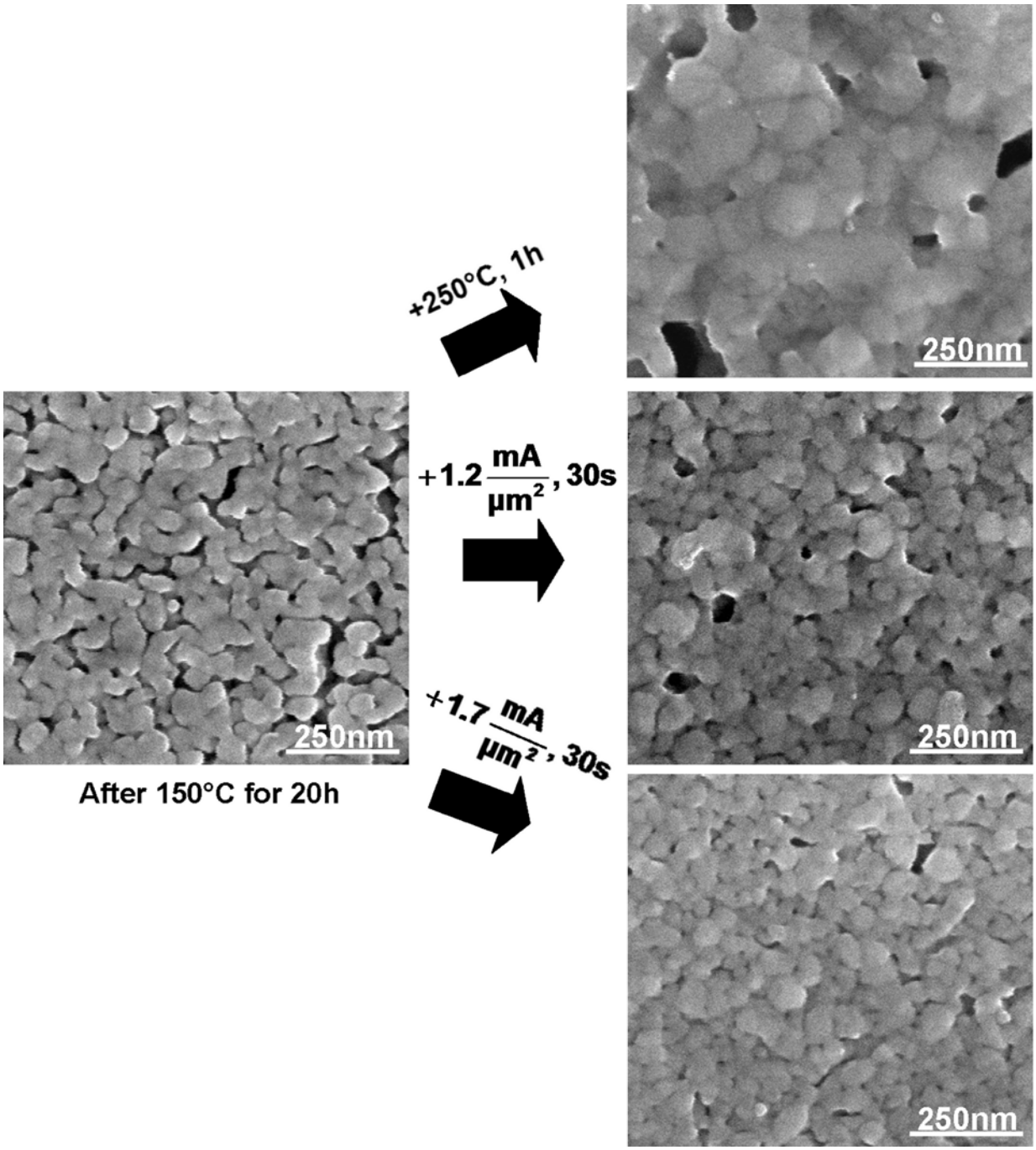

Figure 4.5: The change in microstructure which occurs as a result of an additional thermal cycle of 250°C for 1h compared to a 30s ohmic curing cycles with a current density of 1.2mA/μm^2 and 1.7mA/μm^2 for lines printed from Cabot CCI-300 ink.

The CCI-300 ink is the most comparable ink to that used in the work of Allen *et al.* [13] due to the similar composition of the ink as it is the only silver nanoparticle ink used in our

study. The lowest resistivity attained by Allen *et al.* [13], was 27nΩ·m, roughly 37% lower than the 43nΩ•m achieved in our experiments. One reason for the lower resistivity found in similar prior work may be the difference in silver nanoparticle size as Allen *et al.* [13] reported the silver particle size in their ink range between 10nm and 20nm while the particle size of Cabot CCI-300 is ~40nm.

The equation relating electrical resistivity and particle radius for conductive particles during the sintering process is:

$$\rho(t) = \frac{2\rho_o}{\pi} \times \ln\left\{\frac{r + L(t)/2}{r - L(t)/2}\right\} \tag{4.2}$$

where r is the particle radius, ρ_o, is the bulk resistivity of the conducting material and $\rho(t)$ and $L(t)$ are the resistivity and distance between particle centers at a time, t, during the sintering process [4].

The distance between particle centers during the sintering process is limited by the maximum diameter of the neck, x, which grows during the sintering process defined by the equation:

$$x = \left(E_{Ad}/rG\right)^{1/3} r \tag{4.3}$$

where E_{Ad} is the energy of adhesion between particles and G is the shear modulus of the bulk material [22]. The relationship between neck radius and the distance between particles is described by the equation:

$$L(t) = L(0) \times \sqrt{1 - \left(\frac{x}{r}\right)^2} \tag{4.4}$$

where $L(0)$ is the distance between particles at time $t = 0$ [4]. Due to the fact this model is based on spherical particles of the same size, $L(0)$ can be equated to $2r$ meaning that Equation (4.4) can be rewritten in terms of the minimum attainable distance between particles, L_{min} governed by the maximum diameter the neck will grow:

$$L_{\min} = 2r \times \sqrt{1 - \left(E_{Ad}/rG\right)^{2/3}} \tag{4.5}$$

Now a model describing the minimum resistivity attainable due to sintering can be made by combining Equations (4.5) and (4.1):

$$\rho_{\min} = \frac{2\rho_o}{\pi} \times \ln\left\{\frac{r + L_{\min}/2}{r - L_{\min}/2}\right\} \tag{4.6}$$

A graphical representation of Equation (4.6) is seen in Figure 4.6 for a particle radius ranging from 2nm to 30nm and it can be seen that the minimum resistivity attainable due to sintering is lower for the particle size used in the work of Allen *et al.* [13] compared to the nanoparticle ink used in this study. The model in Equation (6) is dependent on the particles being spherical, the same size, and of a pure material. Cabot CCI-300 is the only ink in this study which meets these criteria as the silver particles in microparticle-loaded inks are anisotropic flakes and the other nanoparticle ink used in this study (Cima NanoTech IJ242-54) is Ag/Cu-based.

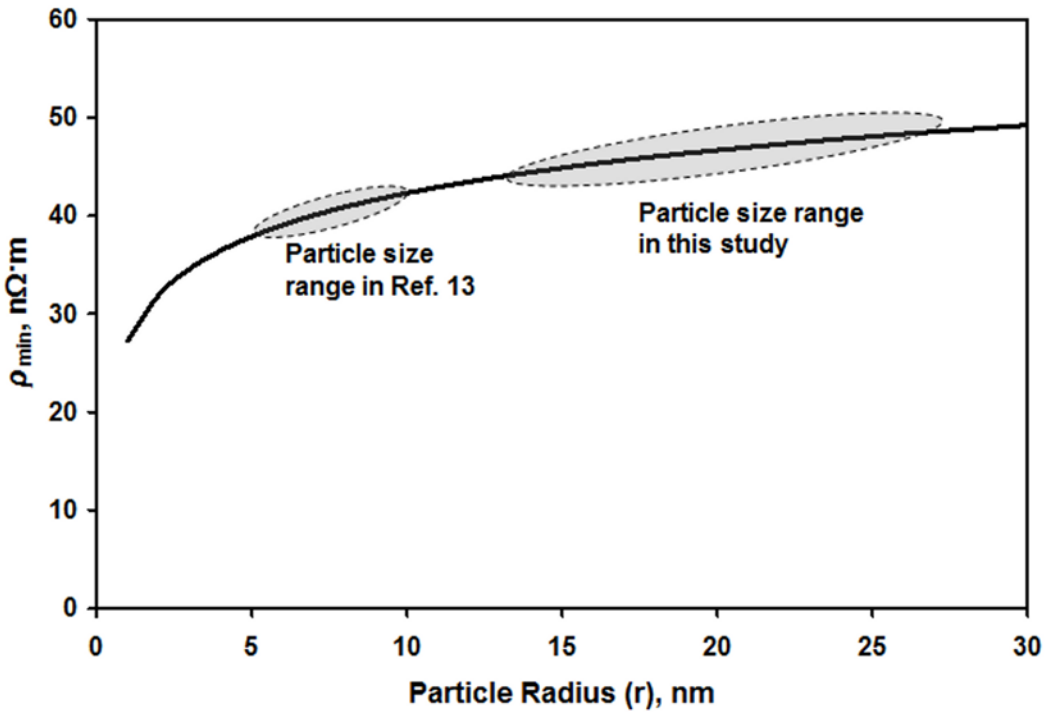

Figure 4.6: Graphical representation of Equation (4.6) for silver nanoparticles comparing the minimum resistivity attainable between the work in Ref. 13 to the experiments in this study involving Cabot CCI-300 conductive ink.

Real-Time Measurement Experiments

Electrical characterization of the ohmic curing process is demonstrated by the real time measurement of resistance by computer-controlled experiments. Repetition of cure cycles demonstrates the effect of the ohmic curing process as seen in Figure 4.7(a). The first curing cycle with an applied current density of 0.33mA/μm^2 began with a higher resistance, which then decreased over the course of the 10s curing cycle. Subsequent curing cycles show the resistance to have dropped by roughly 20% due to the first curing cycle. The application of current density in two 10s steps, the first step, 0.33mA/μm^2 and the second step 0.66mA/μm^2, demonstrated a drop in resistance during the first cycle for both applied current values as seen by observing the plot of resistance versus time in Figure 4.7(d). The drop in resistance is due to the line becoming more conductive during the first cycle. The 0.33mA/μm^2 current step of the second cycle had a resistance value 20% lower than the initial resistance value of cycle one. The slope of voltage versus time is level indicating that no curing is occurring during the second cycle. However, when the current density is ramped up to 0.66mA/μm^2, the resistance value begins to increase. The increase in resistance may be due to the line becoming hotter and temporarily increasing the resistance. The effect of applying electrical current density in a ramped fashion (ramping from 0.33 to 0.66mA/μm^2) reduced the resistance of the conductive trace to the same amount, roughly 50%, as applying a single current density value of 0.66mA/μm^2 (Fig. 4.7(c)) meaning that incrementally increasing the current density will achieve the same conductivity as a single application at the maximum current density. The microstructural changes which occurred as a result of the ohmic curing process are seen in Figures 4.7(b) and (e) and it can be seen that the initial drying cycle at 110°C (Fig. 4.7(f)) left the silver particles in an unsintered state. The application of current densities of 0.33 and 0.66 mA/μm^2 created a sintered microstructure.

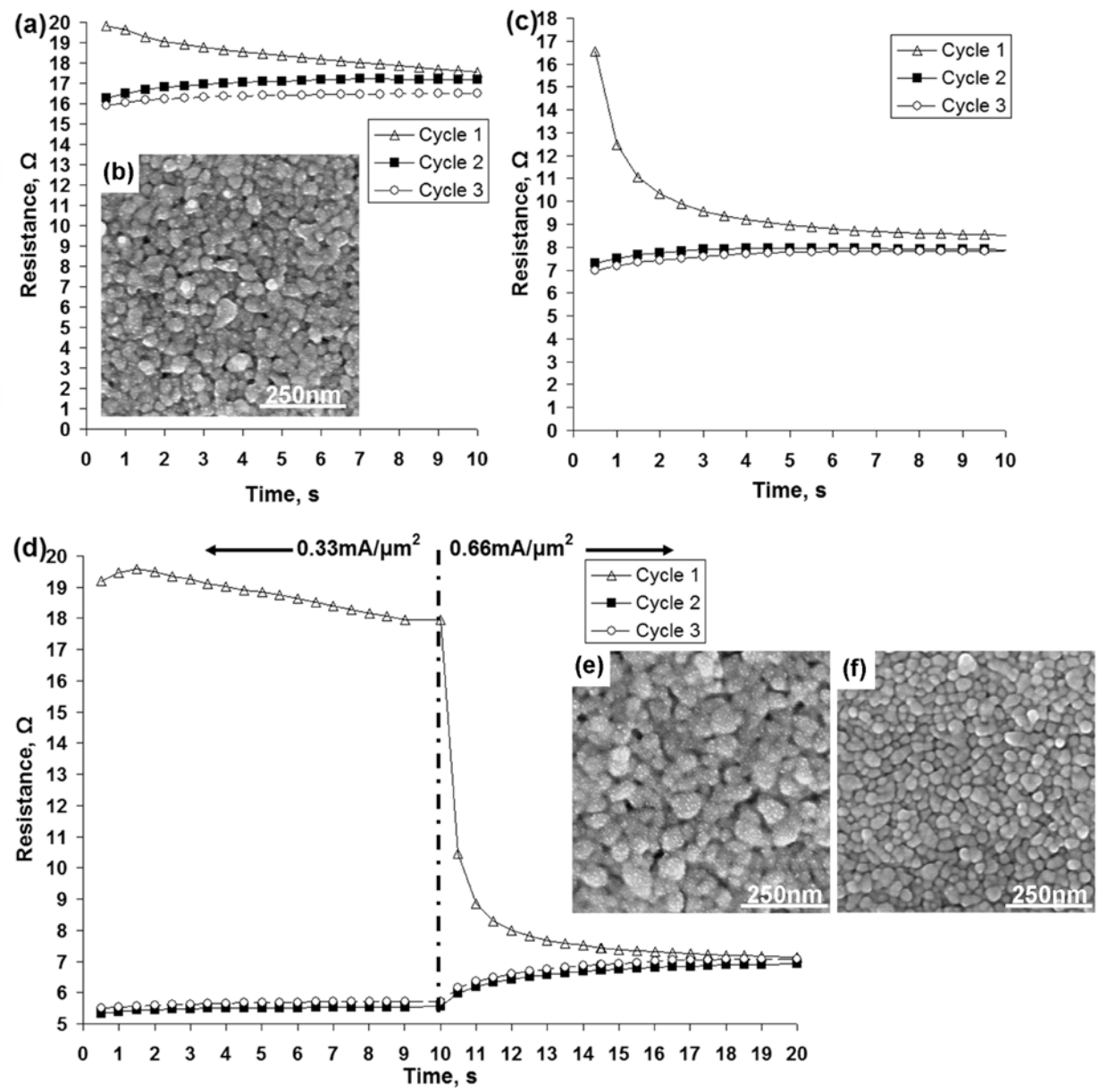

Figure 4.7: Results of computer controlled experiments. Resistance vs. time plot of **(a)** static cycles of 0.33mA/μm^2, and **(b)** the resulting microstructure, **(c)** plot of static cycles of 0.66mA/μm^2, **(d)** plots of cycles which started at 0.33mA/μm^2 and ramped up to 0.66mA/μm^2 and the resulting microstructure **(e)**. The initial microstructure **(f)** after drying at 110°C for 1h shows that the ohmic curing process has created a sintered microstructure.

The process of curing which occurs during the application of electric current is facilitated by localized heat which is transferred by resistance heating mechanisms within the printed line. Expressed as an equation, the transfer of heat can be expressed as:

$$Q = I^2Rt \tag{4.7}$$

where Q is the heat transferred in joules, I is applied current, R is the resistance within the electric circuit and t is the time the circuit is active [23]. Equation (4.7) is Joule's law describing the heat dissipated in an electric circuit [24] and in the case presented here the circuit is the probes of the power supply and the printed conductive line which is composed of conductive particles. The total resistance can be expressed as an equation describing resistors in series:

$$R_{total} = R_{btw\ particles} + R_{btw\ particles\ and\ probes} + R_{particles} \tag{4.8}$$

where the total resistance is the sum of the resistance values of the components in our circuit [25]. The decrease in resistance observed was driven by the change in resistance between the conductive particles as the contact resistance between the probes connected to the power supply and the particles themselves will not change. Ohmic heating is the mechanism which cured the printed conductive lines.

When the plots of resistance vs. time in Figure 4.7 were analyzed, it was apparent that a rapid decrease in resistance occurred during the initial portion of the curing cycle. The initial decrease in resistance is consistent with the findings of Allen *et al*. [13] who described the process of "electrical sintering" in terms of power produced during the application of voltage to printed traces. In general, power generated in is described by the equation:

$$P = I^2R, \tag{4.9}$$

where, P is power in watts, I is applied current and R is the resistance of the printed trace. In the context of ohmic heating, integrating Equation (4.9) over a time interval produces Equation (4.7) and describes the amount of heat transferred [23]. Applying this concept to the ohmic curing of

printed conductive traces; the amount of joules transferred during a time interval early in the cure cycle is greater than the amount of joules produced during a time interval later in the cure cycle. Since the resistance is lower at the beginning of subsequent cycles, fewer joules are transferred and no further curing takes place.

The Effect of Length on the Ohmic Curing Process

Considering the initial wattage produced when 500mA was applied to the 5cm lines was roughly 5W according to Equation (4.9), the electrical current applied to each sample set of given line lengths was scaled based on the measured resistance of the printed lines to ensure 5W would be produced. The measured resistance scaled linearly with line length. The initial resistance measurements are shown graphically in Figure 4.8(a) while the measured resistance after the application of an ohmic curing cycle for each line width is seen in Figure 4.8(b). Most significant is that for each sample set, line lengths of 1 and 2cm failed immediately upon the application of current. Also notable is the behavior of the percent decrease in measured resistance due to ohmic curing which decreases as the line width gets longer as seen in Figure 4.8(c). The microstructure of the printed lines after ohmic curing is that of partially sintered particles as seen in Figure 4.8(d).

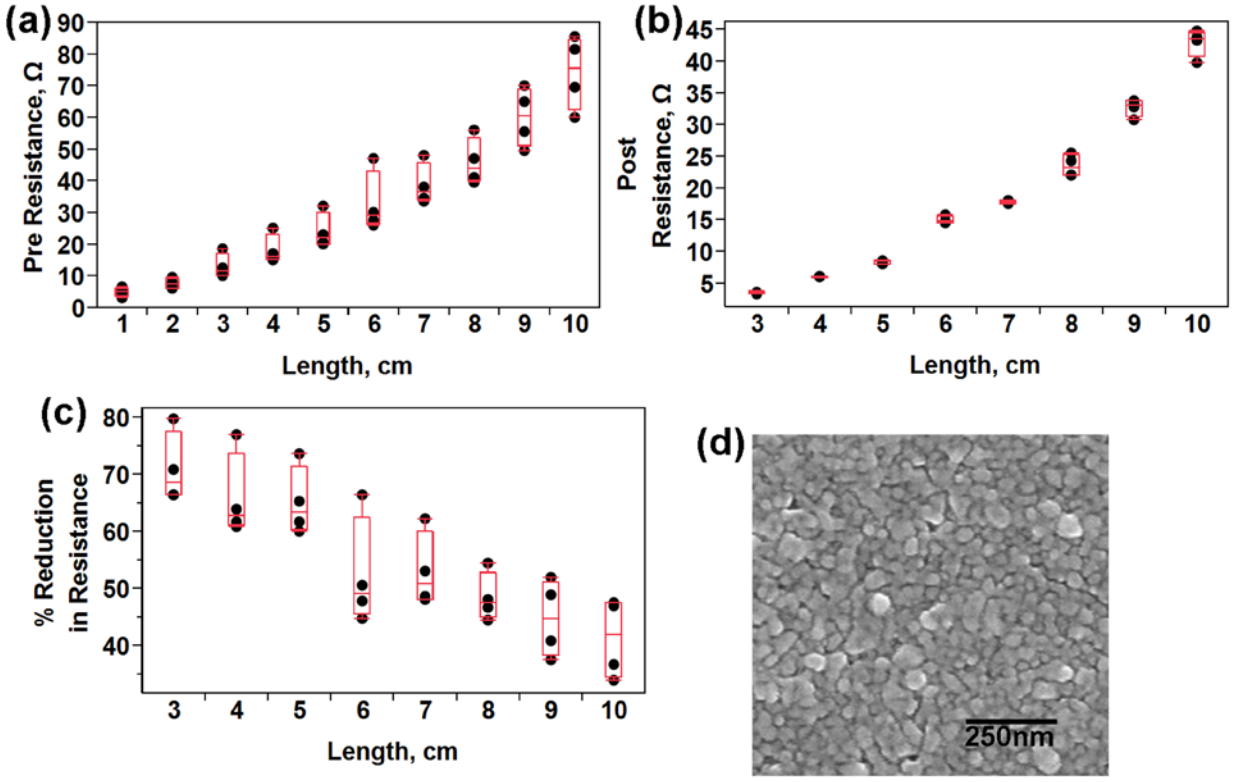

Figure 4.8: Measured resistance **(a)** of printed traces of Cabot CCI-300 for trace lengths ranging from 1cm to 10cm and **(b)** the measured resistance of the same set of lines after application of an ohmic curing cycle of 10s. Note that line lengths 1cm and 2cm failed for each sample set. The % reduction in measured resistance **(c)** decreases with increasing line length. Sample size for each line length was 4. The microstructure resulting from ohmic curing is that of slightly sintered particles.

It should be pointed out that there was no observed damage to the DuPont Kapton® polyimide film substrates once the curing parameters were dialed in to the levels used in the experiments. Table 1 lists the parameters determined using trial and error for experiments one through four performed in this study. The T_g for Kapton® is 360°C [26] and use of ohmic curing on polymers with lower T_g has yet to be explored. Localized damage of the substrate has been documented by Church *et al.* [27] where the application of electric current was utilized to cause the failure of printed conductive traces which were intended for use as fuses.

Beyond electrical characterization of the ohmic curing process the effect on physical properties, namely adhesion to the substrate, of printed traces which have been cured by ohmic heating should also be explored. The scotch tape based test, ASTM D3359 for measuring adhesion [28] has been used in a modified form by Muse *et al.* [29] on conductive traces where the criteria for failure was an open circuit after removal of the Scotch® 600 series tape. Initial results performed on samples cured by ohmic heating show, in the case of DuPont CB028, the adhesion test resulted in a failure while the thermally cured samples passed the adhesion test. The three other inks tested in this study showed the adhesion of samples cured by ohmic heating to be comparable to thermally cured samples as the adhesion test passed for samples cured using both methods. Additional areas of research to pursue pertaining to ohmic curing include the effect of the curing process on low T_g materials (150°C and below) and the use of the ohmic curing process in combination with photonic curing methods. Additionally, a predictive model to determine the optimum current values for the ohmic curing process should be explored.

4.4 Conclusions

A novel method for decreasing the resistivity of printed conductive traces was demonstrated. The application of electric current density to conductive lines printed from microparticle silver ink which were first air dried led to conductive paths with measured resistivity values similar to printed lines which were oven cured according to manufacturer recommendations. However, the ohmic heating approach had the further advantage of only subjecting the substrate to high temperatures in the region of the ink trace and is substantially faster. Increasing the electric current density value applied to conductive traces decreased the resistivity to 80nΩ·m—roughly 6 times the resistivity of bulk silver—compared to 130nΩ·m for lines which were thermally cured at the manufacturer's recommended parameters. In the case of nanoparticle inks, the utilization of ohmic curing was also demonstrated as a method for enhancing conductive traces which were already in a sintered state as a result of thermal pre-curing and, in some cases, the additional ohmic cure cycle further reduced the resistivity of the

printed trace to 43nΩ·m—roughly 3 times the resistivity of bulk silver. Ohmic curing increased the conductance in relatively fast cure cycles of less than 1 minute as compared to thermal cure cycles as long as one hour. A real time measurement of the curing process showed the resistance of the printed trace to drop rapidly upon the application of electric current density. The effect of varying length while scaling the applied electrical current to keep the initial wattage constant across various line lengths resulted in failure of the two shortest line lengths, 1cm and 2cm. Also, the lines which did not fail showed a decrease in resistance, but the amount of decrease was incrementally smaller as the line length increased. The utilization of ohmic curing overcomes constraints imposed by the thermal limitations inherent to polymeric substrates. Utilizing this method may provide more opportunities for more functional printed and flexible electronic devices based on a wider variety of substrate materials.

4.5 References

[1] J.-W. Kim, Y.-C. Lee, J.-M. Kim, W. Nah, H.-S. Lee, H.-C. Kwon, and S.-B. Jung, "Characterization of direct patterned Ag circuits for RF application," *Microelectronic Engineering*, vol. 87, no. 3, pp. 379–382, Mar. 2010.

[2] D. Tobjörk, N.J. Kaihovirta, T. Mäkelä, F.S. Petterson, R. Österbacka, "All-printed low-voltage organic transistors," *Organic Electronics*, vol. 9, no. 6, pp. 931–935, Dec. 2008.

[3] S. Merilampi, T. Laine-Ma, and P. Ruuskanen, "The characterization of electrically conductive silver ink patterns on flexible substrates," *Microelectronics Reliability*, vol. 49, no. 7, pp. 782–790, Jul. 2009.

[4] J. R. Greer and R. A. Street, "Thermal cure effects on electrical performance of nanoparticle silver inks," *Acta Materialia*, vol. 55, no. 18, pp. 6345–6349, Oct. 2007.

[5] D. Kim and J. Moon, "Highly Conductive Ink Jet Printed Films of Nanosilver Particles for Printable Electronics," *Electrochem. Solid-State Lett.*, vol. 8, no. 11, p. J30-J33, Nov. 2005.

[6] N. R. Bieri, J. Chung, S. E. Haferl, D. Poulikakos, and C. P. Grigoropoulos, "Microstructuring by printing and laser curing of nanoparticle solutions," *Applied Physics Letters*, vol. 82, no. 20, pp. 3529–3531, May 2003.

[7] M.-K. Kim, *et al.*, "Laser sintering of the printed silver ink," in *IEEE International Symposium on Assembly and Manufacturing, 2009. ISAM 2009*, 2009, pp. 155-158.

[8] A. J. Lopes, E. MacDonald, and R. Wicker, "Integrating Stereolithography and Direct Print Technologies for 3D Structural Electronics Fabrication," *Rapid Prototyping Journal*, vol. 18, no. 2, p. 4-4, Jan. 2012.

[9] J. Perelaer, B. de Gans, and U. S. Schubert, "Ink‐jet Printing and Microwave Sintering of Conductive Silver Tracks," *Advanced Materials*, vol. 18, no. 16, pp. 2101–2104, Aug. 2006.

[10] J. Perelaer, M. Klokkenburg, C. E. Hendriks, and U. S. Schubert, "Microwave Flash Sintering of Inkjet‐Printed Silver Tracks on Polymer Substrates," *Advanced Materials*, vol. 21, no. 47, pp. 4830–4834, Dec. 2009.
[11] S. Sivaramakrishnan, P.-J. Chia, Y.-C. Yeo, L.-L. Chua, and P. K.-H. Ho, "Controlled insulator-to-metal transformation in printable polymer composites with nanometal clusters," *Nat Mater*, vol. 6, no. 2, pp. 149–155, Feb. 2007.
[12] T. Mattila, A. Alastalo, M. Allen, H. Seppa, U.S. Patent 7,759,160, 20 July, 2010.
[13] M. L. Allen, M. Aronniemi, T. Mattila, A. Alastalo, K. Ojanperä, M. Suhonen, and H. Seppä, "Electrical sintering of nanoparticle structures," *Nanotechnology*, vol. 19, p. 175201, Apr. 2008.
[14] H. Wohltjen and R. Dessy, "Surface acoustic wave probes for chemical analysis. III. Thermomechanical polymer analyzer," *Anal. Chem.*, vol. 51, no. 9, pp. 1470–1475, 1979.
[15] D. A. Roberson, R. B. Wicker, L. E. Murr, K. Church, and E. MacDonald, "Microstructural and Process Characterization of Conductive Traces Printed from Ag Particulate Inks," *Materials*, vol. 4, no. 6, pp. 963-979, May. 2011.
[16] *DuPont CB028 Silver Conductor Technical Data Sheet*, Du Pont, Wilmington, DE, 2009, p. 1.
[17] *Ercon E1660; Technical Data Sheet*, Ercon Incorporated, Wareham, MA, 2007, p. 1.
[18] M. Navarette, A. Lopes, J. Acuna, R. Estrada, E. MacDonald, J. Palmer, R. Wicker, "Integrated Layered Manufacturing of a Novel Wireless Motion Sensor System with GPS," in *Proceedings of the 2009 Solid Freeform Fabrication Symposium*, Austin, Texas, pp. 575-585, 2007.
[19] *Cima NanoTech IJ242-54 Conductive Silver/Copper Ink Data Sheet*, Cima NanoTech, St. Paul, MN:, 2010, p. 1.
[20] *Cabot Conductive Ink CCI-300 Data Sheet*, Cabot Printed Electronic Materials, Albuquerque, NM, 2009, p. 2.
[21] S. O. Kasap, "Electrical and Thermal Conduction in Solids," in *Principles of Electrical Engineering Materials and Devices*, New York, NY: Irwin McGraw Hill, 1997, p. 113.
[22] L.E. Murr, "Properties of Interfaces," in *Interfacial Phenomena in Metals and Alloys*, Massachusetts: Addison-Wesley, 1975, pp. 297–299.
[23] H. Zhang, J. Senkara, "Electrothermal Processes of Welding," in *Resistance Welding: Fundamentals and Applications*, Boca Raton, FL: CRC Press, 2006, p. 19.
[24] J. C. Maxwell, "Electric Current," in *An elementary treatise on electricity*, Oxford: Clarendon Press, 1888, p. 100.
[25] K.-S. Moon *et al*., "Thermal behavior of silver nanoparticles for low-temperature interconnect applications," *Journal of Electronic Materials*, vol. 34, no. 2, pp. 168-175, Feb. 2005.
[26] *DuPont Kapton® HN polyimide film Technical Data Sheet*, DuPont, Wilmington, DE, 2011, p. 3.
[27] K. H. Church, C. M. Newton, A. J. Marsh, E. W. MacDonald, C. D. Soto, and J. C. Lyke, "Print-and-play: a new paradigm for the nearly-instant aerospace system," *Proc. of SPIE*, vol. 7691, no. 1, p. 76910A-76910A-9, Apr. 2010.
[28] ASTM Standard D3359-02, 2002.
[29] D. Muse, S. Pritchard, E. MacDonald, R. Wicker, X. Chen, M. Newton, K.H. Church, in *Proc. of IMAPS 42nd Int. Symp. on Microelectron.*, San Jose, CA, 2009.

CHAPTER 5: FAILURE INVESTIGATION OF DIRECT WRITE PEN TIPS

5.1 Introduction

The emerging technology of printed microelectronics manufacturing involving the use of conductive ink necessitates the development of new equipment. The application of direct-write technology in the creation of microelectronic components has lent itself to a situation where the feature size of the printed element is related to the orifice diameter of the pen tip which, in the case presented here, was less than 100μm. Maintaining a functional pen tip is of great importance to achieving the desired printed feature size and quality control. In the case studied, failure involved any event which causes the orifice dimensions of the pen tip to change.

In this situation alumina ceramic was chosen as the material for a pen tip in an automated direct write microdispense system. These tips were used to print silver-loaded conductive ink or a photo-curable resin. Failure of the pen tips occurred during use and a noticeable difference in print quality was observed by the operator. The pen tips are shown in Figure 5.1. The pen tips were labeled 1, 2, and 3 in order to keep track of the samples during failure analysis.

The size of the failed component presented a quandary in that “typical” steps in performing the failure analysis could not be taken. These steps would ideally include locating the pieces dislocated from the pen tip during failure in order to determine the crack initiation sites and glean information as to the cause of the component failure [1]. However, due to the size of the failed component, the process of failure analysis was totally dependent on electron microscopy and fractography. Microanalysis via scanning electron microscopy (SEM) was carried out in order to examine the fracture surfaces of the pen tips. Fractography was performed based on micrographs taken at various magnifications. Though the component size was small, a large amount of information could be ascertained from analyzing the fracture surfaces. The failure, based on the analysis of the fracture surfaces, was caused by impact loading.

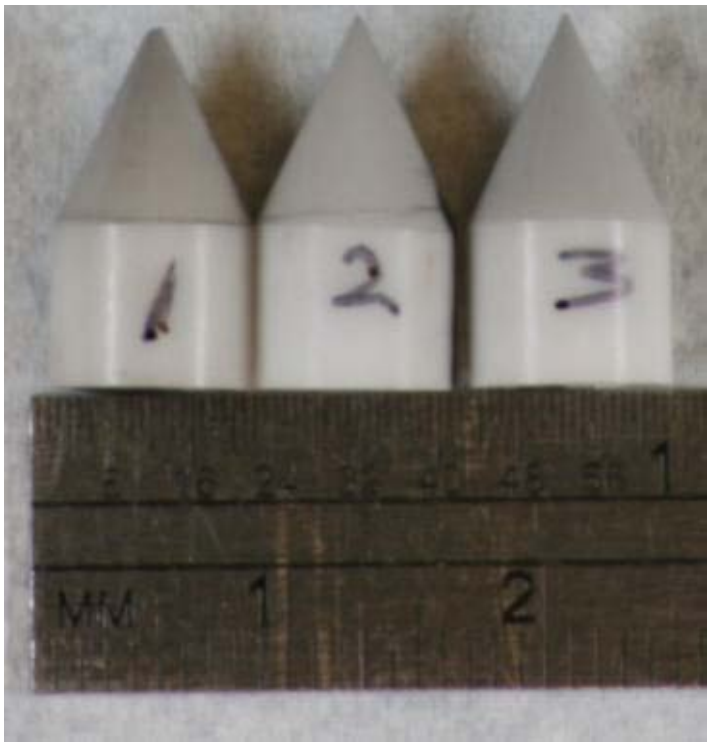

Figure 5.1: The microdispense pen tips examined in this investigation.

5.2 SEM Microanalysis of the Pen Tips

SEM microanalysis was performed with a Hitachi S-4800 Ultra-high Resolution Field Emission Scanning Electron Microscope (Hitachi High-Technologies Corporation, Tokyo, Japan) in order to characterize the fracture surface of the failed tips. To minimize the effects of charging during SEM microanalysis, the pen tips were first subjected to carbon sputtering for 30s in a Gatan Model 682 Precision Etching Coating System (Gatan, Inc., Pleasanton, CA, USA). Energy-dispersive x-ray spectroscopy (EDX) was performed in order to determine the composition of the pen tips. As seen in Figure 5.2, the pen tips were most likely composed of sintered alumina ceramic, a claim which was reinforced by the microstructure both of the fracture surface and the undamaged surfaces of the pen tip. The fracture surfaces matched examples of brittle fracture of sintered alumina found in literature namely, Krell [2]. Close examination of the fracture surfaces revealed a mix of intergranular cleavage and transgranular

cleavage. Figure 5.3 is representative of the fracture surfaces observed while Figure 5.4 indicates porosity in the structure of the pen tip.

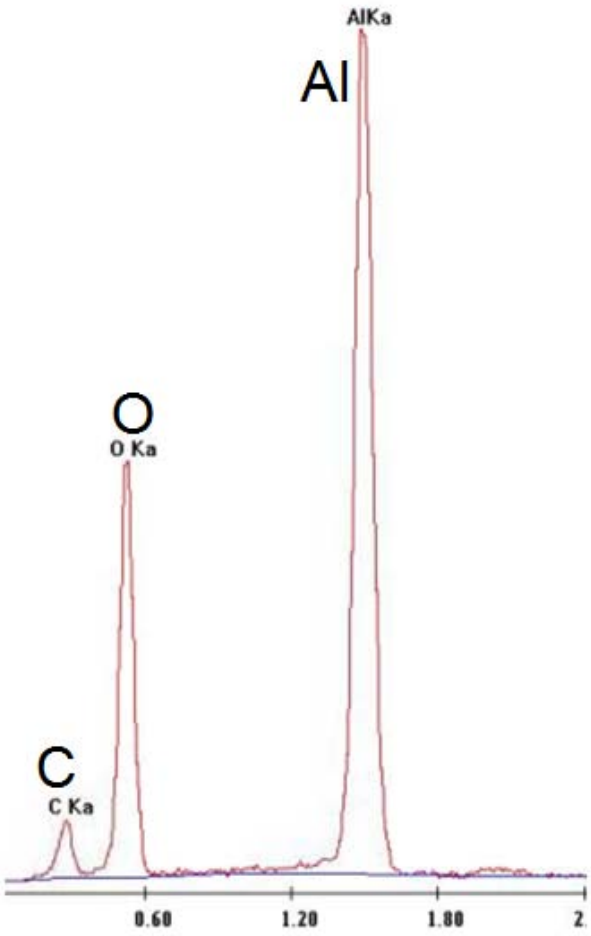

Figure 5.2: Results of EDX analysis of the pen tips.

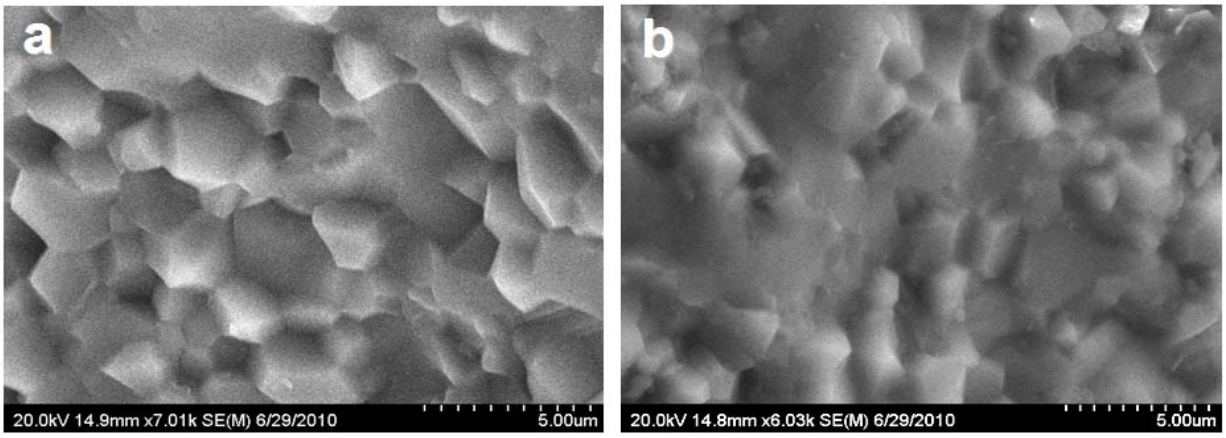

Figure 5.3: (a) Intergranular cleavage and **(b)** a mixture of intergranular and transgranular cleavage.

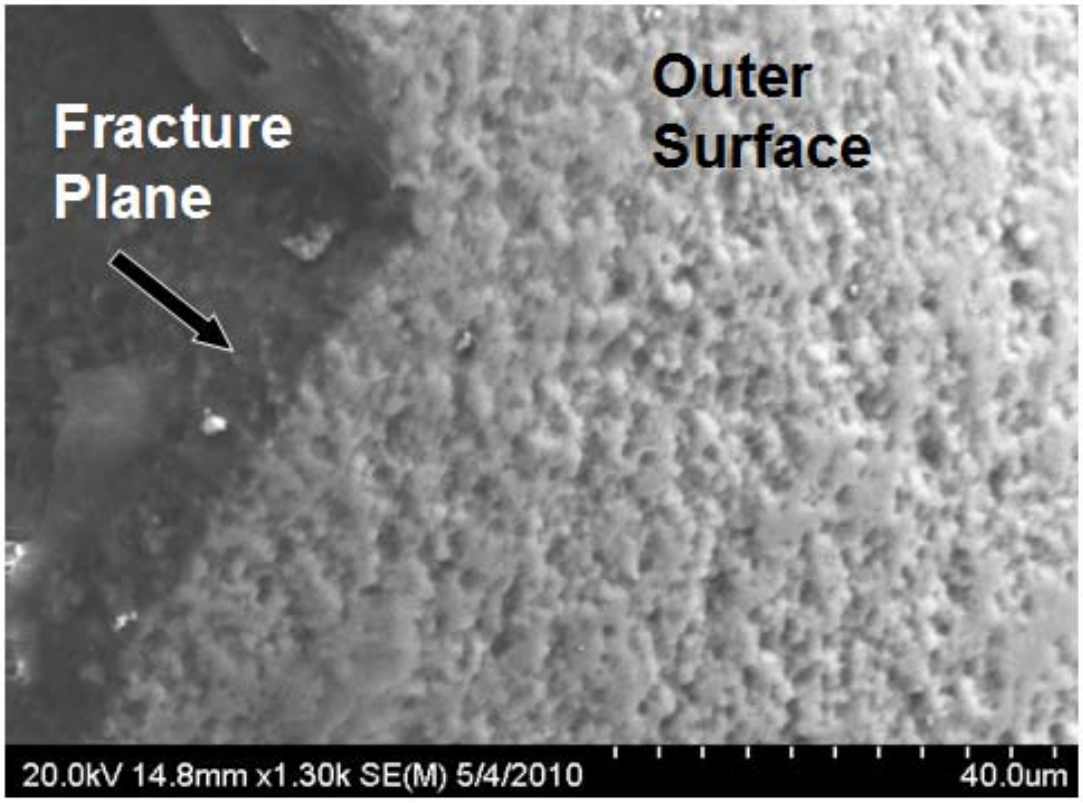

Figure 5.4: Porosity observed on the outer surface of the pen tip material adjacent to a fracture plane. Note the porosity of the outer surface.

SEM micrographs of the three pen tips taken at a 30° tilt are seen in Figure 5.5. All images in the figure are presented at the same magnification, which makes it possible to compare

the amount of damage between pen tips. It was obvious Tip 1 suffered more damage as compared to the other two pen tips. There was far more of the pen tip missing as compared to the other two; which was also discernable optically as seen in Figure 5.1. The fracture surface displayed features which appeared to be conchoidal in nature and resembled the fracture surface of a stone-age tool. These features are characterized by curvature on the fracture surface caused by Hertzian cone crack formation [3]. A concentric ring feature, seen in Figure 5.6, was observed on some of the fracture planes indicating crack growth direction. This ring structure is another characteristic of conchoidal fracture [4].

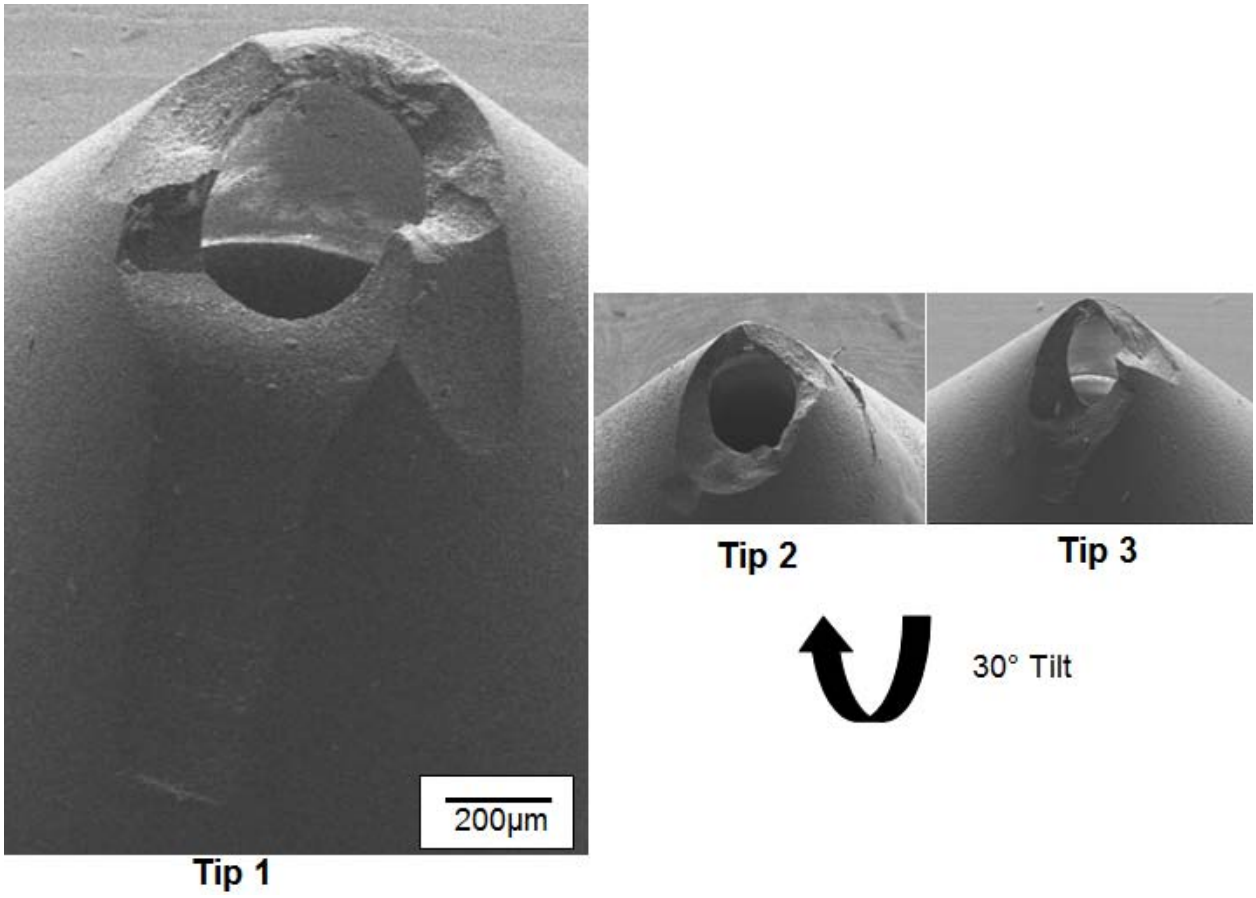

Figure 5.5: Comparison of the damage imposed on the pen tips. All images are the same magnification.

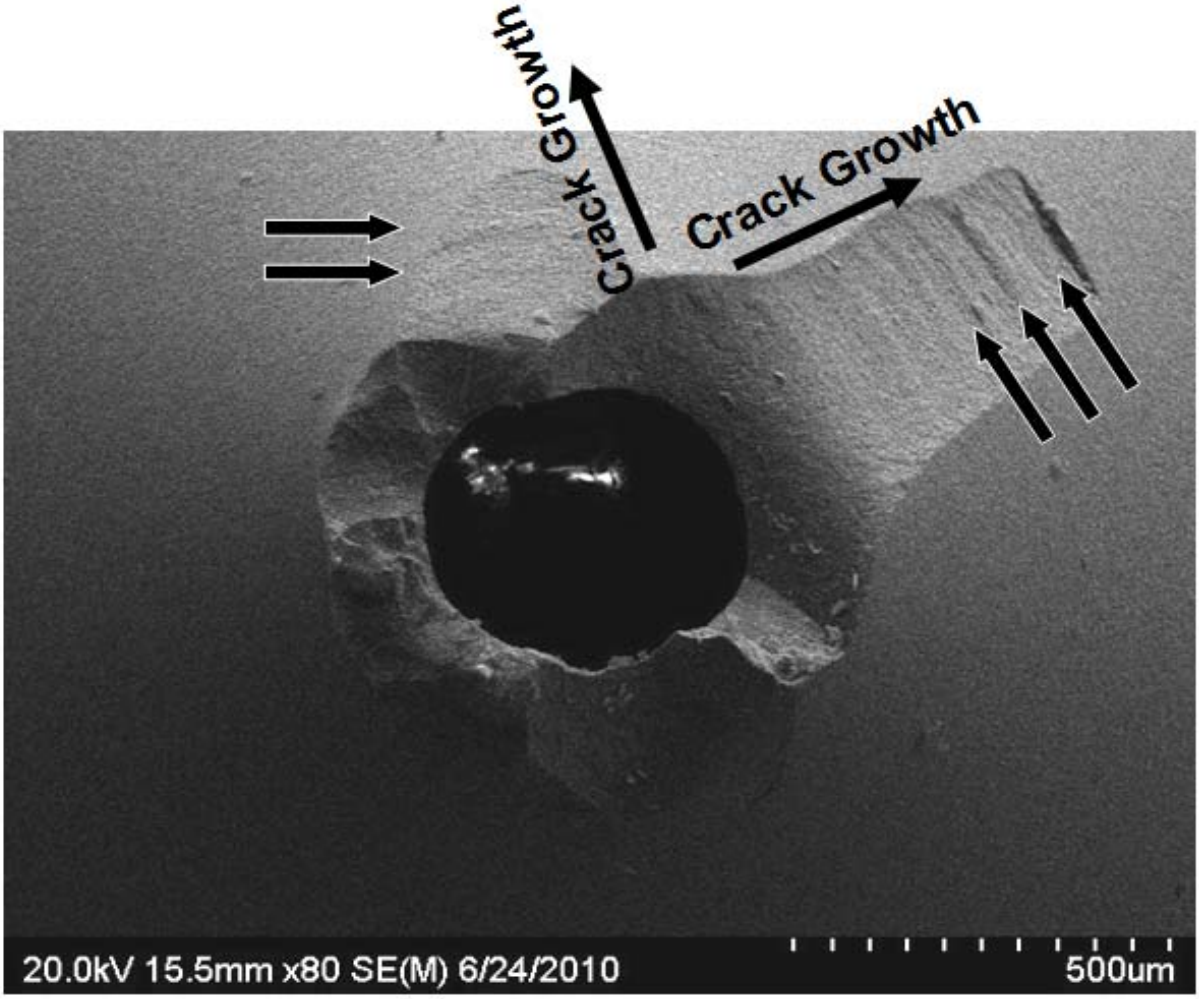

Figure 5.6: Ring pattern highlighted by arrows indicating the direction of crack growth.

The presence of a conchoidal fracture surface is indicative of a fracture caused by impact. This type of fracture surface is typical of brittle materials or ultra fine-grained materials [4]. There is also a distinctive feature which is highlighted by the arrow in Figure 5.7, which was found to be caused by head-on impact. This feature is also conchoidal in nature and if found, the flake produced by the chip would have most likely resembled flakes created during the production of stone-age tools. Tip 2 and Tip 3 also display conchoidal fracture surfaces as well as the distinctive "head-on" feature.

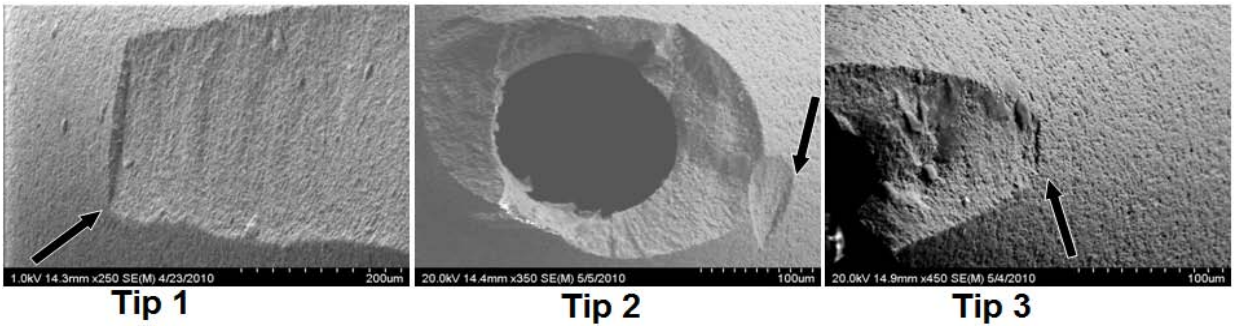

Figure 5.7: Distinctive feature observed on each of the three pen tips.

Proof the distinctive feature was caused by head-on impact came from an error made in the re-analysis of Tip 3. When setting the sample height on the sample holder for SEM microanalysis, the tip was inadvertently pushed into the sample height gage in a head-on manner normal to the orifice of the pen tip. Re-analysis of Tip 3 revealed a new fracture surface had appeared with the characteristic fracture surface as indicated in Figure 5.8. While this was an inadvertent experiment, it provided valuable data in the determination of the cause of the distinctive fracture feature.

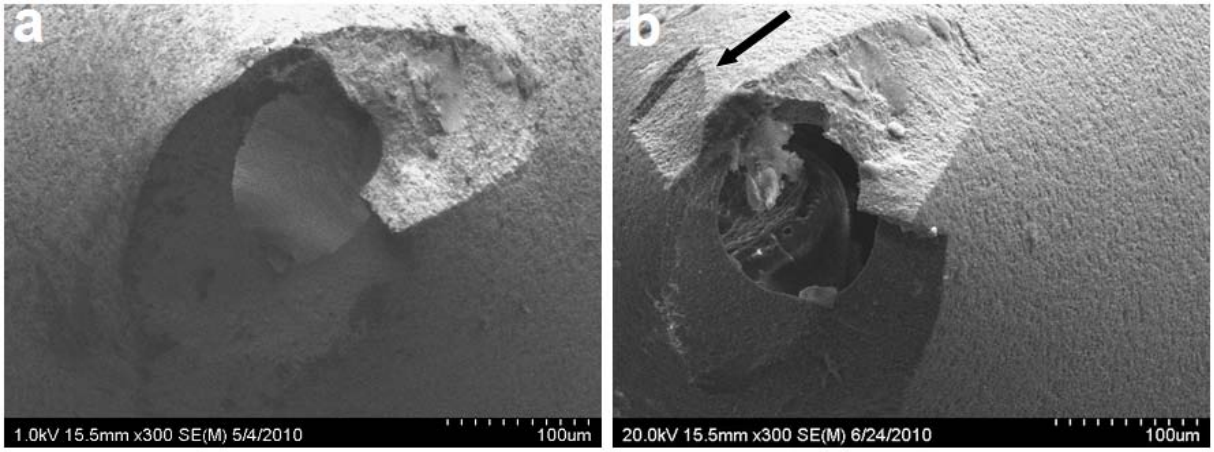

Figure 5.8: Pen tip 3 **(a)** before and **(b)** after additional damage. Note the appearance of the distinctive fracture feature indicated by the arrow.

It is also important to note the fracture surface features which were not observed on the pen tips. There were no mirror, mist and hackle regions on the fracture surfaces. These fracture

surfaces are characteristic of tensile failures of ceramics and glasses [1, 4, 5]. There was also no evidence of wear or erosion observed on the pen tips.

5.3 Conclusion

Based on the fracture evidence, impact was the most likely cause of the failure of the microdispense pen tips. The fracture mode was brittle in nature as evident by the features observed on the crack planes, namely conchoidal fracture features. The presence of a conchoidal fracture surface is not surprising as the sintered structure of the pen tip is essentially a fine-grained material and ceramics are inherently brittle. The presence of porosity is also not a benefit to the mechanical properties of the pen tips. Moreover, the characteristics of fracture caused by tensile loading were not observed. These fracture features would have been present if the failure was caused by too much pressure being applied within the pen tip.

5.4 Recommendations

The microdispense system in which the pen tips were utilized was in the process of being integrated as a component in a prototype. The integration in this particular equipment set was an atypical use. It was recommended to implement safeguards to prevent impact of the pen tip into the print media as part of the system integration.

5.5 References

[1] G. W Powell, "Engineered and Electronic Materials," in *ASM Handbook Volume 11 Failure Analysis and Prevention*, Ohio: ASM International, 1995, pp. 745-757

[2] A. Krell, "Fracture Origin and Strength in Advanced Pressureless-Sintered Alumina," *Journal of the American Ceramic Society*, vol. 81, no. 7, pp. 1900-1906, Jul. 1998.

[3] B. Cotterell, J. Kamminga, and F. P. Dickson, "The essential mechanics of conchoidal flaking," *International Journal of Fracture*, vol. 29, no. 4, pp. 205-221, Dec. 1985.

[4] D. Hull, "Observing, describing, and measuring fracture surface topography: some basics using Ketton stone as an example," in *Fractography: observing, measuring, and interpreting fracture surface topography*. Cambridge University Press, 1999, pp. 38-40.

[5] J. R. Kelly, S. D. Campbell, and H. K. Bowen, "Fracture-surface analysis of dental ceramics," *The Journal of Prosthetic Dentistry*, vol. 62, no. 5, pp. 536-541, Nov. 1989.

CHAPTER 6: OVERCOMING SUBSTRATE-IMPOSED THERMAL LIMITATIONS ON THE PROCESSING OF 3D STRUCTURAL CONDUCTIVE INK INTERCONNECTS

6.1 Introduction

The integration of printing methodologies into the creation of electronic components has created a new realm of electronics manufacturing. Figure 6.1 illustrates the relative simplicity of creating metal interconnects via direct printing (DP) techniques compared to traditional metallization methods Though there are examples of all-printed functional devices such as junction transistors described by Tobjörk *et al*., [1], the current state of the art of electronic components which make use of printing methodologies falls in to the realm of hybrid electronic devices such as a physically flexible graphics driver [2] which is a hybridization of ink-based electrical interconnects printed on a flexible Kapton® substrate with commercially available microchips components integrated into the system. The combination of additive manufacturing (AM) techniques with direct printing (DP) techniques has created another paradigm of electronics manufacturing—structural or 3D electronics. A profound feature of 3D electronic components is the lack of a printed circuit board (PCB) as the component to be created is essentially the PCB as all the chips are housed within the structure. Examples of functional components created via the integration of AM and DP techniques include a GPS sensor, [3], a 3-axis magnetometer, [4] and a conformal helmet insert with an integrated accelerometer and motion sensor [5].

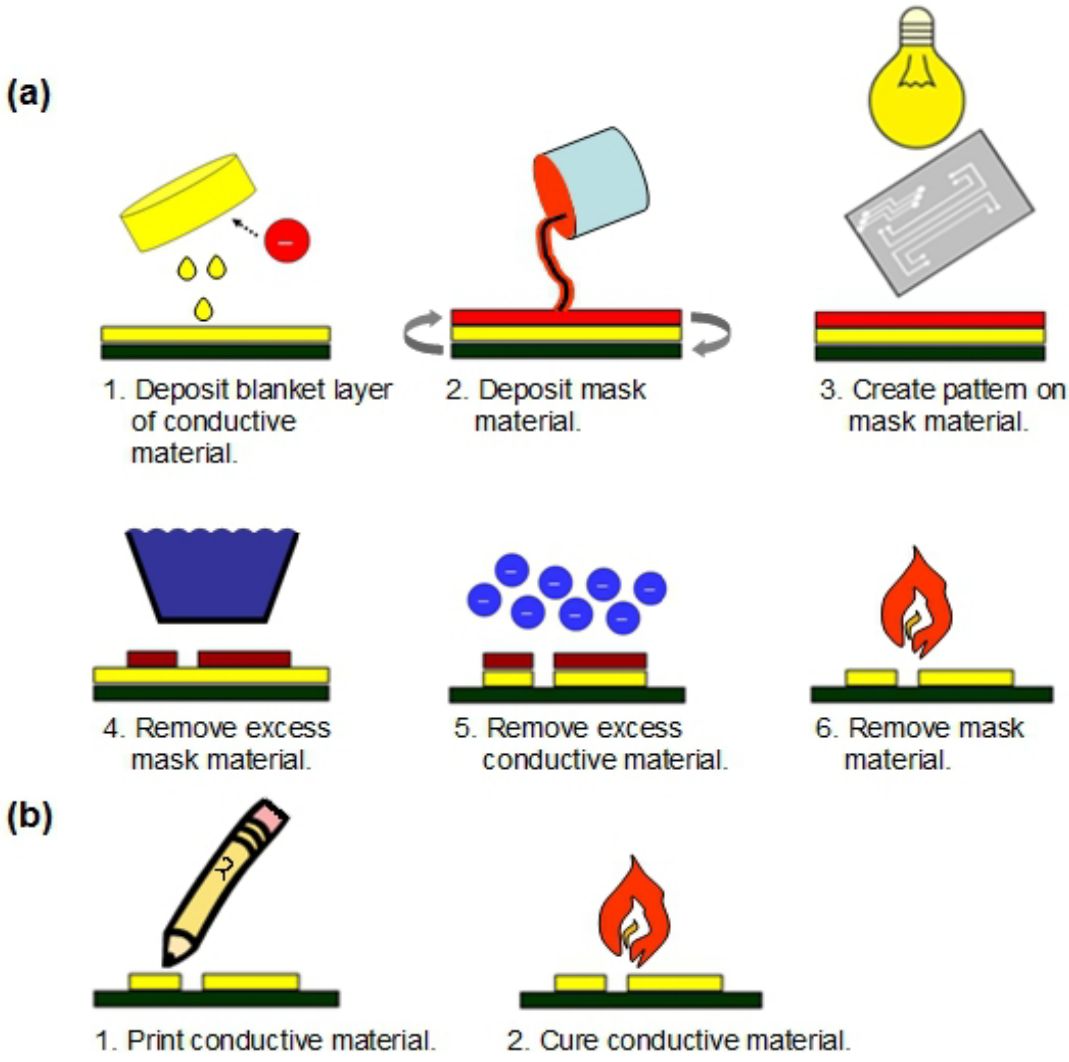

Figure 6.1: Typical metallization process **(a)** compared with **(b)**, the utilization of direct print (DP) to create conductive traces on a substrate.

The AM process of stereolithography (SL) is seen in Figure 6.2 while Figure 6.3 shows a rechargeable die system developed at the W.M. Keck Center for 3D innovation and features a charging base which can wirelessly recharge the dice. The rechargeable dice each contain DP created interconnects, an accelerometer, a microcontroller, a lithium polymer battery with supporting safety circuitry, and LEDs which blink when a given side is facing up after the dice are rolled. The charging base consists of an induction coil, DP manufactured interconnects, and supporting microchips. The fact that an entire system was created by the integration of SL and

DP serves an example of the ability to utilize the two technologies to create unique and fully functional hybridized electronic systems an expand the concept of rapid prototyping (RP) from the creation of models to the creation of fully functional systems.

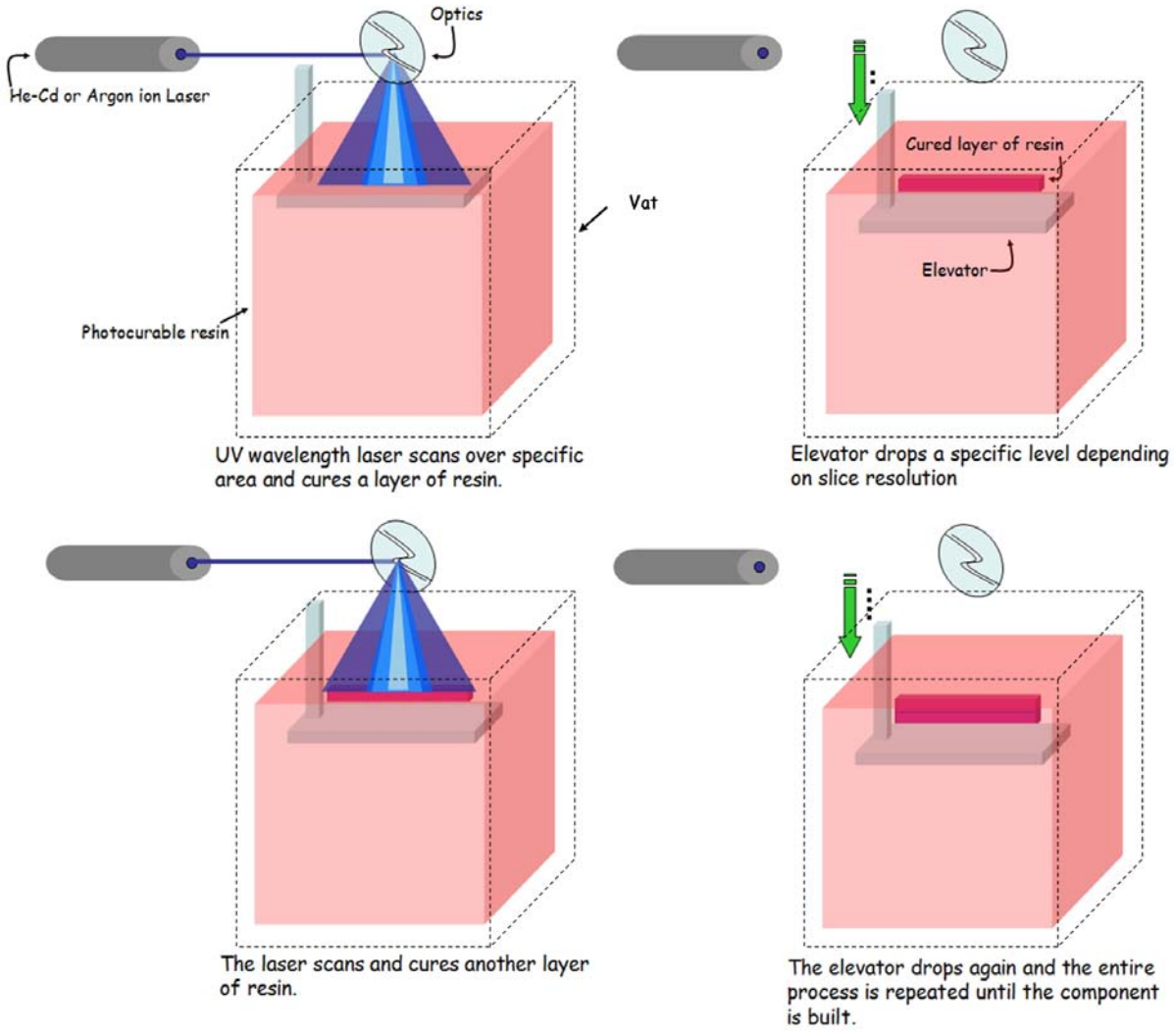

Figure 6.2: Simple depiction of the SL process. Adapted from [5, 6].

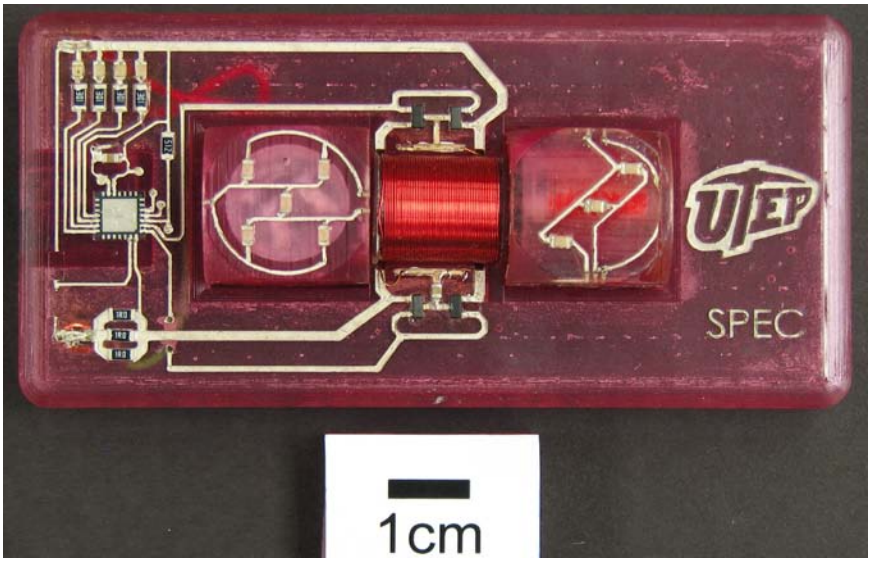

Figure 6.3: Example of a complex electronic component created through the hybridization of DP and SL techniques.

A critical step in the manufacture of electronic devices involving printed interconnects is the curing of the conductive traces. The limiter of the thermal curing process is the temperature constraints of the substrates. Consider the use of SL involving a photocurable resin to create 3D substrates; two commercially available photocurable resins manufactured by DSM Somos®, (DSM Somos®, Elgin, IL, USA) ProtoTherm™ 12120 and WaterShed™ 11120, have a glass transition temperatures (T_g) of 74°C and 46°C respectively (ProtoThem™ Datasheet; WaterShed™ Datasheet) whereas the recommend thermal cure temperatures of most conductive inks are greater than 100°C [7].

Lopes [8] demonstrated the capability to cure a printed conductive trace *in situ* with the laser of a 3D Systems (3D Systems, Rock Hill, SC) SLA® 250/50 system on straight line traces on one plane SL created substrates. Utilizing measured resistance of the printed trace as a metric, it was found the best results came when the laser was directed on the edge of the printed trace, however there was some damage to the SL substrate. The number of times the laser was passed over the over the printed trace was also found to have an effect on the measured resistance as the measured resistance dropped with each subsequent pass of the laser.

The interconnect scheme in a 3D structural electronic occupies multiple planes, making curing via laser somewhat difficult from an equipment point of view as some manipulation of the laser would have to be achieved especially if vertical interconnects are utilized. This paper explores the utilization of ohmic curing as described by Roberson *et al.* [9] as a method for decreasing the resistance of ink printed interconnects and vias which occupy multiple planes in 3D space without damaging the substrate. The mal-effects of curing the inks to the manufacturer recommended specifications are also demonstrated.

6.2 Experimental

The test structure in Figure 6.4 was manufactured in a 3D Systems Viper™ SLA® system. As can be seen in Figure 6.4, the test structure possess two interconnect structures with exposed and internal sections occupying multiple planes. Each test structure was considered a sample, designed to give paired data for experimental purposes. Two photocurable resins were utilized, DSM Somos®, ProtoTherm™ 12120 and WaterShed™ 11120. Two conductive inks were tested, Ercon E1660 (Ercon Incorporated, Wareham, MA) and DuPont CB028, (DuPont, Wilmington, DE, USA) and DuPont CB028, (DuPont, Wilmington, DE, USA). Additionally, two via/plug, pastes were tested, DuPont CB100 and CB102.

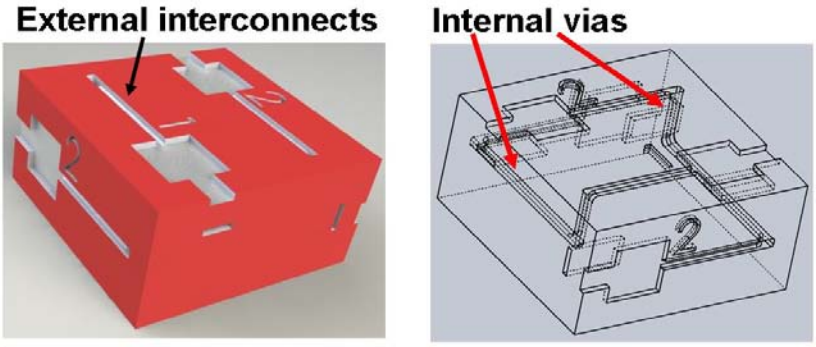

Figure 6.4: The test structure used in this study which featured internal vias and external interconnects.

Thermal pre-curing is needed to dry the ink and also to attain a level of conductivity for ohmic heating to be possible. Thermal pre-curing as well as thermal curing for benchmark samples was carried out in a VWR Signature™ Horizontal Air Flow Oven model 1370FM (VWR International, West Chester, PA, USA). Electrical current for ohmic curing cycles was supplied in the same fashion as described in Roberson *et al.* [9] where a Kepco model ABC 25-4DM programmable power supply (Kepco, Inc, Flushing, NY, USA) was connected to a personal computer (PC) through a National Instruments SC-2345 Signal Conditioning Connector Block (National Instruments, Austin, TX, USA) and controlled by a LabVIEW-created program. Electrical resistance was measured with a Fluke model 179 True RMS multimeter (Fluke Corporation, Everett, WA, USA).

Thermal benchmark parameters are listed in Table 6.1 and were based on manufacturer specified curing temperatures with the exception of Ercon E1660, which was cured at 138°C instead of the recommended cure temperature of 121°C as there are several examples of 138°C being the optimum cure temperature for this ink [3, 7, 8].

Table 6.1: Critical parameters for the inks tested in this study.

Ink	Viscosity, cP	Benchmark Cure Parameters
Ercon E1660	17,500 ± 7,500	138°C 30min
DuPont CB028	15,000 – 30,000	160°C for 1h
DuPont CB100	115,000 – 145,000	Dry at 110°C 115°C for 30min then cure at 160°C for 60min.
DuPont CB102	83,000	150°C for 60min

A key component in deciding the success of an individual cure experiment was evaluating substrate damage. Photography and microscopy were utilized in the evaluation process. Macro photography was performed with a Canon Powershot S2IS 5MP Camera (Canon U.S.A, Inc., Lake Success, NY) while optical microscopy was performed with a Leica model MZ16 stereoscope (Leica Microsystems, Buffalo Grove, IL) outfitted with a Regita 2000R Fast 1394 digital CCD camera (QImaging Corp., Surrey, BC, Canada). Scanning electron

microscopy was performed with a Hitachi TM-1000 Tabletop Microscope operating at 15keV (Hitachi High-Technologies Europe GmbH, Germany).

For all experiments, ink was applied with a BD 10ml luer-lock syringe (BD, Franklin Lakes, NJ) with a Nordson EFD precision dispensing tip (Nordson EFD, Providence, RI) with a 0.008in (0.2mm) orifice diameter for DuPont CB028 and Ercon E1660 inks. A precision tip with an orifice diameter of 0.023in (0.6mm) was needed for DuPont CB100 and CB102 due to the higher viscosity of the pastes. Viscosity values for all the printable conductors are listed in Table 6.1.

6.3 Results

6.3.1 Via/interconnect Structures in ProtoTherm™

Initial experimentation led to the abandonment of DuPont CB028 as no conducting traces could be created on the test structured created from Somos ProtoTherm™. The ink was found to not adhere well to the substrate particularly in the interior via section as seen in Figure 5. Attempts to create traces from DuPont CB028 on Somos WaterShed™ substrates indicate there are surface energy-related issues with using this ink as the ink ejected itself from the via portion of the structure as is also seen in Figure 6.5. DuPont CB100 was also abandoned due to the fact that samples produced with this paste could not attain a reliable level of conductivity in terms of variability between samples. Preliminary experimentation also found the application of 4A of current to be the optimum applied current value to induce an improvement in the electrical conductivity of the printed trace regardless of ink type. Electrical current was applied in three 10s cycles. The current value of 4A was the maximum current value capable by the equipment available to us so attempts at higher current values were not possible.

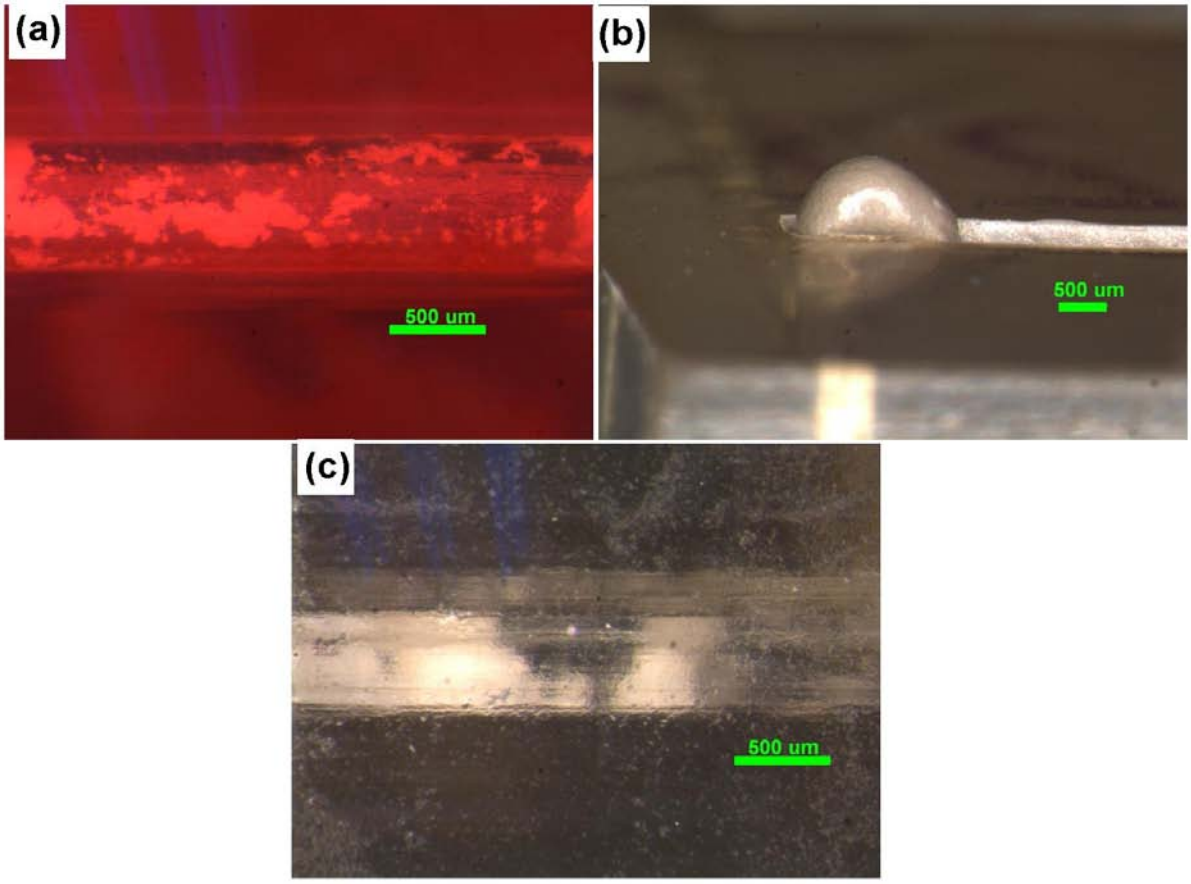

Figure 6.5: Examples of the problems encountered when trying to use DuPont CB028 ink on 3D structures; **(a)** separation in the via structure of a ProtoTherm™ structure, **(b)** ejection of the ink during the thermal curing process in a WaterShed™ structure and **(c)** separation in the via portion of a WaterShed™ structure.

Figure 6 illustrates the goal of this study, attaining the lowest resistance possible without damaging the substrate. In the case of Somos ProtoTherm™ substrate damage is predominately scaling of the bottom of the substrate cured at 138°C for 30min—the optimum curing temperature for Ercon E1660. It should be noted that scaling could be avoided at the temperatures used in this study if the substrate was created on a polycarbonate film (note the structure on the right in Figure 6.6) without the use of support structures. However, if non

monolithic forms are to be created, support structures must be used; therefore avoidance of scaling is a priority.

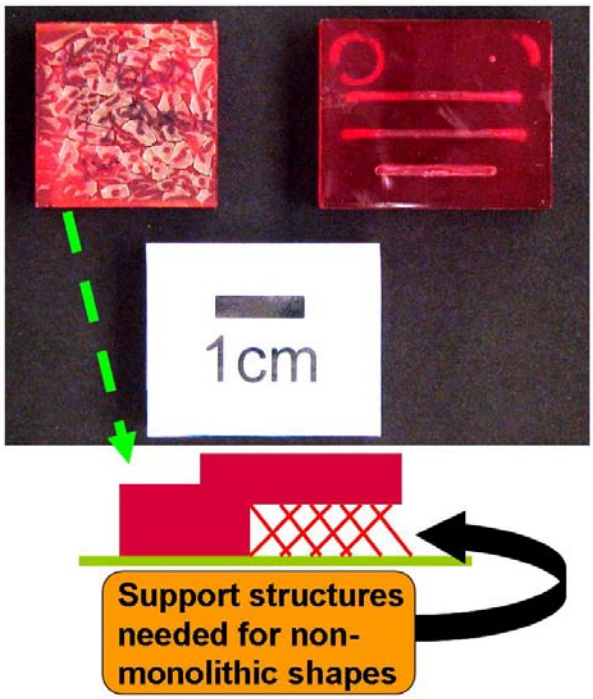

Figure 6.6: Example of the substrate damage imposed by curing a ProtoTherm™ structure for 30min at 138°C, the optimum cure temperature for the conductive ink used. Building the structure without the use of support structures could avoid scaling as illustrated by the sample on the right which was also cured at 138°C for 30min.

The lowest temperature which resulted in functional samples for E1660 was 100°C. Results of additional ohmic curing cycles are seen in Figure 6.7 and it is notable that the addition of ohmic curing cycles dropped the measured resistance to levels matching the resistance of samples cured at 138°C for 30min. Using CB102 for the creation of vias and E1660 for the external interconnects ink use pushed the lower thermal limit for producing functional samples to 74°C, the T_g of Somos ProtoTherm™. In this case the benchmark samples were subjected to two cure cycles, the first cure cycle was for the curing of the vias and followed the specified cuing parameters of CB102: 150°C for 1h. The second cure sample was meant to cure the external interconnects and took place at 138°C for 30min. As is seen in Figure 6.7, the additional ohmic

curing cycles allowed for samples subjected to two separate via/interconnect cure cycles of 74°C for 1h to attain a measured resistance matching the benchmark samples. Additionally, sample sets cured at 100°C for a shorter cure time of 15min were also able to attain a resistance matching that of benchmark samples after the application of additional ohmic curing cycles.

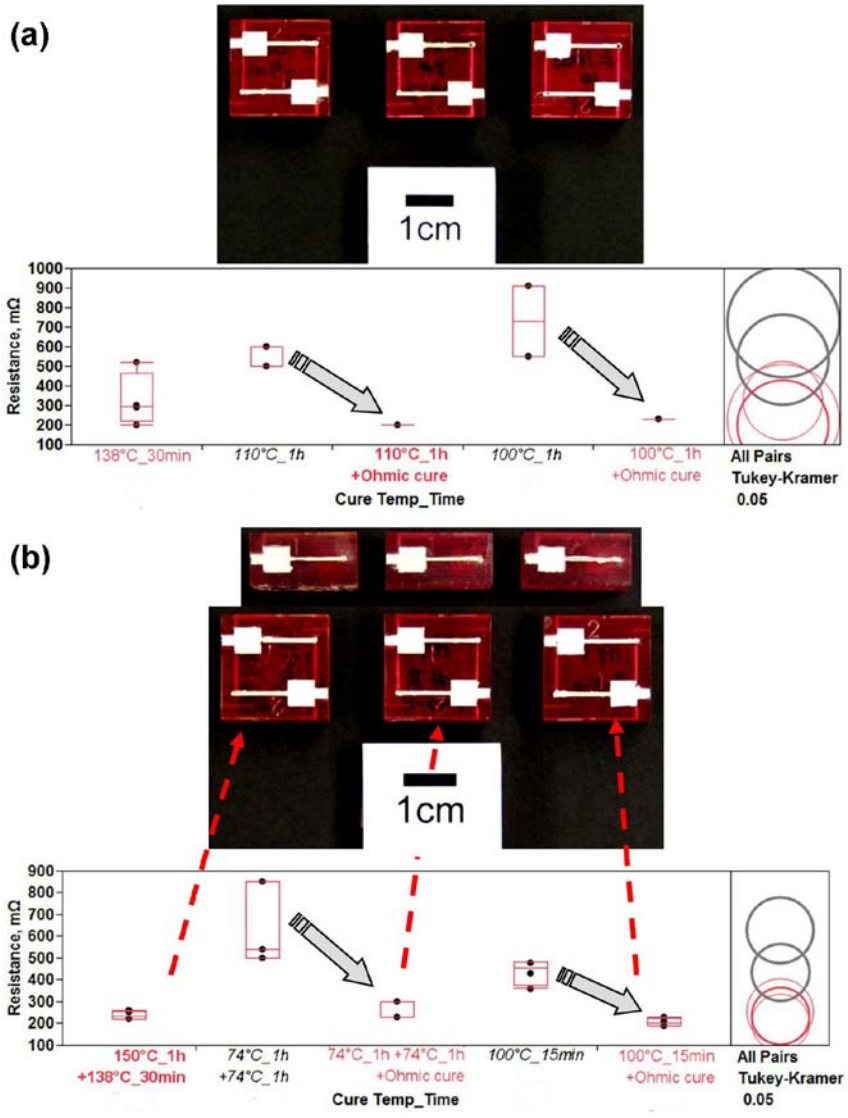

Figure 6.7: Results of **(a)** E1660 used as vias and interconnects on ProtoTherm™ substrates and **(b)** CB102 used as vias and E1660 used as interconnects on ProtoTherm™ substrates.

Dual paste/ink use also overcame the failure of components which utilized right angles in the via structure. As pointed out by Olivas [10], right angles in interconnect paths can lead to

failures in the conductive path. Indeed, earlier versions of the via/interconnect structure possessed right angles within the design and were subject to failure after 3 or less cycles of applied current as seen in Figure 6.8.

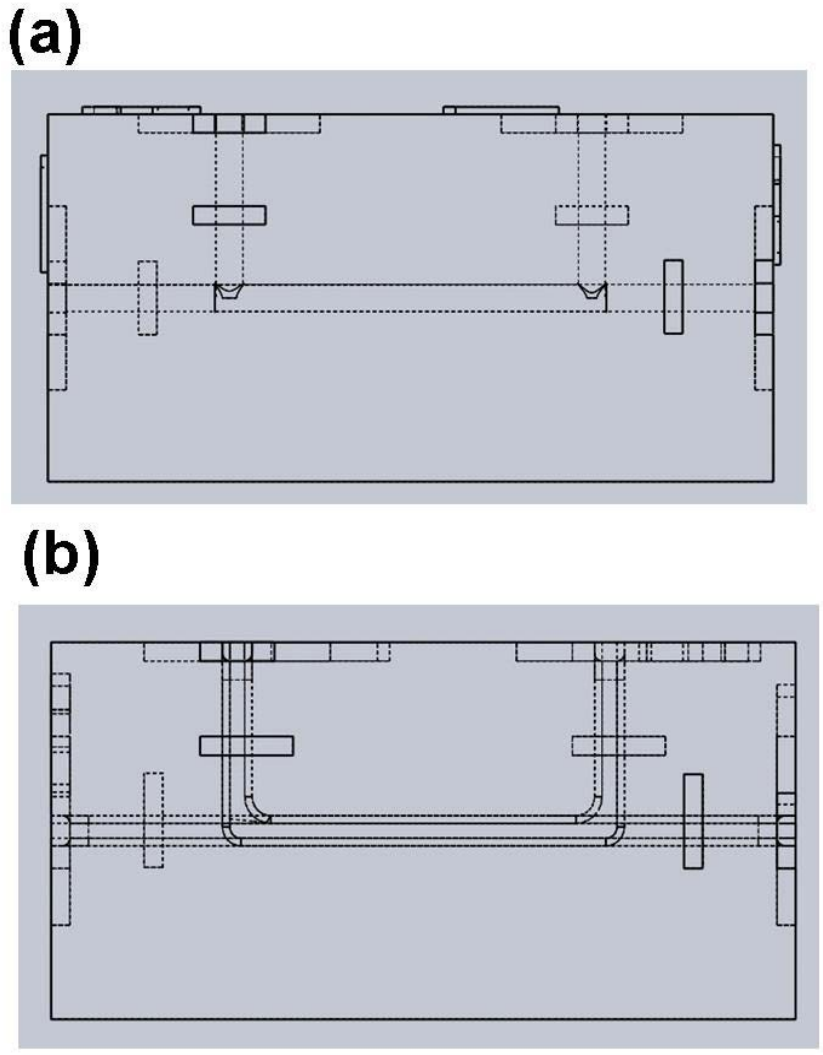

Figure 6.8: Earlier design **(a)** which incorporated right angles and **(b)** design with rounded vias.

Figure 6.9 illustrates the mechanics of the ohmic curing process. The first applied cycle at 2A did not produce enough initial heat to permanently change the resistance of the conductive trace though the resistance rises slightly due to ohmic heating. The first cycle at 3A displays a drop in resistance as this current value supplied enough initial heat to make a change to the

properties of the conductive trace, which is noticeable during the second 3A cycle as the initial resistance was lower than the initial resistance of cycle 1. The first 4A cycle produces the same behavior as the first 3A cycle as the higher current again produced enough heat to permanently alter the resistance of the printed trace.

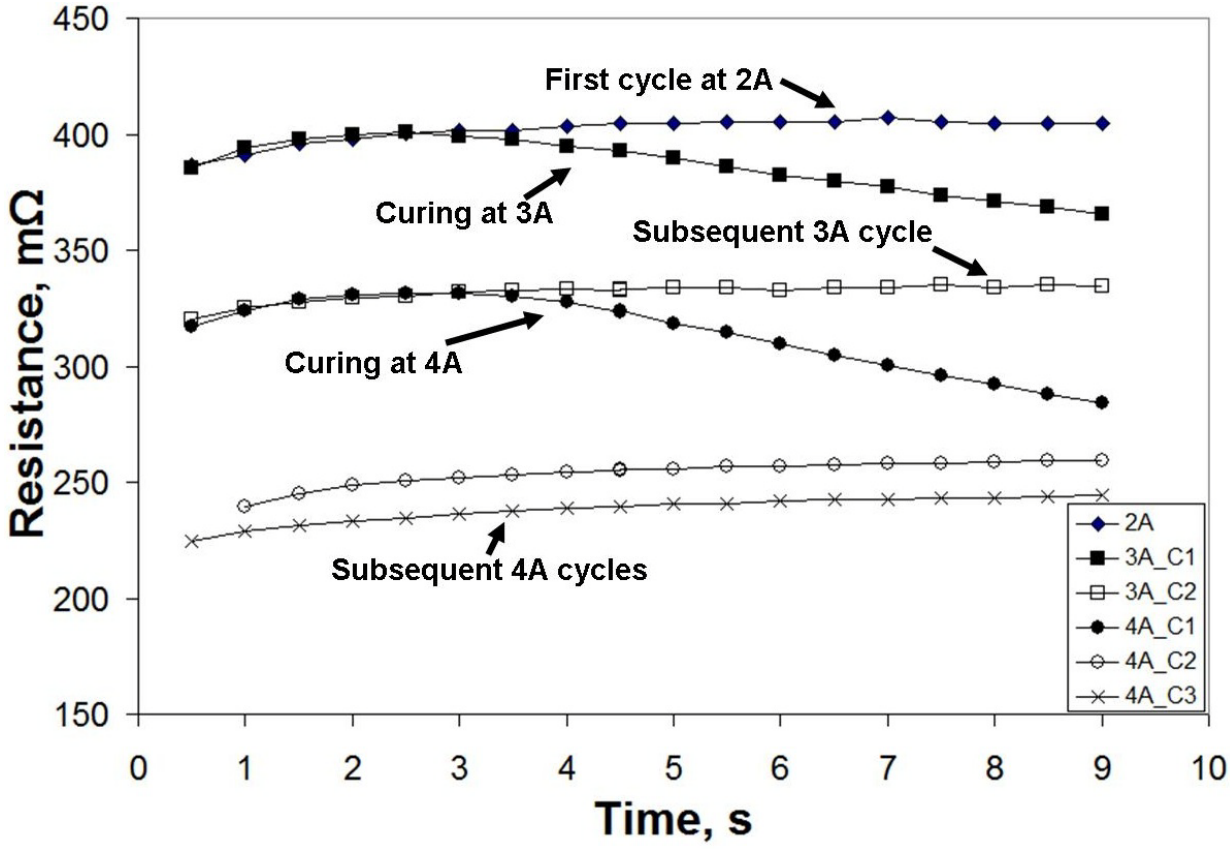

Figure 6.9: Graphical representation of the application of ohmic curing cycles to right angles via structures (Figure 6.8(a)) when DuPont CB102 paste was used in the internal vias and Ercon E1660 was used as external interconnects.

6.3.2 Via/interconnect Structures in WaterShed™

In the case of Somos WaterShed™ yellowing of the substrate is the predominant indicator of substrate damage as illustrated in Figure 6.10. Utilization of E1660 in the creation of both interconnects and vias was found to not necessitate the use of an additional ohmic cure as

samples cured at the lowest temperature an at which functional conductive traces could be attained (100°C for 1h) possessed lower resistance values than the benchmark samples.

When DuPont CB102 was used to create vias and E1660 used to create interconnects, the shorter cure time of 15min was capable of producing functional samples at a cure temperature of 110°C, whereas the longer cure time of 1h was necessary when solely using E1660 to ink the entire via/interconnect structure. The results of the DuPont CB102/Ercon E1660 experiments are seen in Figure 6.10. Experiments with a cure temperature of 46°C (the specified T_g for WaterShed™) for 1h produced functional samples, but with resistance values in the MΩ range, which was beyond our equipment capability to induce ohmic heating.

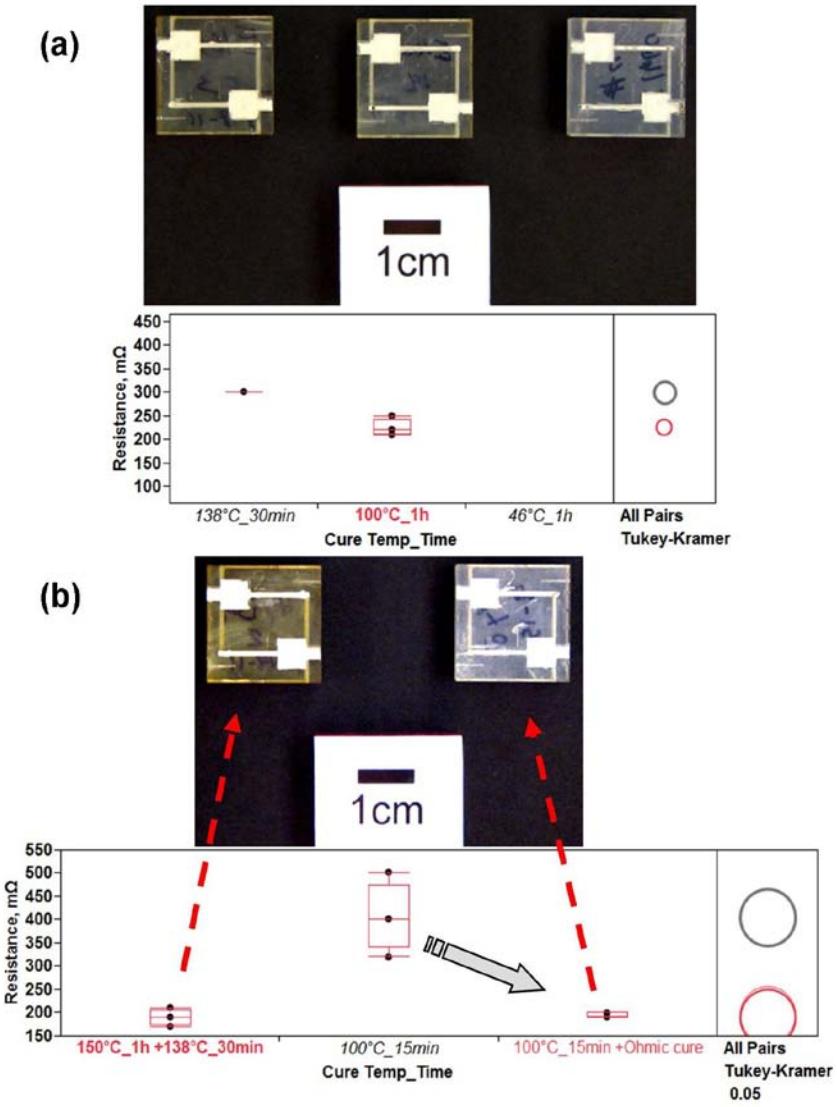

Figure 6.10: Results of experiments involving WaterShed™ substrates where **(a)** E1660 used as vias and interconnects and **(b)** CB102 used as vias and E1660 used as interconnects.

6.3.3 Special Processing of Outliers

Though the sample sets used in this study were small, there were experiments which produced outliers with resistance values greater than 1000mΩ. It was found that the power used in the 4A cure cycles was roughly 7 to 8W. Applying current values which equated to this range

of power applied to the conductive trace provided a successful avenue to apply ohmic curing without causing failure of the trace. As seen in Figure 6.11, an initial ohmic curing cycle at a current lower than 4A lowered the resistance of the outlier samples to a point that subsequent 4A cycles could be applied resulting in resistance values on par with non-outlier samples.

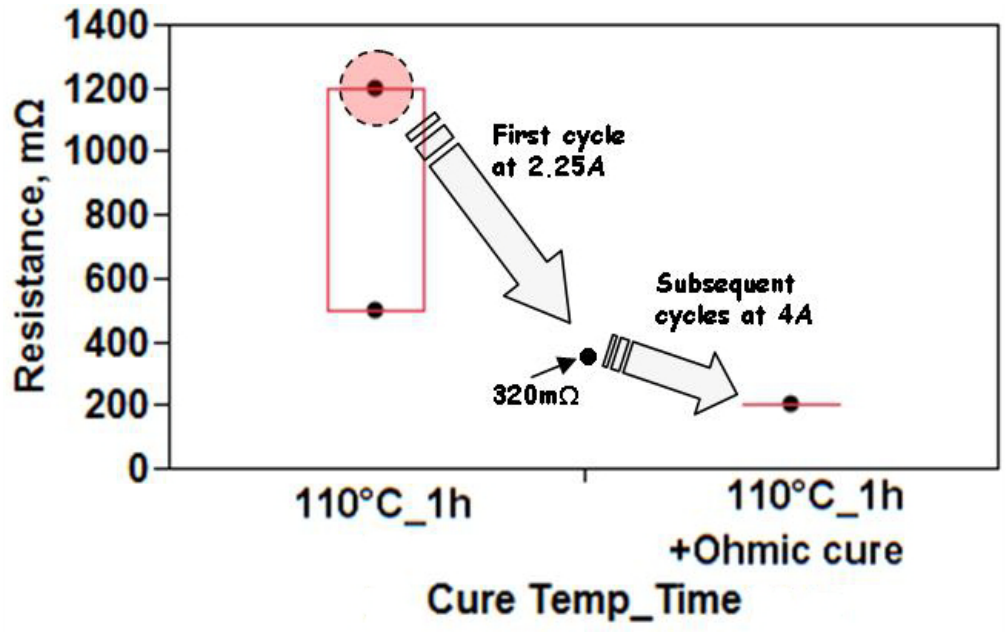

Figure 6.11: Example of applying incrementally increasing current values to process outliers.

6.4. Discussion

Initial wattage is driving parameter of the ohmic curing process. Figure 6.12 shows the typical resulting cure cycle profile of resistance vs. time. For a given applied current value, the resistance drops sharply during the initial portion of the cure cycle. Subsequent cycles at the same applied current value do not result in a further decrease of the resistance of the conductive trace, but rather an increase in resistance due to ohmic heating is observed. In order to reduce the resistance of the conductive trace further, a higher current would have to be applied. This phenomenon is also visible in Figure 6.9 where the initial cycles of applied current at 3A and 4A show a sharp decrease in resistance, but the subsequent cycles.

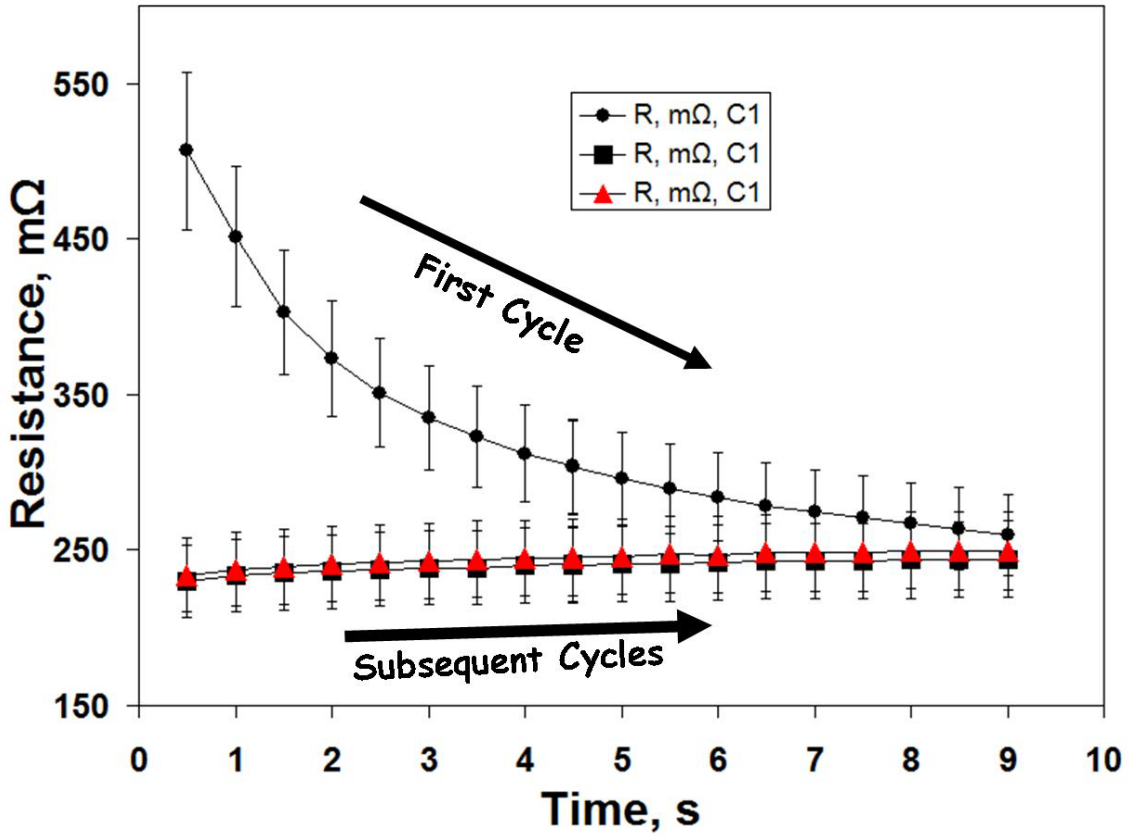

Figure 6.12: Typical resistance vs. time behavior for an ohmic curing cycle. The first cycle at a given applied current causes a sharp drop in resistance. The subsequent cycles are not able to cause further significant curing effect. In this case the applied current was 4A.

However, in the case of the structure presented in this study, the maximum applied current of 4A seemingly creates the most conductive path possible. Higher currents applied manually with a different power supply (Kepko model JQE 3615) showed little to no improvement for applied current values of up to 8A.

Substrate damage appears to be limited to that imposed by the initial thermal cure cycle or cycles. Neither substrate material appears to have been damaged by the ohmic curing process, though CB102 seems to be subject to charring as seen in Figure 6.13. Corresponding SEM micrographs show the charring to be limited to the paste itself.

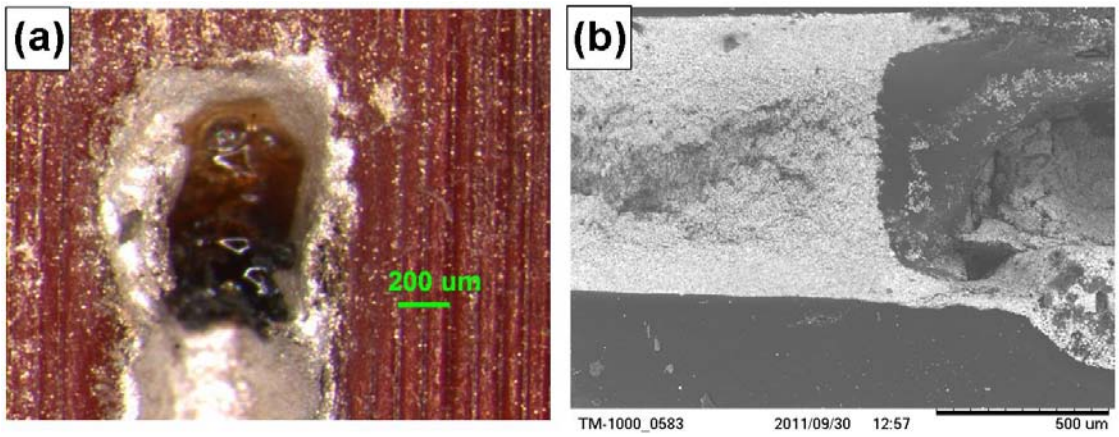

Figure 6.13: (a) Optical micrograph showing evidence of charring of DuPont CB102 on a ProtoTherm™ substrate and **(b)** a SEM micrograph showing charring of DuPont CB102 near the via/interconnect interface of a dual E1660/CB102 interconnect/via structure on a WaterShed substrate.

6.5. Conclusions

Ohmic heating can be used as a method to improve the conductivity of 3D via/interconnect systems for silver microparticulate-based inks. Using DuPont CB102 via/plug paste for the internal via structures in conjunction with Ercon E1660 conductive ink as external interconnects produced several benefits. Among these benefits was the creation of functional samples at lower pre cure as low as 74°C whereas utilizing E1660 alone did not allow for the creation of functional samples at cure temperatures lower than 100°C. Utilizing separate printable conductors for internal vias and external interconnects also allowed for shorter cure times to be realized as functional samples were created at 100°C after curing for only 15min whereas utilizing only E1660 necessitated the longer cure time of 1h. The utilization of CB102 in the creation of the via structure also removed design limitations as functional samples were created with via structures which possessed right angles in the conductive path. Finally, no substrate damage was introduced by the ohmic curing process.

6.6 References

[1] D. Tobjörk, N. J. Kaihovirta, T. Mäkelä, F. S. Pettersson, and R. Österbacka, “All-printed low-voltage organic transistors,” *Organic Electronics*, vol. 9, no. 6, pp. 931-935, Dec. 2008.

[2] K. H. Church, *et al.*, “Printed Electronic Processes for Flexible Hybrid Circuits and Antennas,” *Proceedings of the Flexible Electronics and Displays Conference*, Phoenix, AZ, Feb 2009.

[3] M. Navarette, A. Lopes, J. Acuna, R. Estrada, E. MacDonald, J. Palmer, R. Wicker, *Proc. 18th Solid Freeform Fabr. Symp.,* (Austin, TX: 2007), pp. 575-585.

[4] E. DeNava, M. Navarette, A. Lopes, M. Alawneh, M. Contreras, D. Muse, S. Castillo, E. MacDonald, R. Wicker, “Three-Dimensional Off-Axis Component Placement and Routing, “for Electronics Integration using Solid Freeform Fabrication in *Proceedings of the 2008 Solid Freeform Fabrication Symposium*, Austin, Texas, pp. 362-369, 2008.

[5] S. Castillo, D. Muse, F. Medina, E. MacDonald, R. Wicker, “Electronics Integration in Conformal Substrates with Additive Layered Manufacturing,” in *Proceedings of the 2009 Solid Freeform Fabrication Symposium*, Austin, Texas, pp. 730-737, 2009.

[6] K. Arcaute Cantu, "Stereolithography of poly (ethylene glycol) hydrogels with application in tissue engineering as peripheral nerve regeneration scaffolds" Ph.D. dissertation, Dept. Mat. Sci. and Eng., The Univeristy of Texas at El Paso, El Paso, TX, 2008.

[7] D. A. Roberson, R. B. Wicker, L. E. Murr, K. Church, and E. MacDonald, “Microstructural and Process Characterization of Conductive Traces Printed from Ag Particulate Inks,” *Materials*, vol. 4, no. 6, pp. 963-979, May. 2011.

[8] A. J. Lopes, "Hybrid manufacturing: Integrating stereolithography and direct print technologies," Ph.D. dissertation, Dept. Mat. Sci. and Eng., The Univeristy of Texas at El Paso, El Paso, TX, 2010.

[9] D. A. Roberson, R. B. Wicker, E. MacDonald, “Ohmic Curing of Printed Conductive Traces,” *Journal of Electronic Materials*, In Revision

[10] R. I. Olivas, “Conformal electronics manufacturing through additive manufacturing and micro-dispensing,” M.S. thesis, Dept. of Electrical and Computer Eng., The University of Texas at El Paso, El Paso, TX, 2011.

CHAPTER 7: MICROSTRUCTURAL CHARACTERIZATION OF ELECTRICALLY FAILED CONDUCTIVE TRACES PRINTED FROM Ag NANOPARTICLE INKS

7.1 Introduction

Ink-printed conductive traces are gaining interest due to the relative simplicity and low cost of printing methodologies as compared to typical metallization processes [1, 2]. A key obstacle for the use of polymeric substrates is the temperature limitation to thermal curing of printed conductive traces due to the low glass transition temperatures of polymeric substrates such as polycarbonate—which has a T_g of ~150°C [3]. Sintering via the application of DC current has been shown as a method for creating a sintered microstructure within conductive traces printed from nanoparticle inks [4]. The ohmic heating resulting from the application of DC current has also been shown as a method for decreasing the resistivity of conductive traces printed from both microparticle and nanoparticle loaded inks consisting of both a sintered and unsintered microstructure [5]. Both methods focused on the decrease in measured resistance and resistivity of a printed trace; however, characterizing the failures of printed traces is also important in the development of curing methods alternative to the application of thermal energy through use of an oven.

The goal of the work presented in this paper is to characterize the microstructures found in electrically failed regions of conductive traces printed from nanoparticle loaded inks. The non-homogeneous nature of the microstructure found within the failed region was discussed.

7.2 Experimental

DuPont Kapton® (DuPont, Wilmington, DE, USA) polyimide film measuring 300μm in thickness was subjected to UV-ozone cleaning in a UVO Cleaner Model 342A (Jelight Company, Inc., Irvine, CA, USA) for 10min to create a clean surface and to enhance the wetting of the ink on the substrate surface. Conductive traces measuring ~850μm wide with a 5mm by 5mm test pad structure on either end were printed in sample sets of five in two lengths (1 and

2cm) with a Dimatix 2800-Series Materials Printer (Fujifilm Dimatix, Inc., Santa Clara, CA, USA) operating at 1270 DPI using a nanoparticle ink (CCI-300, Cabot Corporation, Albuquerque, NM, USA) with a particle size of 40nm. The traces were printed twice upon one another to optimize the electrical properties [6]. The traces were oven cured in air for 1h at 110°C to dry the ink. For comparison, the failed zone of a 5cm trace was also examined utilizing the same substrate material, pretreatment and thermal cure parameters. Different printing parameters were used as the trace was printed ten times upon itself at 635 DPI resulting in the same cross-sectional area as the 1 and 2cm traces. Also characterized was the failed zone of a 4mm fuse printed from another nanoparticle Ag ink (JS-015, Novacentrix, Austin, TX, USA) with an nScrypt 3Dn 450 micro-dispensing system (nScrypt, Inc., Orlando, Florida, USA) on Kapton® with no prior substrate treatment and then cured for 20min at 110°C. The fuse is similar to those described by Church *et al.* [7].

Resistance was measured with a multimeter (Fluke model 289, Fluke Corporation, Everett, WA, USA). Electrical current was supplied manually to the conductive traces with a programmable power supply (ABC 25-4DM, Kepco, Inc, Flushing, NY, USA). For both resistance measurement and the application of electrical current, flat Cu test probes with a contact area of ~2.25mm^2 were used. Scanning electron microscopy (SEM) was performed with a Hitachi S-4800 Ultra-high Resolution Field Emission Scanning Electron Microscope (Hitachi High-Technologies Corporation, Tokyo, Japan) utilizing a 20keV accelerating voltage after first subjecting the samples to a 30sec Au/Pd sputtering with a Gatan Model 682 Precision Etching Coating System (Gatan, Inc., Pleasanton, CA, USA). The applied current values are found in Table 7.1.

Table 7.1: The experimental data for the conductive traces examined in this study.

Ink	Initial Cure	Length, cm	Area, μm^2	Initial Resistance, Ω	Sample Size, n	Applied Current, mA	Applied Current Density, $mA/\mu m^2$
CCI-300	1h at 110°C	1	510	4.8 ± 1.3	5	1000	1.96
CCI-300	1h at 110°C	2	510	8 ± 1.7	5	800	1.56
CCI-300	1h at 110°C	5	510	19	1	1000	1.96
JS-015	20min at 110°C	0.4	77	25	1	150	1.95

7.3 Results

Figure 7.1(a) shows that there is no substrate damage under the failed region of the 1cm trace. The failed region itself resembles a ruptured pipe. Examining the microstructures at different areas in and around the failure zone reveals a variety of different microstructures due to non-uniform heating. White dashed arrows indicate the corresponding zoomed region for each area of the failed zone examined. The SEM micrograph zooming in on a folded-over portion of material near the center of the rupture zone reveals a grainy microstructure while a zoomed in region of a folded-over portion of material at the bottom left of the failed area shows the microstructure to be that of sintered particles. The contrast difference in the area around the failed zone was examined and it was found that the darker region corresponds to a film of sintered particles while the lighter region more closely matches the initial (prior to the application of electric current) microstructure of the printed trace—unsintered particles. Also notable is the cracking which occurred within the printed trace. The densification of the grainy region is significant as it is an indicator of the amount of heat transferred to the localized region in the conductive trace. For comparison, a micrograph (Figure 7.1(b)) of the same material printed in the same manner, but subjected to a thermal cure of 250°C for 1h shows a grainy film, but far less dense. Figure 7.1(c) shows no sintering occurred far away from the failure region.

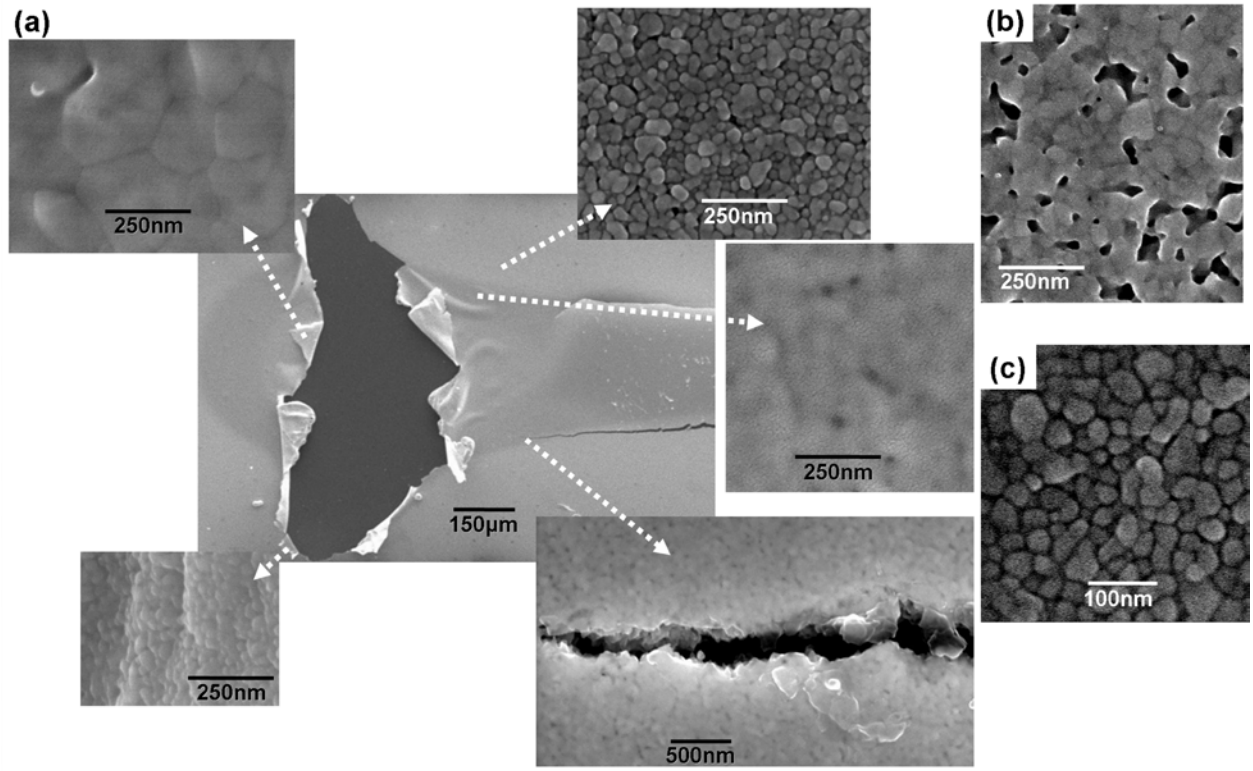

Figure 7.1: (a) The different microstructures observed in the failure zone of a 1cm long printed conductive trace. Note the presence of a grainy film which is denser than **(b)** the microstructure of the same ink thermally cured at 250°C for 1h. Note the drastic difference of the microstructure of the ink far away from the failure zone **(c)**.

The failed region of the 2cm trace is seen in Figure 7.2(a) and also resembles a ruptured pipe. Again, a contrast difference was observed where the darker region corresponded to sintered particles. The microstructure of the lighter region as well as an area further away from the failed zone (Figure 7.2(b)) was that of unsintered particles. The magnified image of a crack near the center edge of the ruptured zone has both intergranular and transgranular fracture indicating the crack in this area developed after the formation of grains. Examining the area at the top and bottom of the ruptured zone shows material to have been pushed outward as was the case when examining the 1cm trace. In every instance for both the 1 and 2cm samples, failure of the trace occurred immediately upon the manual application of electrical current.

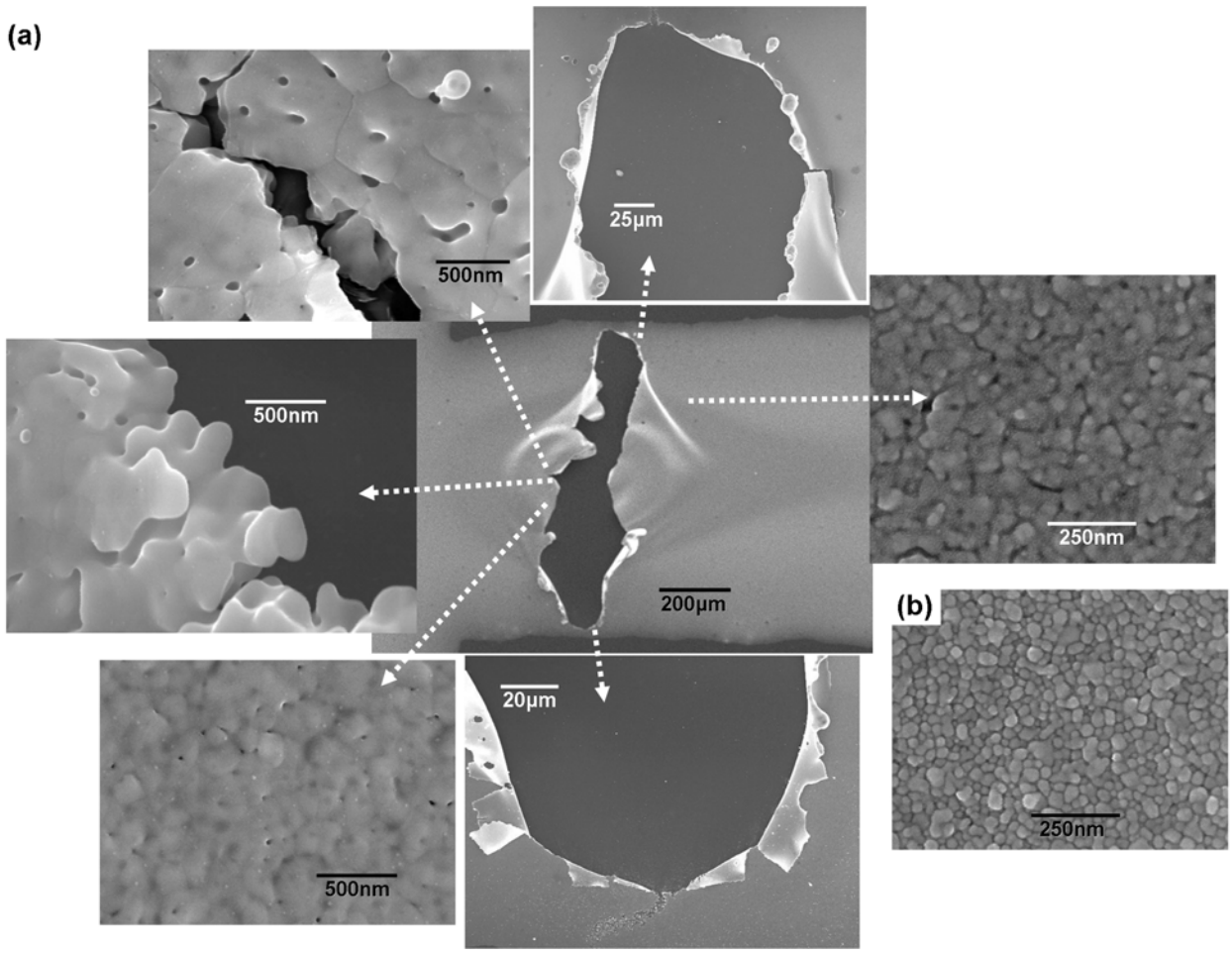

Figure 7.2: (a) The different microstructures observed in the failure zone of a 2cm long printed conductive trace compared to **(b)** the microstructure of the trace away from the failure zone.

Examining the failure area of the 5cm trace reveals substrate damage to have occurred as seen in Figure 7.3(a). Again, the failed zone resembles a ruptured pipe. The substrate damage does not seem to have occurred under the rupture area, but rather in the area above and below the failed zone. The microstructure of the ruptured area is that of a grainy film. Smaller ruptures are found adjacent to the failed area also consisting of a grainy film. The initial microstructure was that of unsintered particles as seen in Figure 7.3(b).

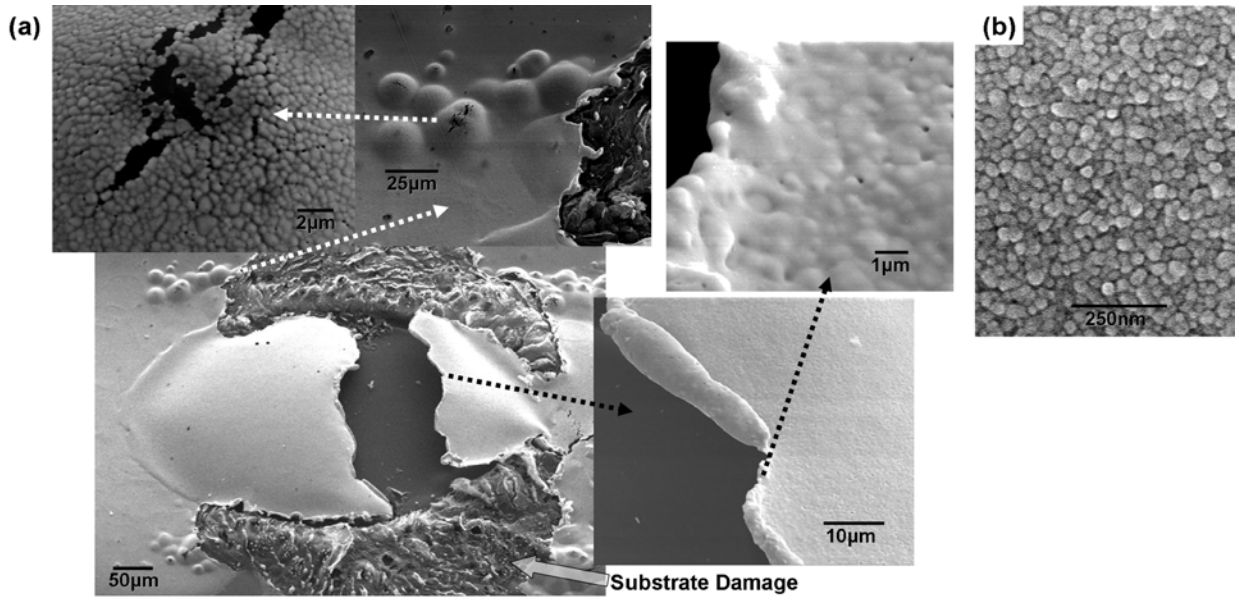

Figure 7.3: (a) The different microstructures observed in the failure zone of a 5cm long conductive trace. Note the initial microstructure **(b)** was that of unsintered nanoparticles.

The blister-like ruptures found in the above three examples may be due to the shrinkage which occurs during the sintering process as documented in literature [8-10]. The drastic difference in microstructure found in close proximity to one another would lead to localized tension within the conductive traces which led to the rupture and cracking observed as illustrated in the schematic in Figure 7.4 where the magnitude of the force associated with the different microstructures is indicated by the relative size of the arrows. The amount of force is directly influenced by the amount of shrinkage associated with the different microstructures, for example, the formation of grains causes more shrinkage than sintering [8-10]. The microstructural differences give an indication of the thermal profile. The heat transferred to the conductive trace is greater in the center as evident by the presence of grains in the center of the failed zone. The samples failed before a significant amount of heat could be transferred to the rest of the conductive trace as especially evident by the unsintered particles observed outside the failed zone.

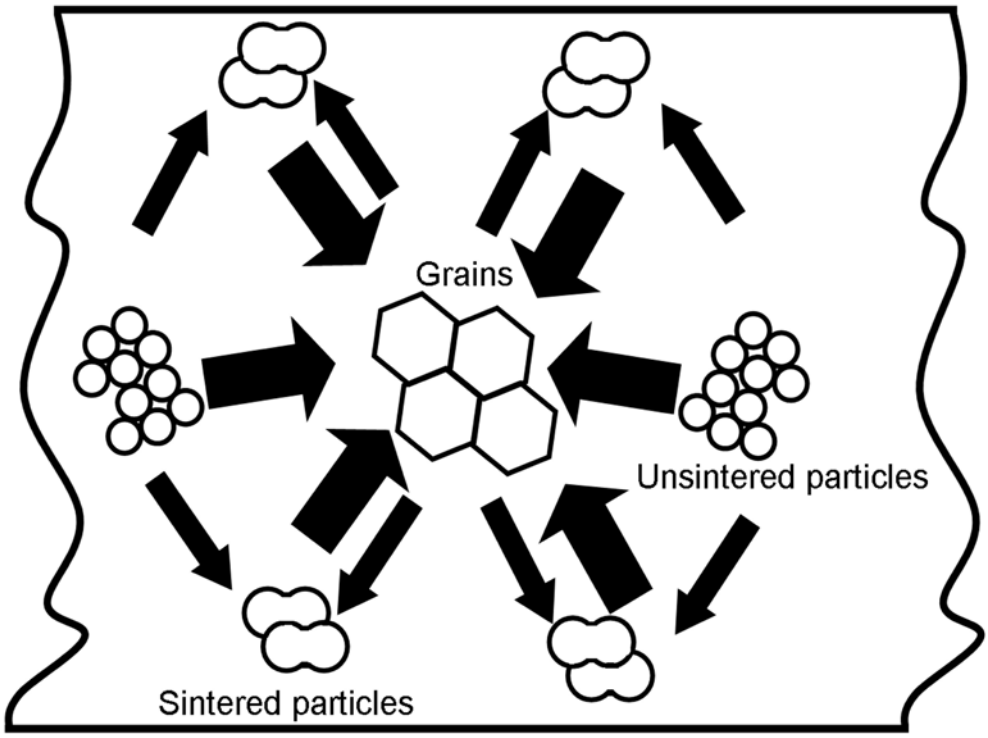

Figure 7.4: Schematic illustrating the magnitude of forces applied within the conductive trace due to the differing shrinkage amounts associated with the non-homogeneous microstructures present within the trace.

The microstructure of the trace intended for use as a fuse shows a drastic difference in microstructure when compared to the first three examples because the trace is considerably smaller in both length and cross sectional area—concentrating the transferred heat to a smaller area. The applied current of 150mA is much lower than the other samples observed in this study, but the applied current density—which accounts for dimensional differences—is similar as indicated in Table 7.1. The initial microstructure (Figure 7.5(a)) was that of unsintered particles while the failed zone's microstructure (Figure 7.5(b)) is a web-like matrix consisting of grains and melted particles. There is a small portion at the point of failure which resembles the "ruptured pipe" feature discussed earlier. Figure 7.5(c) shows a sharp contrast between the failed and non-failed region within the trace. In the area of the failed region, there appears to be some

substrate damage indicating that a temperature greater than the 360°C T_g of Kapton® [5] was reached.

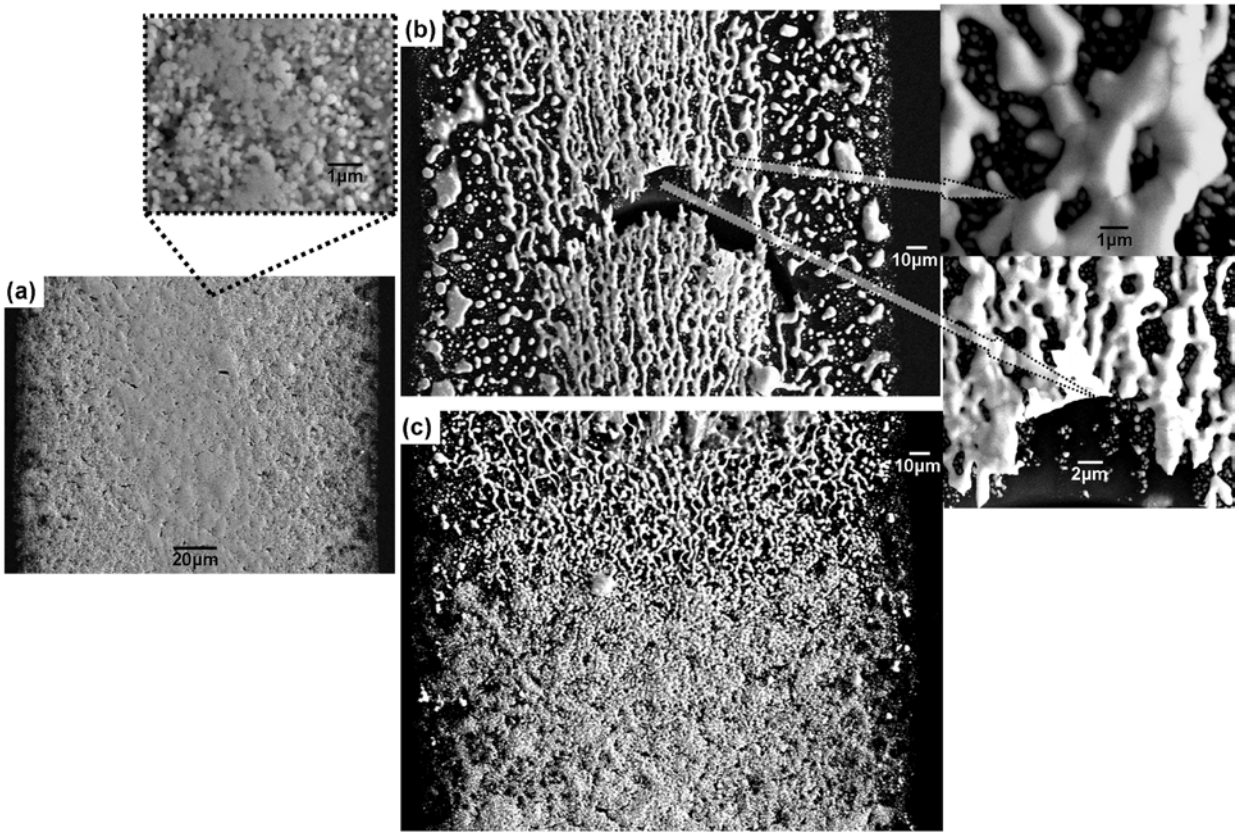

Figure 7.5: (a) The initial microstructure of a fuse printed from Novacentrix nanoparticle ink compared to **(b)** the failure zone of the fuse. Note the web-like matrix of grains and melted particles. There is a sharp contrast **(c)** between the failure zone and the remainder of the printed trace.

7.4 Conclusions

In all of the cases discussed in this paper, a significant amount of energy was transferred to the conductive ink particles as indicated by the presence of grains, sintering and melted particles. In some cases, the energy transfer was sufficient to damage the polyimide substrate. The application of electrical current is capable of producing significant microstructural changes within conductive traces printed from nanoparticle loaded inks.

7.5 References

[1] B. K. Park, D. Kim, S. Jeong, J. Moon, and J. S. Kim, “Direct writing of copper conductive patterns by ink-jet printing,” *Thin Solid Films*, vol. 515, no. 19, pp. 7706-7711, Jul. 2007.

[2] J.-W. Kim *et al.*, “Characterization of direct patterned Ag circuits for RF application,” *Microelectronic Engineering*, vol. 87, no. 3, pp. 379-382, Mar. 2010.

[3] H. Wohltjen and R. Dessy "Surface acoustic wave probes for chemical analysis. III. Thermomechanical Polymer Analyzer", *Anal. Chem.*, vol. 51, pp.1470 - 1475, 1979.

[4] M. L. Allen, M. Aronniemi, T. Mattila, A. Alastalo, K. Ojanperä, M. Suhonen, and H. Seppä, “Electrical sintering of nanoparticle structures,” *Nanotechnology*, vol. 19, p. 175201, Apr. 2008.

[5] D. A. Roberson, R. B. Wicker, E. MacDonald, “Ohmic Curing of Printed Conductive Traces,” *Journal of Electronic Materials*, In Revision

[6] D. A. Roberson, R. B. Wicker, L. E. Murr, K. Church, and E. MacDonald, “Microstructural and Process Characterization of Conductive Traces Printed from Ag Particulate Inks,” *Materials*, vol. 4, no. 6, pp. 963-979, May. 2011.

[7] K. H. Church, C. M. Newton, A. J. Marsh, E. W. MacDonald, C. D. Soto, and J. C. Lyke, “Print-and-play: a new paradigm for the nearly-instant aerospace system,” *Proc. of SPIE*, vol. 7691, no. 1, p. 76910A-76910A-9, Apr. 2010.

[8] J. R. Greer and R. A. Street, “Thermal cure effects on electrical performance of nanoparticle silver inks,” *Acta Materialia*, vol. 55, no. 18, pp. 6345-6349, Oct. 2007.

[9] K.-S. Moon *et al.*, “Thermal behavior of silver nanoparticles for low-temperature interconnect applications,” *Journal of Electronic Materials*, vol. 34, no. 2, pp. 168-175, Feb. 2005.

[10] K. Park, D. Seo, and J. Lee, “Conductivity of silver paste prepared from nanoparticles,” *Colloids and Surfaces A: Physicochemical and Engineering Aspects*, vol. 313_314, no. 0, pp. 351-354, Feb. 2008.

CHAPTER 8: SUPPLEMENTAL CHARACTERIZATION AND CONCLUDING REMARKS

8.1 DTA/TG Characterization

Throughout this work, the most utilized nanoparticle ink was Cabot CCI-300. Differential thermal analysis and thermogravimetric analysis (DTA and TG) were used to characterize the thermal behavior of this ink. Specifically a LabSys Evo (Seatram, Inc., Hillsboro, NJ) using an argon atmosphere to prevent sample oxidation. As can be seen in Figure 8.1 the rate of weight decrease increases sharply at ~150 -160°C meaning the binder is evaporating quickly in this temperature range. By ~260°C the weight decrease stops. Noticeably absent from the DTA curve in Figure 8.1 is any indication of an exothermic process in the temperature range of 150 -160°C indicating the sintering process has begun [1]. Sintering starting in this temperature range would be consistent with the results seen in Figures 1.8 and 3.7. The DTA curve in Figure 8.1 indicates an exothermic reaction occurring at ~210°C with another exothermic reaction starting at ~225°C and may be associated with the densification and solid-state grain growth which occurs in this temperature range as indicated by Figures 1.8 and 3.7.

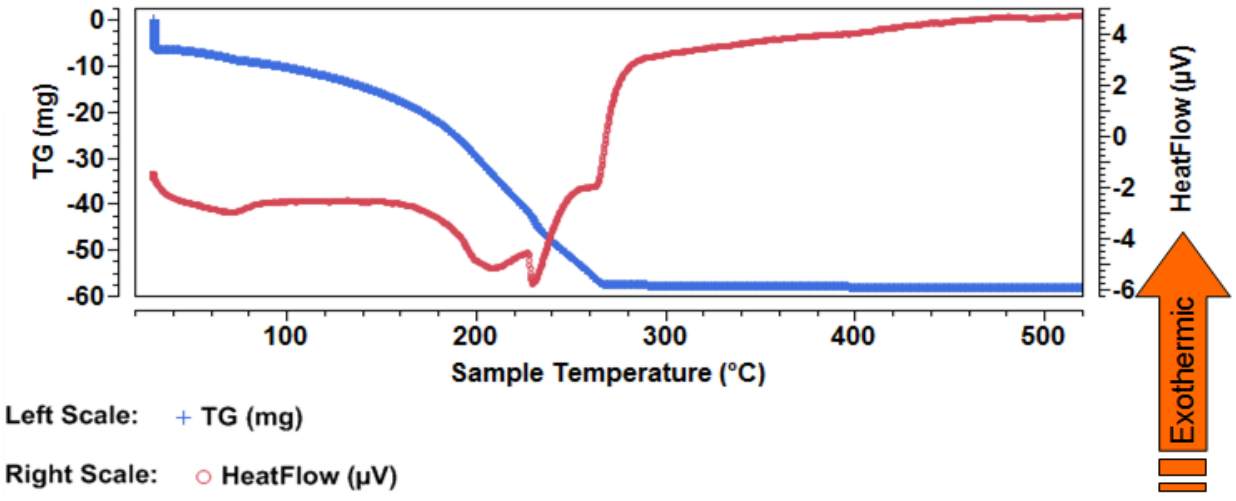

Figure 8.1: Graph of the TG and DTA curves for Cabot CCI-300 nanoparticle ink.

A microparticle loaded ink used the most in this study was Ercon E1660. DTA/TG curves of this ink are seen in Figure 8.2 where a rapid decrease in weight begins at around 180°C corresponding with an endothermic reaction; most likely the evaporation of the solvent in the binder. The rapid decrease in weight ends at ~200°C which corresponds with an exothermic reaction. The weight loss levels off at roughly 460°C. The recommended cure temperature for Ercon E1660 is 121°C [2] indicating perhaps the manufacturer intended the binder to remain in the ink during use.

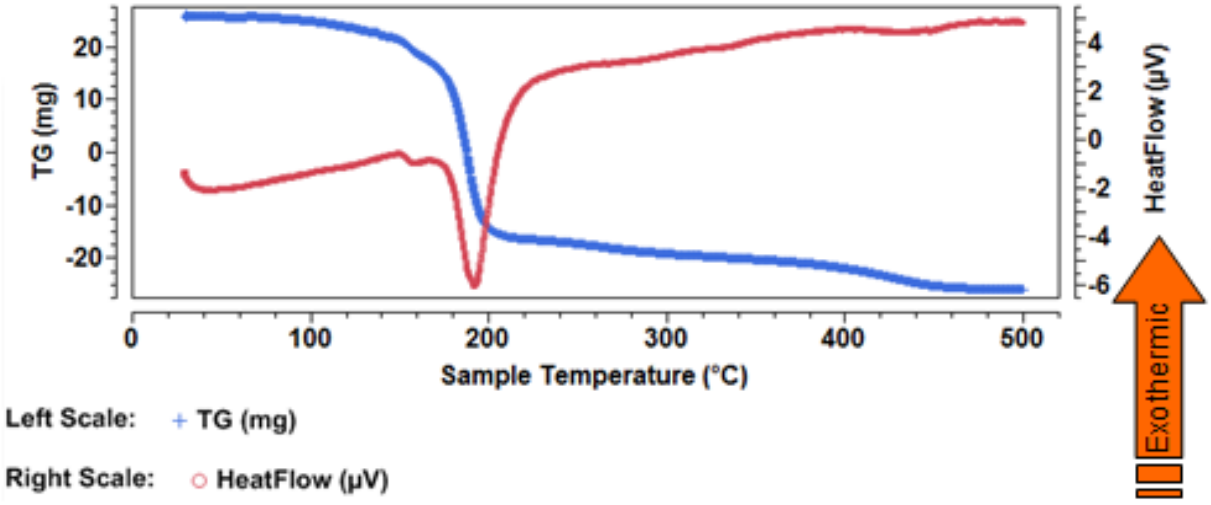

Figure 8.2: Graph of the TG and DTA curves for Ercon E1660 microparticle ink.

8.2 Temperature modeling of the Ohmic Curing Process

Method 1: Heat and Mass Model

If we revisit the data presented in the real-time measurement of the ohmic curing process, (Figure 4.6(a) and (c)) real-time plots of power, P, and consequently heat Q, can be calculated from the measured resistance data as the readings were taken every 0.5s based on Equations (4.7) and (4.9). Modeling of the heat is relatively straightforward and graphs of the heat derived from the cycles in Figure 4.6 are seen in Figure 8.3.

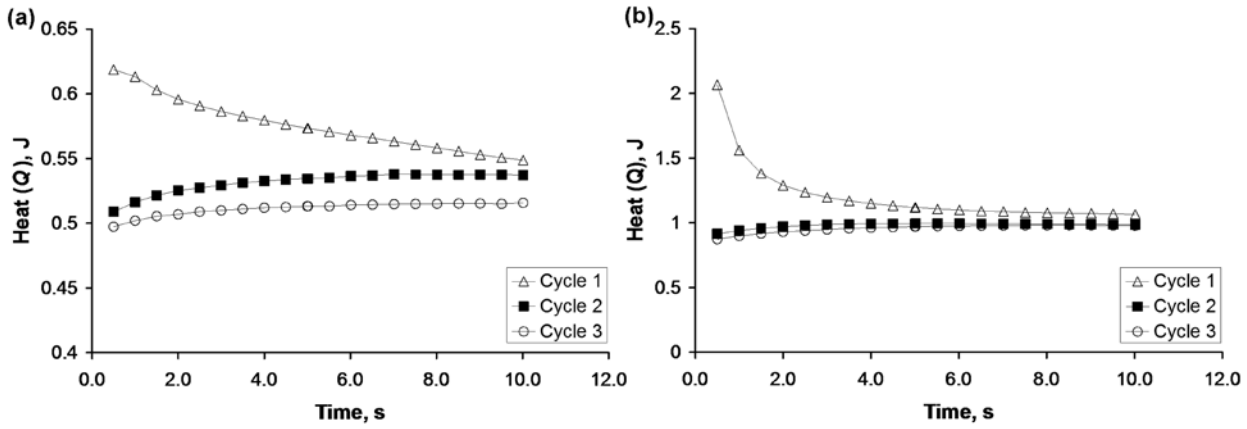

Figure 8.3: Graphical representation of the heat generated during the ohmic curing process after the application of **(a)** 0.25A and **(b)** 0.5A of electrical current. Calculated from data in [3].

As an aside it should be noted for Figure 8.3, the application of 0.25A (0.33mJ/μm^2) the second cycle was hotter than the third whereas the second cycle for the application of 0.5A (0.66mJ/μm^2) was almost identical to the third cycle in terms of heat. Because of this behavior it can be deduced the application of 0.25A did not effectively cure the printed trace during the first application of current.

From a calculation of the heat, *Q*, in Joules, the change in temperature, *ΔT*, can be approximated by the equation:

$$Q = mc\Delta T\,, \tag{8.1}$$

Where *m*, is mass and *c* is the specific heat capacity of the material [4]. It is at this step in the process where the modeling breaks down. Assuming the heat is confined within the printed trace, the mass of the printed trace is ~3.7 X 10^{-4} grams, meaning the change in temperature at the beginning of Cycle 1 in Figure 8.3(b) is ~24,000°C—an impossibility!

Method 2: Temperature Effect on Resistance Model

The equation describing the effect of temperature on the resistivity of a metal is:

$$\rho = \rho_o[1+\alpha_o(T-T_o)], \tag{8.2}$$

where α_o temperature coefficient of resistivity [5]. For simplicity we assume the dimensions of the printed trace, $\frac{A}{l}$, do not change during the ohmic curing process. Therefore Equation (8.2) can be rewritten in terms of resistance, *R*:

$$R = R_o[1 + \alpha_o(T - T_o)] \tag{8.2}$$

We also assume that T_o, the initial temperature, is equal to 20°C (room temperature) and that R_o is the measured resistance of the printed trace prior to the application of each ohmic curing cycle. Applying Equation 8.2 to the ohmic curing cycles yields the results seen in Figure 8.4.

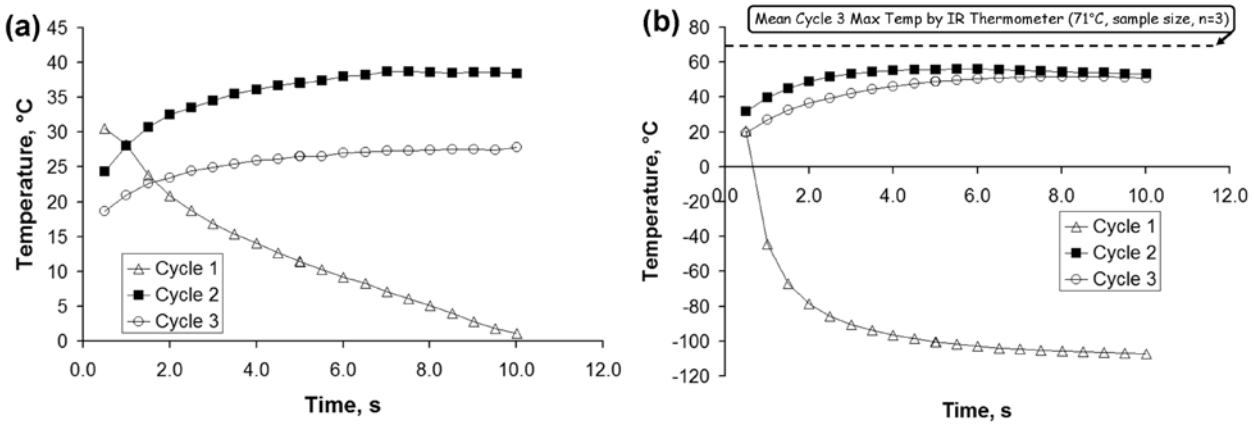

Figure 8.4: Graphical representation of the temperature of the printed trace during the ohmic curing process after the application of **(a)** 0.25A and **(b)** 0.5A of electrical current. Note the breakdown of the model for the first curing cycles. Calculated from data in [3].

As is evident by the behavior of the plot for the first cycle for both ohmic curing experiments, the temperature effect on resistance model breaks down during the first cycle—the cycle in which the most appreciable curing takes place. However, the modeling of subsequent cycles produces temperature values which are reasonably close to measurements made with an infrared (IR) thermometer (Fluke 62 Mini IR Thermometer, Fluke Corporation, Everett, WA, USA) readings of 71°C for Cycle 3 for experiments involving an applied current density of 0.66mA/μm^2.

Method 3: Utilizing Stefan's Law

At room temperature, the equation describing power radiated in a wire used in a heating element or light bulb—known as Stefan's Law—is:

$$P_{radiated} = \varepsilon \sigma_S A T^4 . \tag{8.3}$$

In the above equation Stefan's constant is represented by σ_S, A is the area of the conducting wire, T is the temperature of the conducting wire, and ε is the emissivity of the material the wire is composed of.[5] Equation (8.3) is also known as the Stefan-Boltzmann law and σ_S, the Stefan-Boltzmann constant [4]. Assuming that all the dissipated power in the trace is converted into heat and that the emissivity of the silver nanoparticles is 0.4 [6], a model can be created based on the power dissipated in the conductive trace during the ohmic curing process. The assumption of 0.4 being the emissivity of our silver nanoparticles is based on the findings in Reference [6], where the emissivity of a similar silver nanoparticle-loaded ink (Silverjet DGP-30LT-15C) decreased from 0.64 to 0.17 due to an electrical sintering process. The value of 0.4 (the midpoint between 1.7 and 0.64) as the emissivity of the Cabot CCI-300 traces is valid due to the 110°C thermal pre cure which did not sinter the nanoparticles, but left the ink somewhere between a cured and uncured state.

Graphical results of the application of this emissivity model to our two ohmic curing examples at 0.25 and 0.5A of electrical current are seen in Figure 8.5 where the emissivity is assumed to remain constant between cycles. As can be seen the temperature values for both electrical current values are below the melting temperature of silver making them plausible temperature values. The shape of the temperature vs. time curves match the shape of the heat vs. time curves for the same cycles in Figure 8.3. However, if the values of Cycle 3 for the 0.66mA/μm^2 ohmic curing cycle are compared to the model of Cycle 3, there is a difference in temperature of an order of magnitude (~10X). It should be noted also, that for a model based on Stefan's law to work, the emissivity of the printed conductive trace would have to be ~28.8—an impossibility yet again.

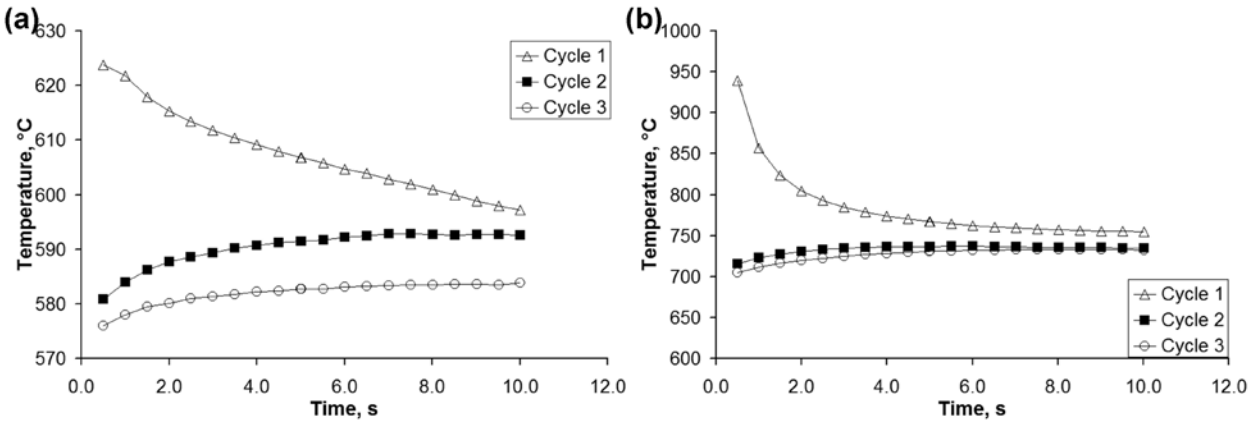

Figure 8.5: Graphical representation of the temperature (based on Stefan's Law) of the conductive trace during the ohmic curing process during the application of **(a)** 0.25A and **(b)** 0.5A of electrical current. Calculated from data in [3].

Applying Scaling Laws to Methods One and Three

Temperature modeling of the ohmic curing process presents an interesting exercise in the effects of scaling laws. The scenario described below is similar to those found in literature pertaining to the nano vs. beyond macro world namely [7, 8]. The nano-scale dimension in our printed traces is the thickness of the trace at ~600nm, if this dimension were to be multiplied by 10 it would no longer be nano; essentially meaning our traces are too small by a factor of 10^{-1}. Mathematically, Method 1 for modeling the temperature of the conductive trace during the ohmic curing process fails because the mass of the conductive trace is extremely small; ~3.7 X 10^{-4} grams. Assuming the IR thermometer readings of the third 0.5A ohmic curing cycle are correct, a factor of 4.5 X 10^{-3} should be applied to the ΔT calculations of the ohmic curing cycles. This factor is essentially the application of the scaling law for mass which scales based on volumetric linear dimension (L^3) [7, 8].

Applying this law to our factor of 10^{-1}, based on the mass the change in temperature would have to scale by a factor of 10^{-3}; on the order of the factor we actually scaled by. Adding a large amount of heat to a small mass and then saying, the mass does not increase very much in temperature seems somewhat counter intuitive, however if we revisit the microstructures of the failed printed traces in Chapter 7, it should be recalled that the microstructures in the center of

the printed lines indicated that the conductive trace was hottest in the center of the printed line. Recalling the profilometry of printed traces in Chapter 3, shows the printed traces are thicker in the center. This relationship between thickness and higher temperature in the center of the printed trace was also observed utilizing an IR camera during the electrical sintering process by Alastalo *et al.* [6]. A graphical representation of this scaled model is seen in Figure 8.6.

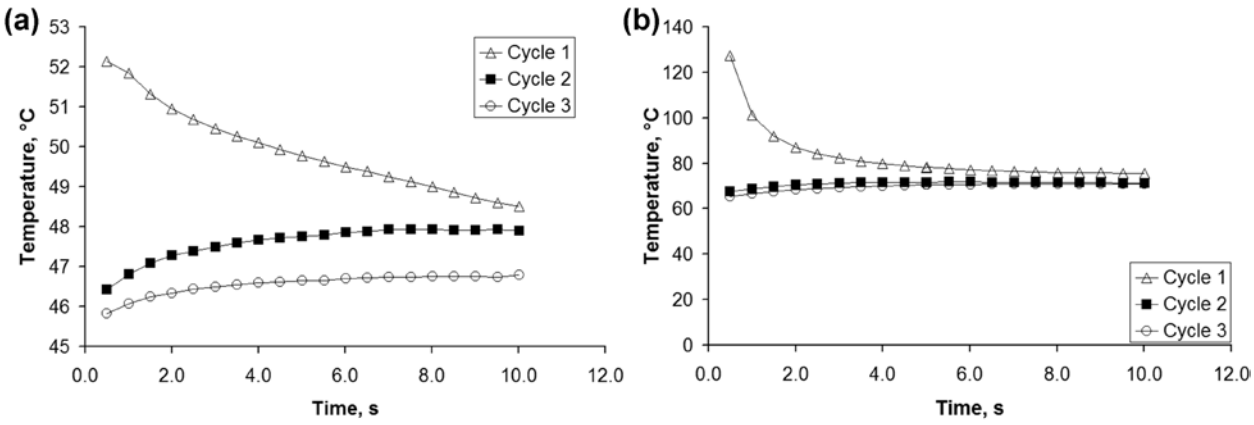

Figure 8.6.: Graphs resulting form applying a scaling factor to the modeling (based on heat and mass) of the temperature of conductive traces subjected to ohmic curing cycles of **(a)** 0.25 and **(b)** 0.5A. Calculated from data in [3].

Revisiting the emissivity model based on Stefan's law (Method 3) we may assume that amount of power dissipated as heat scales to some degree. Again using the IR thermometer reading as a baseline, Cycle 3 of the 0.5A ohmic curing cycle, a factor of 1.4 X 10^{-2} would have to be applied to the power dissipated in the emissivity model. According to scaling laws, power dissipated in the form of radiated heat scales by a linear dimension factor of L^2 [8]. Again, considering our trace is small by a factor of 10^{-1}, our scaling factor should be 10^{-2}, in the neighborhood of the factor we used to scale the dissipated power. A graphical representation of the scaled emissivity model is seen in Figure 8.7. Application of the concept of scaling the dissipated power by the same factor of 1.4 X 10^{-2} was made to the heat and mass model (Method 1) and is graphically represented in Figure 8.8.

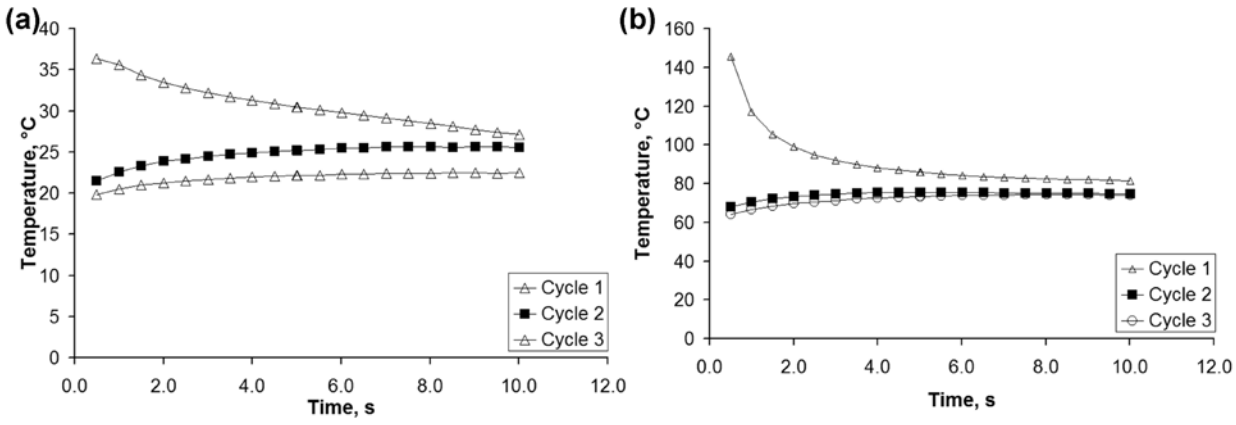

Figure 8.7: Graphical representation of the temperature after applying a scaling factor to the model based on Stefan's Law for ohmic curing cycles of **(a)** 0.25A and **(b)** 0.5A of applied electrical current. Calculated from data in [3].

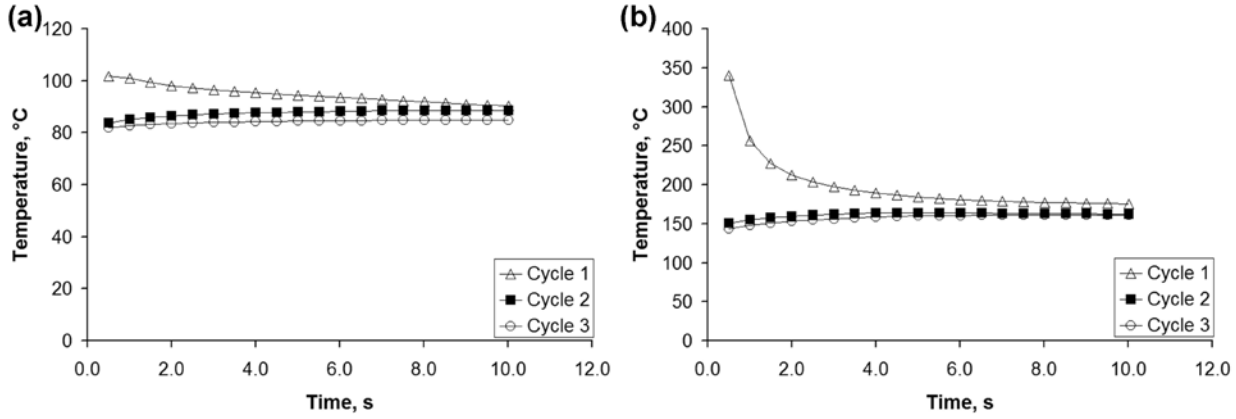

Figure 8.8: Graphical representation of applying the scaling factor based on power dissipation (as used in Figure 8.7) on the heat and mass model for ohmic curing cycles of **(a)** 0.25A and **(b)** 0.5A of applied electrical current. Calculated from data in [3].

A notable item is more electrical power is expected to be dissipated as is observed in microchips, as electrical power dissipates by a dimensional factor, L^{-1} [8]. Scaling the emissivity model by a factor of 10^{-1} in order to take into account the scaling of radiated power and

dissipated electrical power (L^{-1} X $L^2 = L$) results in the results seen in Figure 8.9. As can be seen the model produces a resulting temperature much higher than the IR thermometer readings of 71°C.

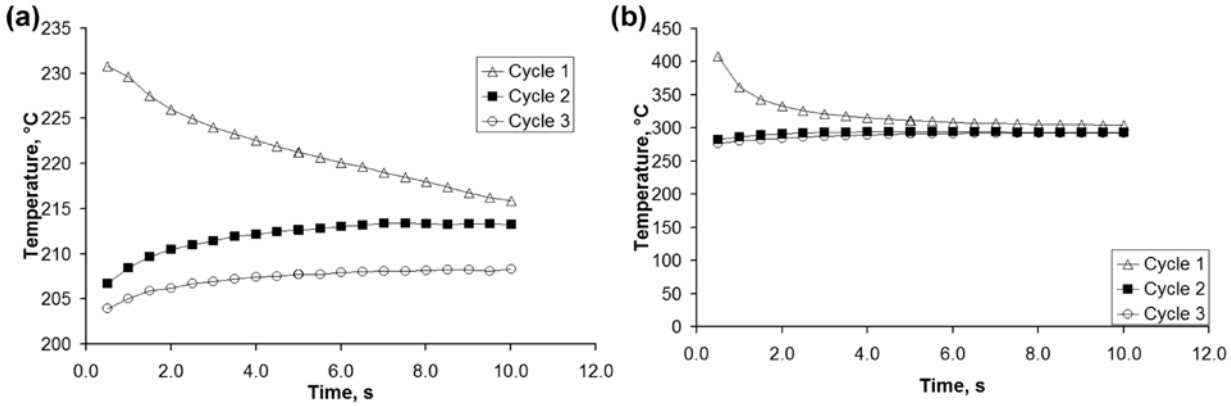

Figure 8.9: Graphical representation of applying the scaling factor based on electrical and radiated power dissipation on the emissivity model for ohmic curing cycles of **(a)** 0.25A and **(b)** 0.5A of applied electrical current. Calculated from data in [3].

Other Matters Related to Temperature

SEM microscopy of the samples used in DTA/TG analysis shed some light on the temperature reached by the electrically failed samples printed from Cabot CCI-300 ink examined in Chapter 7. The densified sintered microstructure of the ink used in DTA/TG analysis is seen in Figure 8.10 and is similar to the failed region of the conductive trace seen in Figure 7.1. The DT/TGA sample was subjected to a temperature of 500°C meaning that regions with similar microstructure in the failed conductive trace reached a similar temperature. Figure 7.1 also shows regions with a well-defined grain structure, meaning that the corresponding temperature was in excess of 500°C due to the fact that a higher temperature would be required to initiate grain growth than the temperature required to create the densified sintered structure.

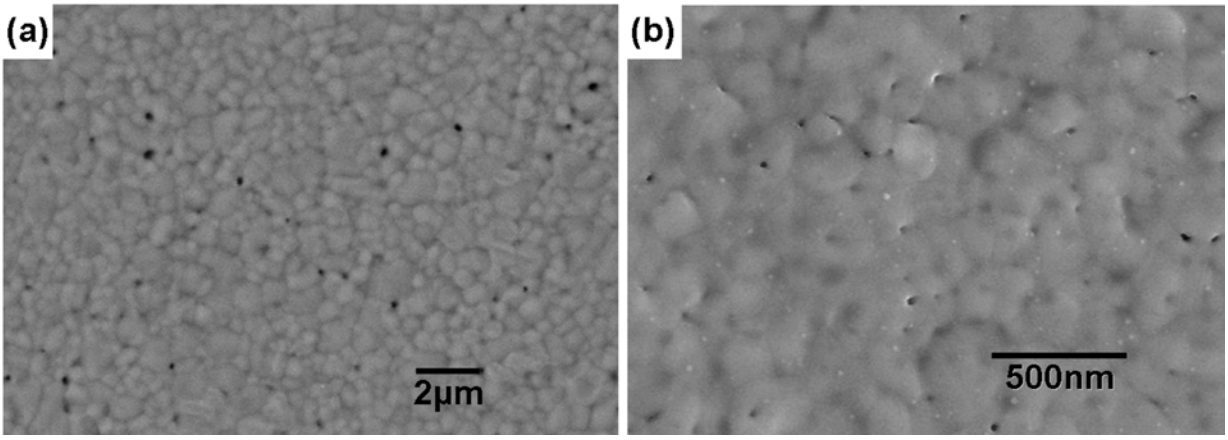

Figure 8.10: (a) SEM micrograph of CCI-300 subjected to 500°C during a DTA/TG analysis compared to **(b)** the failure zone of an electrically failed conductive trace. The similar microstructures indicate the temperature of the printed trace during failure was ~500°C. Image in (b) from [9].

Examining the microstructure of a DTA/TG sample which was subjected to a temperature of 800°C reveals the binder has not completely disappeared, as is apparent by the white chalky film seen in Figure 8.11(a), meaning that the binder is meant to play a role in the final electrical performance of this particular ink. Furthermore, no grain growth occurred though there appears to have been some particle melting which may actually be the polyester binder as seen in Figure 8.11(d). In contrast, the densified grain structure of the Ferro 3309F cured at 850°C seen in Chapter 3, indicates the binder used in that particular ink is designed to not play a role in the final electrical performance.

Also of interest was the exothermic reaction occurring at ~200°C for the Ercon E1660 sample subjected to DTA/TG testing with a maximum temperature of 500°C. SEM microanalysis revealed no difference between a sample of Ercon E1660 cured at 200°C (after ramping the sample to that temperature) and a sample cured 130°C for 30min. It is plausible that the exothermic reaction was caused by the binder rather than the silver flakes.

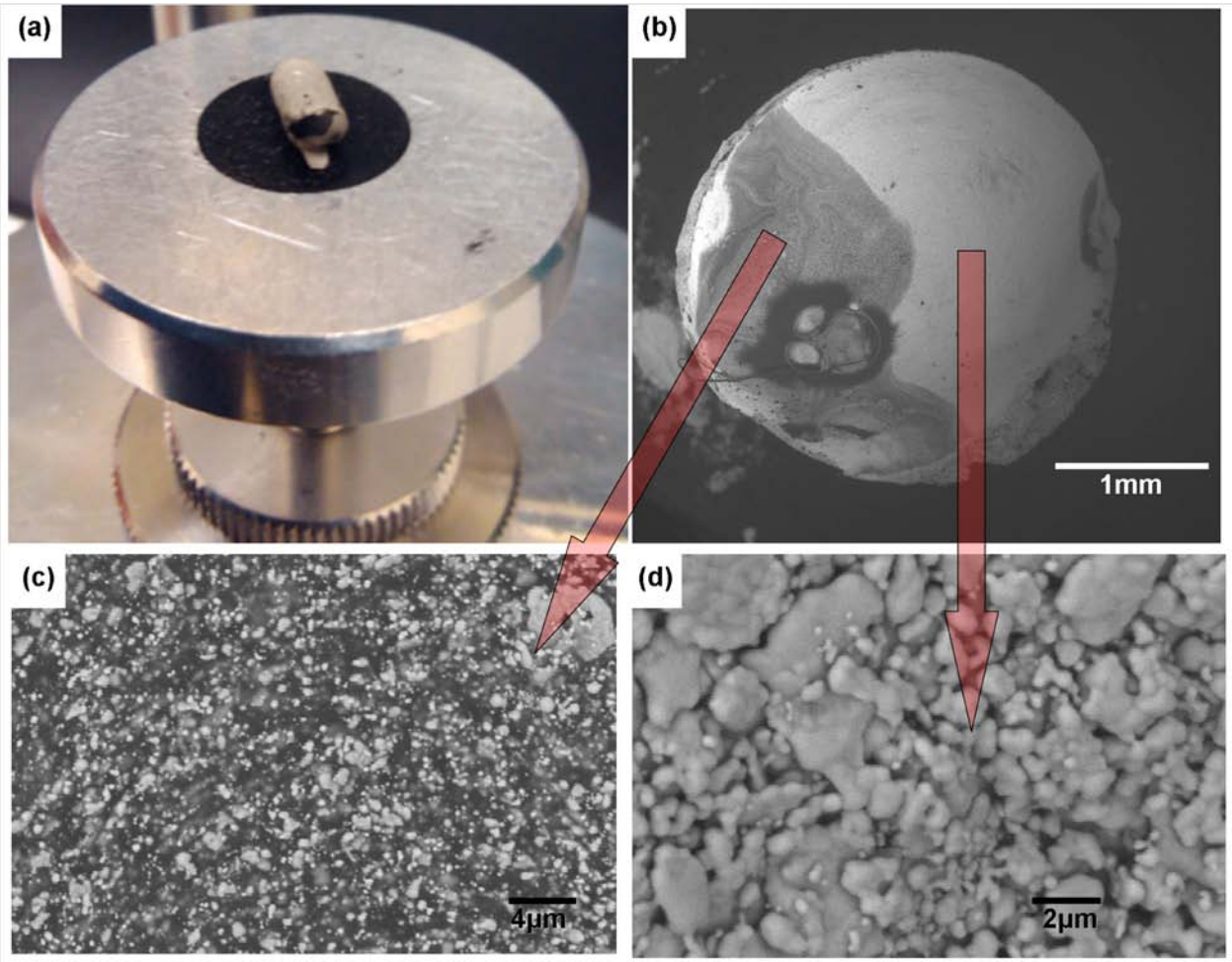

Figure 8.11: (a) Photograph of an Ercon E1660 sample subjected to 800°C in a DTA/TG test. Note the white substance which is most-likely the polyester binder. Corresponding SEM micrograph **(b)** of the top of the sample (the side pointing out in the photograph) long with SEM micrographs of **(c)** the darker region and **(d)** the lighter region.

8.3 Conclusions

The inherent resistance of a conductive printed trace can be harnessed to produce ohmic heating capable of increasing the conductivity of printed conductive traces. The utilization of ohmic curing in conjunction with or in lieu of thermal processing makes the use of polymeric substrates possible. Moreover, a clear pathway for the integration of ohmic curing in the creation of 3D structural electronics exists.

The creative thinking which goes into the development of novel ideas such as the integration of seemingly different technologies such as DW and AM in the creation of something

unique is the pathway for continued innovation. Equally as innovative is the utilization of inherent flaws such as the undesirably high resistance of a printed trace to improve or remove the undesirable characteristic.

8.4 References

[1] K.-S. Moon *et al*., "Thermal behavior of silver nanoparticles for low-temperature interconnect applications," *Journal of Electronic Materials*, vol. 34, no. 2, pp. 168-175, Feb. 2005.

[2] *Ercon E1660; Technical Data Sheet*, Ercon Incorporated, Wareham, MA, 2007, p. 1.

[3] D. A. Roberson, R.B. Wicker, E. MacDonald, "Ohmic Curing of Printed Conductive Traces," *Journal of Electronic Materials*, In Revision

[4] H. D. Young and R. A. Freedman, "Chapter 15 Temperature and Heat" in *University Physics 9th Edition*, Massachusetts: Addison-Wesley, 1996, pp. 471-484.

[5] S. O. Kasap, "Electrical and Thermal Conduction in Solids," in *Principles of Electrical Engineering Materials and Devices*, New York, NY: Irwin McGraw Hill, 1997, pp. 112-118.

[6] A. T. Alastalo, T. Mattila, M. L. Allen, M. J. Aronniemi, J. H. Leppäniemi, K. A. Ojanperä, M. P. Suhonen, and H. Seppä "Rapid electrical sintering of nanoparticle structures," *Materials Research Society Symp.—Low-Cost Solution-Based Deposition of Inorganic Films for Electronic/Photonic Devices*, D. B. Mitzi, D. Ginley, B. Smarsly, D. V. Talapin, Eds., 2008, vol. 1113E, pp. 1–6, paper 1113-F02-07.

[7] D. Duvivier and M. Wautelet, "From the microworld to King Kong," *Physics Education*, vol. 41, no. 5, pp. 386–390, Sep. 2006.

[8] M. Wautelet, "Scaling laws in the macro-, micro- and nanoworlds," *European Journal of Physics*, vol. 22, no. 6, pp. 601–611, Nov. 2001.

[9] D. A. Roberson, R. B. Wicker, E. MacDonald, "Microstructural characterization of electrically failed conductive traces printed from Ag nanoparticle inks," *Materials Letters*, In Press, 2012.

APPENDIX A: PERMISSION TO INCLUDE MATERIAL FROM THE JOURNAL *MATERIALS*

Re: Request to use published material in a dissertation

From:**Materials Editorial Office** (materials@mdpi.com)
Sent: Tue 8/09/11 1:56 AM
To: David Roberson (droberson@miners.utep.edu)

Dear Dr. Roberson,

Thank you very much for your e-mail and the request. You are free to use the following paper as long as it is properly cited:

Roberson, D.A.; Wicker, R.B.; Murr, L.E.; Church, K.; MacDonald, E. Microstructural and Process Characterization of Conductive Traces Printed from Ag Particulate Inks. *Materials* **2011**, *4*, 963-979.

In case of any questions, please feel free to contact us.

Best regards,
Emma Ma
Managing Editor
Materials (http://www.mdpi.com/journal/materials)

--
Ms. Emma Ma, M.Sc.
Materials Editorial Office
MDPI AG, Postfach, CH - 4005 Basel, Switzerland
E-Mail: materials@mdpi.com
Tel. +41 61 683 77 34; Fax: +41 61 302 89 18

On 8/5/2011 3:05 AM, David Roberson wrote:
David A. Roberson

The University of Texas at El Paso
500 W. University Ave
W.M. Keck Center for 3D Innovation
College of Engineering Building – Room E-108
El Paso, Texas 79968, USA
e-mail: droberson@miners.utep.edu <mailto:droberson@miners.utep.edu>

Materials Editorial Office
MDPI AG, Postfach, CH-4005 Basel, Switzerland
E-Mail: materials@mdpi.com mailto:materials@mdpi.com

Dear Editors,

I am currently a Ph.D. candidate at The Univerisity of Texas at El Paso, El Paso Texas, USA. I recently published an article in *Materials*. The Citation for this article is as follows:

Roberson, D.A.; Wicker, R.B.; Murr, L.E.; Church, K.; MacDonald, E. Microstructural and Process Characterization of Conductive Traces Printed from Ag Particulate Inks. *Materials* **2011**, *4*, 963-979.

I am writing to request permission to use the material presented in the above article in my dissertation. My University will accept permission to use the material published in *Materials* in the form of a reply to this e-mail.

Thanks!
David A. Roberson

APPENDIX B: PERMISSION TO INCLUDE MATERIAL FROM *JOURNAL OF ELECTRONIC MATERIALS*

From: Alfred, Edita [Edita.Alfred@springer.com]
Sent: Thursday, February 16, 2012 6:36 PM
To: David Roberson
Subject: JEMS-2815R2...

Dear Dr. Roberson,

I would like to let you know that permission has been granted to use the material. Please find below the response from the editor.

Thank you very much.

Best regards,

Edita

Edita Alfred (Mrs)

Springer

Journals Editorial Office

JEO Assistant

---

tel +91 44 42197752

fax + 91 44 42197763

Edita.Alfred@springer.com

---

www.springer.com

Editor Response:

Kindly provide appropriate reference to the journal article in the thesis.

From: Alfred, Edita
Sent: Thursday, February 16, 2012 10:13 AM
To: 'David Roberson'
Subject: JEMS-2815R2...

Dear Dr. Roberson,

I have forwarded the mail to the editor and would get back to you once I hear from her.

Thank you very much.

Best regards,

Edita

Edita Alfred (Mrs)

Springer

Journals Editorial Office

JEO Assistant

---

tel +91 44 42197752

fax + 91 44 42197763

Edita.Alfred@springer.com

-----Original Message-----
From: em.jems.f2b.291df2.45d74c5c@editorialmanager.com
[mailto:em.jems.f2b.291df2.45d74c5c@editorialmanager.com] On Behalf Of David Roberson
Sent: Thursday, February 16, 2012 2:43 AM
To: Alfred, Edita
Subject: My Manuscript - #JEMS-2815R2

Dear Editor,

I am writing to request permission to use the material in the article entitled "Ohmic curing of printed conductive traces" in my Ph.D. dissertation. The third revision of this article is currently under review, however, the material in the article is integral to my dissertation and I am set to graduate this semester. My university will accept permission to use the material contained within the article in the form of a reply to this e-mail.

Thank you,

David A. Roberson

APPENDIX C: PERMISSION TO INCLUDE MATERIAL FROM *JOURNAL OF FAILURE ANALYSIS AND PREVENTION*

Request to use material published in Journal of Failure Analysis and Prevention in a Dissertation

From:**Diane Whitelaw** (diane.whitelaw@asminternational.org)
Sent: Tue 8/23/11 8:33 AM
To: 'droberson@miners.utep.edu' (droberson@miners.utep.edu)

Yes, you have permission to use information in the article listed below in your dissertation:

D. A. Roberson, E. MacDonald, K. Church, and R. B. Wicker, "Failure Investigation of Direct Write Pen Tips," *Journal of Failure Analysis and Prevention*, vol. 10, no. 6, pp. 504-507, Aug. 2010.

Just be sure to cite this reference.

Thanks so much, and best wishes.

Diane M. Whitelaw

Production Coordinator

ASM International

9639 Kinsman Road

Materials Park, OH 44073

440.338.5151 ext. 5240

fax: 440.338.4634

diane.whitelaw@asminternational.org

----- Forwarded by Mcintyre Louthan/SRNL/Srs on 08/23/2011 08:30 AM -----

From: David Roberson <droberson@miners.utep.edu>

To: <mcintyre.louthan@srs.gov>
Date: 08/15/2011 01:18 PM
Subject: Request to use material published in Journal of Failure Analysis and Prevention in a Dissertation

---

David A. Roberson
The University of Texas at El Paso
500 W. University Ave
W.M. Keck Center for 3D Innovation
College of Engineering Building – Room E-108
El Paso, Texas 79968

e-mail: droberson@miners.utep.edu
Phone: 915-747-7443
Fax: 915-747-5019

McIntyre R. Louthan, Jr.
Editor, *Journal of Failure Analysis and Prevention*

Dr. Louthan,

I am a Ph.D. candidate at The University of Texas at El Paso, El Paso, TX, USA. An article I have written was published in *Journal of Failure Analysis and Prevention*. The citation for the article is as follows:

D. A. Roberson, E. MacDonald, K. Church, and R. B. Wicker, "Failure Investigation of Direct Write Pen Tips," *Journal of Failure Analysis and Prevention*, vol. 10, no. 6, pp. 504-507, Aug. 2010.

I am writing to request the use of the material in the article cited above in my dissertation. The University of Texas at El Paso will accept permission to use the material published in *Journal of Failure Analysis and Prevention* in a form of a reply to this e-mail. I appreciate your time and look forward to receiving a reply to this message.

Thanks!
David A. Roberson

APPENDIX D: PERMISSION TO INCLUDE MATERIAL FROM *MATERIALS LETTERS*

From: Pritchard, Laura (ELS-OXF) [L.Pritchard@elsevier.com]
Sent: Friday, February 17, 2012 3:33 AM
To: droberson@miners.utep.edu
Cc: Jayakumar, Balasaraswathi (ELS-CHN)
Subject: RE: Your Submission MLBLUE-D-11-04971R1

Dear Mr Roberson,

Thank you for your permission request below.

Please note that, as one of the Authors of this article, you retain the right to include the journal article, in full or in part, in a thesis or dissertation. You do not require permission to do so.

For full details of your rights as a Journal Author, please visit:

http://www.elsevier.com/wps/find/authorsview.authors/copyright#whatrights

Please feel free to contact me if you have any queries.

Kind regards

Laura

Laura Pritchard

Senior Rights Associate | ELSEVIER | The Boulevard| Langford Lane | Kidlington | Oxford OX5 1GB |

Tel: +44 1865 843517 Fax: +44 1865 853333

l.pritchard@elsevier.com

From: David Roberson [droberson@miners.utep.edu]

Sent: 09 February 2012 06:02

To: Material

Subject: RE: Your Submission MLBLUE-D-11-04971R1

Dear Professor Willoughby,

Thank you for accepting my submission to Materials Letters. I am writing to request permission to use the letter entitled "Microstructural characterization of electrically failed conductive traces printed from Ag nanoparticle inks" in my Ph.D. dissertation. My university will accept permission in the form of a reply to this e-mail.

Thanks in advance,

David A. Roberson

CURRICULUM VITA

David Adrian Roberson was born May 7, 1976 in El Paso, TX to Charles and Susan Roberson. David is a third generation El Pasoan. The Ph.D. in Materials Science and Engineering is the third degree awarded to David by The University of Texas at El Paso, the first two being a B.S. in Metallurgical and Materials Engineering in 1999 and a M.S. in Metallurgical and Materials Engineering in 2001. Between earning his Master of Science in Metallurgical and Materials Engineering and the pursuit of his Doctorate, David worked eight years in the semiconductor industry for Intel Corporation and Qimonda North America.

Selected Publications

Roberson, D. A.; Wicker, R. B.; MacDonald, E. Microstructural characterization of electrically failed conductive traces printed from Ag nanoparticle inks, *Materials Letters* **2012**, 76, 51-54

Roberson, D. A.; Wicker, R. B.; MacDonald, E. Ohmic Curing of Printed Conductive Traces, *Journal of Electronic Materials* **2012**, In Revision

Roberson, D. A.; Wicker, R. B.; Murr, L. E.; Church, K.; MacDonald, E. Microstructural and Process Characterization of Conductive Traces Printed from Ag Particulate Inks. *Materials* **2011**, *4*, 963-979.

Irwin, Michael D.; **Roberson, D. A.**; Olivas, R. I.; Wicker, R. B.; MacDonald, E. W. Conductive Polymer-Coated Threads as Electrical Interconnects in e-Textiles. *Fibers and Polymers* **2011**, 12, 904-910.

Roberson, D. A.; MacDonald, E.; Church, K.; Wicker, R. B. Failure Investigation of Direct Write Pen Tips. *Journal of Failure Analysis and Prevention*, **2010**, *10*, 504-507.

Permanent address: 867 Via Bonita Ln.

El Paso, TX 79912

droberson@miners.utep.edu

This dissertation was typed by David Adrian Roberson.